AD-A123 380 CAPABILITIES AND POTENTIAL OF MILLIMETER-WAVE IMPATT DEVICES(U) MICHIGAN UNIV ANN ARBOR ELECTRON PHYSICS LAB R K MAINS ET AL. NOV 82 TR-159 AFWAL-TR-82-1141 1/2

UNCLASSIFIED F33615-81-K-1429 F/G 9/1 NL

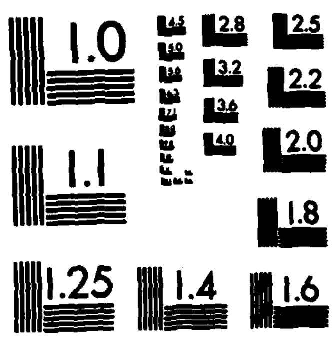
1.0
2.8
2.5
3.2
2.2
3.6
4.0
2.0
1.1
1.8
1.25
1.4
1.6

(12)

AFWAL-TR-82-1141

CAPABILITIES AND POTENTIAL OF MILLIMETER-WAVE IMPATT DEVICES

One of a series of Reports on Millimeter-Wave Circuit Analysis and Synthesis

R. K. Mains
G. I. Haddad

Electron Physics Laboratory
Department of Electrical and Computer Engineering
The University of Michigan
Ann Arbor, Michigan 48109

November 1982

Interim Report for Period March 1981-August 1982

Approved for public release; distribution unlimited.

AVIONICS LABORATORY
AIR FORCE WRIGHT AERONAUTICAL LABORATORIES
AIR FORCE SYSTEMS COMMAND
WRIGHT-PATTERSON AIR FORCE BASE, OHIO 45433

NOTICE

When Government drawings, specifications, or other data are used for any purpose other than in connection with a definitely related Government procurement operation, the United States Government thereby incurs no responsibility nor any obligation whatsoever; and the fact that the government may have formulated, furnished, or in any way supplied the said drawings, specifications, or other data, is not to be regarded by implication or otherwise as in any manner licensing the holder or any other person or corporation, or conveying any rights or permission to manufacture, use, or sell any patented invention that may in any way be related thereto.

This report has been reviewed by the Office of Public Affairs (ASD/PA) and is releasable to the National Technical Information Service (NTIS). At NTIS, it will be available to the general public, including foreign nations.

This technical report has been reviewed and is approved for publication.

Jon E. Griggs

JON E. GRIGGS, CAPT, USAF
Project Engineer
Microwave Techniques &
Applications Gp

FOR THE COMMANDER

Donald S. Rees

DONALD S. REES, Chief
Microwave Technology Branch
Avionics Laboratory

If your address has changed, if you wish to be removed from our mailing list, or if the addressee is no longer employed by your organization please notify AFWAL/AADM, W-PAFB, OH 45433 to help us maintain a current mailing list.

Copies of this report should not be returned unless return is required by security considerations, contractual obligations, or notice on a specific document.

Unclassified

SECURITY CLASSIFICATION OF THIS PAGE (When Data Entered)

REPORT DOCUMENTATION PAGE		READ INSTRUCTIONS BEFORE COMPLETING FORM
1. REPORT NUMBER AFWAL-TR-82-1141	2. GOVT ACCESSION NO. AD-A123310	3. RECIPIENT'S CATALOG NUMBER
4. TITLE (and Subtitle) CAPABILITIES AND POTENTIAL OF MILLIMETER-WAVE IMPATT DEVICES		5. TYPE OF REPORT & PERIOD COVERED Interim Tech March 1981-August 1982
		6. PERFORMING ORG. REPORT NUMBER Tech. Report No. 159
7. AUTHOR(s) R. K. Mains, G. I. Haddad		8. CONTRACT OR GRANT NUMBER(s) F33615-81-K-1429
9. PERFORMING ORGANIZATION NAME AND ADDRESS Electron Physics Laboratory, The University of Michigan, Ann Arbor, MI 48109		10. PROGRAM ELEMENT, PROJECT, TASK AREA & WORK UNIT NUMBERS 20020392
11. CONTROLLING OFFICE NAME AND ADDRESS Avionics Laboratory (AFWAL/AADM-2) Air Force Wright Aeronautical Laboratories, AFSC Air Force Systems Command, WPAFB, OH 45433		12. REPORT DATE November 1982
		13. NUMBER OF PAGES 157
14. MONITORING AGENCY NAME & ADDRESS(if different from Controlling Office)		15. SECURITY CLASS. (of this report) Unclassified
		15a. DECLASSIFICATION/DOWNGRADING SCHEDULE N/A

16. DISTRIBUTION STATEMENT (of this Report)

Approved for public release; distribution unlimited.

17. DISTRIBUTION STATEMENT (of the abstract entered in Block 20, if different from Report)

18. SUPPLEMENTARY NOTES

The findings in this report are not to be construed as an official Department of the Air Force position, unless so designated by other authorized documents.

19. KEY WORDS (Continue on reverse side if necessary and identify by block number)

Millimeter-wave IMPATT devices
Theoretical investigations
GaAs diodes
Si diodes
InP diodes
Single-drift doping profiles
Double-drift doping profiles
CW performance
Pulsed performance

20. ABSTRACT (Continue on reverse side if necessary and identify by block number)

Theoretical investigations of IMPATT diodes are carried out at 30, 40, 60 and 94 GHz. GaAs, Si and InP diodes are simulated. Several single- and double-drift doping profiles are considered. Extensive results as a function of RF voltage amplitude and dc current density are presented. Taking thermal resistance into account, the expected CW performance of each structure is presented, such that the maximum allowable diode temperature is 525°K. Matching each device to 1-Ω circuit resistance gives an estimate of maximum obtainable

DD FORM 1 JAN 73 1473

Unclassified

SECURITY CLASSIFICATION OF THIS PAGE (When Data Entered)

20. (Contd.)

pulsed power. Finally, CW and pulsed performance for all structures and materials are compared over the entire frequency range simulated.

FOREWORD

This report describes the theoretical investigations of IMPATT diodes at the Electron Physics Laboratory, Department of Electrical and Computer Engineering, The University of Michigan, Ann Arbor, Michigan. The work was sponsored by the Air Force Systems Command, Air Force Avionics Laboratory, Wright-Patterson Air Force Base, Ohio under Contract No. F33615-81-K-1429.

The work reported herein was performed during the period March 1981 to August 1982 by Drs. R. K. Mains and G. I. Haddad. The report was released by the authors in August 1982.

The authors wish to thank Captains Jon Grigus and Alan Mertz for their insightful comments and suggestions during the course of this work.

TABLE OF CONTENTS

LIST OF ILLUSTRATIONS

FIGURE PAGE

LIST OF TABLES

TABLE		PAGE
14	Large-Signal Results for the GaAs Double Read Profile in Figure 11a and Power Levels Obtained by Matching to 1-Ω Resistance (f = 40 GHz, V_{RF} = 23 V).	47
15	CW Results for the Profile in Figure 11a at 40 GHz Taking into Account the Thermal-Resistance Expressions.	49
16	Large-Signal Results for the GaAs Single-Drift Read Profile in Figure 13a and Power Levels Obtained by Matching to 1-Ω Resistance (f = 40 GHz, V_{RF} = 13.5 V).	52
17	Large-Signal Results for the Si Hybrid Profile in Figure 15a and Power Levels Obtained by Matching to 1-Ω Resistance (f = 40 GHz, V_{RF} = 29 V).	56
18	CW Results for the Profile in Figure 15a at 40 GHz Taking into Account the Thermal-Resistance Expressions.	57
19	Large-Signal Results for the InP Hybrid Profile in Figure 17a and Power Levels Obtained by Matching to 1-Ω Resistance (f = 40 GHz, V_{RF} = 33 V).	61
20	CW Results for the Profile in Figure 17a at 40 GHz Taking into Account the Thermal-Resistance Expressions.	62
21	Large-Signal Results for the GaAs Single-Drift Read Profile in Figure 19a and Power Levels Obtained by Matching to 1-Ω Resistance (f = 60 GHz, V_{RF} = 10 V).	67
22	CW Results for the Profile in Figure 19a at 60 GHz Taking into Account the Thermal-Resistance Expressions.	68
23	Large-Signal Results for the GaAs Hybrid Profile in Figure 21a and Power Levels Obtained by Matching to 1-Ω Resistance (f = 60 GHz, V_{RF} = 18 V).	72
24	CW Results for the Profile in Figure 21a at 60 GHz Taking into Account the Thermal-Resistance Expressions.	74

TABLE | PAGE

SECTION 1.

INTRODUCTION

In a previous report,[1] results of computer simulations of GaAs IMPATT diode structures operating at X-band frequencies were presented, and a description of the finite-difference computer program and the method of analysis were described. This report presents similar theoretical results for IMPATT diode structures designed to operate from 30 to 94 GHz. In addition to investigating GaAs devices, results for Si and InP are also presented. For each frequency range and material some doping profile optimization was carried out, although time did not permit extensive variation of all the parameters. Therefore, the profiles presented in this report are nearly optimum, although further adjustment of parameters may result in slightly better performance. Systematic optimization of some of these structures is currently being done, and the results will be reported at a future time.

Since efficiency of these devices decreases with increasing frequency and since dimensions become smaller, heat sinking becomes even more of a problem than at X-band. Therefore, thermal limitations are taken into account in this report when calculating expected output power for the various structures.

Comparisons among the uniform double-drift, hybrid double-drift, and double Read double-drift profiles are made at different frequencies and for different materials. While it was found[1] that for GaAs at X-band the double Read profile is optimum, at millimeter-wave frequencies it is found that the hybrid double-drift profile

or the uniformly doped profile is optimum depending on the frequency. This can be related to the fact that the ionization rates vs. electric field in GaAs are saturated for electric-field strengths typically found in millimeter-wave IMPATTs.

Throughout this report the static drift-diffusion model is employed, although it is known that for GaAs and InP nonequilibrium effects become significant at millimeter-wave frequencies. An improved model including energy and momentum balance equations has been developed for Si IMPATT simulation,[2] and results have shown very little discrepancy with the static results up to 200 GHz. A similar model for GaAs IMPATT simulation is currently being implemented and in the near future a similar comparison will be made for GaAs.

SECTION 2.

MATERIAL PARAMETERS

The results of the IMPATT simulations strongly depend on the assumed material parameters, and unfortunately some of the parameter values at the high fields encountered in millimeter-wave IMPATTs are uncertain. Table 1 gives the material parameters assumed for GaAs. The sources for these parameters are given by Bauhahn.[3] In addition, the saturated velocity for holes and the ionizations rates used are in accordance with recent measurements carried out at Raytheon.[4] For previous calculations at X-band,[1] a saturated diffusion coefficient of 20 cm^2/V-s had been used. However, it was found that at higher frequencies the calculated efficiency is very dependent on the high-field diffusion coefficient, and since this value is uncertain, the diffusion coefficient was varied until the best fit to experimentally obtained efficiencies in the 35-GHz range was obtained. This occurred when a diffusion coefficient of 15 cm^2/s was assumed. Since there is some numerical diffusion in the program, the effective diffusion coefficient is somewhat larger than 15 cm^2/s but still less than 20 cm^2/s.

The material parameters used for the Si and InP simulations are given in Tables 2 and 3, respectively. The sources for the Si parameters are given by Bauhahn.[3] The InP parameters[3,5-11] in Table 3 were obtained as follows. The InP ionization rates of Kao and Crowell[5-6] at T = 500°K presented at the Cornell Hot-Electron Workshop were used. (The measurement technique and previous measurements at room temperature are given in Reference 7.) The electron

TABLE 1

GaAs MATERIAL PARAMETERS

$$v_n(E) = \frac{\mu_n|E| + v_{nsat}\left(\frac{E}{E_v}\right)^4}{1 + \left(\frac{E}{E_v}\right)^4}$$

$$v_p(E) = v_{psat}[1 - \exp(-\mu_p|E|/v_{psat})]$$

$$D_n(E) = \frac{D_{no} + D_{nsat}\left(\frac{E}{E_d}\right)^4}{1 + \left(\frac{E}{E_d}\right)^4}$$

$$D_p(E) = 15 \text{ cm}^2/\text{s}$$

$$\alpha_n(E) = \alpha_p(E) = A \exp[-(b/E)^2]$$

T (°K)	μ_n (cm²/V-s)	v_{nsat} (cm/s)	E_v (V/cm)	v_{psat} (cm/s)	μ_p (cm²/V-s)	D_{nsat} (cm²/s)	E_d (V/cm)
300	5000	$8\text{x}10^6$	$4\text{x}10^3$	$8\text{x}10^6$	400	15	$5.8\text{x}10^3$
500	4000	$5\text{x}10^6$	$4\text{x}10^3$	$5.2\text{x}10^6$	200	15	$5.8\text{x}10^3$

T (°K)	A (cm⁻¹)	b (V/cm)	D_{no} (cm²/s)
300	$1.61\text{x}10^5$	$5.42\text{x}10^5$	129
500	$1.84\text{x}10^5$	$6.47\text{x}10^5$	172

TABLE 2

Si MATERIAL PARAMETERS (T = 500°K)

$$v_n(E) = v_{nsat}[1 - \exp(-\mu_n|E|/v_{nsat})]$$

$$v_p(E) = v_{psat}[1 - \exp(-\mu_p|E|/v_{psat})]$$

$$D_n(E) = D_p(E) = 18.2 \text{ cm}^2/\text{s}$$

$$\alpha_n(E) = A_n \exp(-b_n/E)$$

$$\alpha_p(E) = A_p \exp(-b_p/E)$$

$$\mu_p = 250 \text{ cm}^2/(\text{V-s})$$

$$\mu_n = 550 \text{ cm}^2/(\text{V-s})$$

$$v_{psat} = 1.02 \times 10^7 \text{ cm/s}$$

$$v_{nsat} = 8.5 \times 10^6 \text{ cm/s}$$

$$A_n = 1.8 \times 10^6 \text{ cm}^{-1}$$

$$b_n = 1.64 \times 10^6 \text{ V/cm}$$

$$A_p = 1.0 \times 10^7 \text{ cm}^{-1}$$

$$b_p = 3.2 \times 10^6 \text{ V/cm}$$

$$\epsilon_r = 11.8$$

TABLE 3

InP MATERIAL PARAMETERS (T = 500°K)

Parameters have the same functional form as in Table 1 except:

$$\alpha_n(E) = A_n \exp(-b_n/E)$$

$$\alpha_p(E) = A_p \exp(-b_p/E)$$

$$\mu_p = 90 \text{ cm}^2/(\text{V-s})$$

$$\mu_n = 2760 \text{ cm}^2/(\text{V-s})$$

$$v_{psat} = 5.68 \times 10^6 \text{ cm/s}$$

$$v_{nsat} = 6.0 \times 10^6 \text{ cm/s}$$

$$A_n = 7.121 \times 10^6 \text{ cm}^{-1}$$

$$b_n = 4.072 \times 10^6 \text{ V/cm}$$

$$A_p = 3.502 \times 10^7 \text{ cm}^{-1}$$

$$b_p = 3.852 \times 10^6 \text{ V/cm}$$

$$E_v = 11.0 \times 10^3 \text{ V/cm}$$

$$D_{nsat} = D_p = 15 \text{ cm}^2/\text{s}$$

$$E_d = 10.0 \times 10^3 \text{ V/cm}$$

$$D_{no} = 119 \text{ cm}^2/\text{s}$$

$$\epsilon_r = 14.0$$

saturated velocity was suggested by Blakey[5] and is close to the value obtained from Monte Carlo calculations by Fawcett and Hill.[8] The electron low-field mobility was derived from References 5 and 8 through 11. E_v, the field corresponding to the peak electron velocity, was also obtained from the calculations by Fawcett and Hill.[8] The high-field diffusion coefficient for electrons, D_{nsat}, is close to the value obtained by Fawcett and Hill.[8] The low-field electron diffusion coefficient D_{no} is given by the Einstein relationship and is close to the value calculated by Bauhahn, Haddad and Masnari.[11] The field E_D used in the $D_n(E)$ expression was obtained from Bauhahn.[3] The values for hole diffusion coefficient, low-field mobility and hole saturated velocity were suggested by Blakey.[5]

SECTION 3.

THERMAL RESISTANCE

In order to calculate the expected power output for millimeter-wave IMPATTs, the thermal resistance of the diode must be known. For double-drift GaAs IMPATTs, the thermal resistance is given approximately by [12]

$$R_{TH} = \frac{2}{\pi K_{hs} d} + R_{PKG} + \frac{4\ell_1 T_1}{120\ \pi d^2} + \frac{4\ell_2 T_2}{300\pi d^2}\ , \qquad (1)$$

where d is the device diameter in cm, K_{hs} is the thermal conductivity of the heat-sink material in W/cm-°K, R_{PKG} is the portion of the thermal resistance due to the package and bonding (°K/W), ℓ_1 is the buffer or substrate thickness (cm), T_1 is the average temperature (°K) of the buffer layer, ℓ_2 is the active layer thickness (cm) between the junction and the buffer layer, and T_2 is the average temperature (°K) in the active layer.

The first term in Equation 1 is the spreading resistance which occurs at the interface between the diode and heat sink. It is the result obtained by Kennedy[13] for the case of a uniform circuit heat flux density incident on a large cylindrical heat sink of thermal conductivity K_{hs}. (It should be noted that the quantity H in Equation 9 of Reference 13 limits to 1 for this case; also conversions from calories to joules and inches to centimeters are necessary in k and A, respectively, in order for the spreading resistance expressions to agree). The third term in Equation 1, which is the thermal resistance of the buffer layer of length

ℓ_1, can be derived from the expression in Appendix B of the Olson paper[14] for thermal resistance assuming one-dimensional heat flow:

$$R = \frac{\Delta x}{kA} \quad , \tag{2}$$

where Δx is the length of the section, k the thermal conductivity, and A the cross-sectional area. Setting $\Delta x = \ell_1$ and equating these two terms obtains the following expression for the thermal conductivity of GaAs in the buffer layer:

$$k = \frac{120}{T_1} \frac{W}{cm-{}^{\circ}K} \quad . \tag{3}$$

Equation 3 agrees well with the expression given in Appendix A of the Olson paper[14] and also with the experimental conductivity data in Figure 7 of the Maycock paper.[15] The final term in Equation 1, representing the thermal resistance of the active layer, is of the same form as the buffer-layer term but is reduced by the factor 0.4. This is because in deriving the active-layer term, uniform heat generation throughout the active region is assumed.[12]

For these calculations, the thermal conductivity[12] of a diamond heat sink is taken as 11.7 W/cm-°K and that of a copper heat sink is 3.9 W/cm-°K. Since R_{PKG} is very dependent on the package and bonding technique, it is taken to be zero in the thermal resistance calculations.

From the expressions given in Appendix A of Olson,[14] it is seen that the thermal conductivity of Si is approximately three times that of GaAs. Therefore, it is expected that the last two terms of Equation 1 will be reduced by a factor of 1/3 for Si calculations.

Also, from Figure 8 of Maycock[15] it is seen that the thermal conductivity of InP is slightly higher than for GaAs by approximately the factor 5/4. Therefore, the final two terms of Equation 1 are reduced by 4/5 in InP calculations.

The use of multiple mesas or ring geometries will reduce the first term in Equation 1, as explained in the previous X-band report.[1] As was done in that report, it will be assumed here that an improvement of the spreading term by the factor 0.55 is possible by utilizing more efficient geometries than the single-round mesa structure.

Once the thermal-resistance expression is known, the diode junction temperature T (°K) under large-signal CW conditions is given by

$$T = 300 + R_{th}(1 - \eta)V_{dc}J_{dc}A \quad , \tag{4}$$

where η is the fractional RF generation efficiency, V_{dc} is the diode dc voltage in V, J_{dc} is the diode dc current density in A/cm^2, and A is the device area in cm^2. Equation 4 will be taken into account when estimating the power output expected from these devices.

SECTION 4.

ESTIMATION OF OPTIMUM CURRENT DENSITY AND DOPING LEVELS AT DIFFERENT FREQUENCIES

As the frequency of operation is varied in the 30 to 94 GHz range, it is useful to develop expressions which roughly predict the optimum current density and doping level at each frequency.

The small-signal impedance expression of Gilden and Hines[16] may be used to estimate the optimum current density for a Read structure as follows. If it is assumed that the avalanche and drift lengths are specified such that the optimum transit angle ($\theta \cong \pi$) is obtained and the desired operation frequency ω is specified, the avalanche resonance frequency ω_a can be derived which yields the maximum small-signal negative conductance. Since ω_a is related to J_o, the following expression for optimum current density is obtained:

$$J_o = \frac{\dfrac{\varepsilon\omega^2}{2\alpha' v_d}}{1 + \dfrac{4(\ell_d)^3\omega}{v_d\pi^2(\ell_a + \ell_d)^2} + \dfrac{\ell_a}{\ell_a + \ell_d}} , \qquad (5)$$

where J_o is in A/cm^2, ε is the dielectric constant in F/cm, v_d is the saturated velocity in cm/s, ℓ_d and ℓ_a are the drift and avalanche region lengths in cm, respectively, and α' is the derivative of the ionization rate with respect to electric field in the avalanche region in V^{-1}. The quantity α' is found by first determining E_a, the field in the avalanche region, such that $\alpha(E_a)\ell_a = 1$. Then $\alpha'(E_a)$ is calculated from the ionization rate expression.

Of course, Equation 5 is based on many simplifying assumptions and can only give a rough estimate of the optimum current density.

The optimum doping in the drift region of a Read structure can be estimated if the diode is designed to operate in the pre-collection mode as follows. If the terminal voltage is $V_{dc} + V_{RF} \sin(\omega t)$, then dV/dt at 315° in the cycle is $(0.707)\omega V_{RF}$. (315° is chosen because it is halfway into the last quarter cycle.) Recalling that the expression for the velocity of the depletion edge on the n-side is[1]

$$\frac{dw}{dt} = \frac{\varepsilon}{qwN_D(w)} \frac{dV}{dt} \qquad (6)$$

(where the diode is punched through on the p-side and w is the width of the depleted region), an approximate expression for N_D is obtained if it is required that the depletion edge moves at the peak velocity, v_{max}, at 315° in the cycle. This gives

$$N_D = \frac{\varepsilon\omega V_{RF}}{\sqrt{2}\, qwv_{max}} . \qquad (7)$$

Once V_{dc} is known for the structure (by assuming a favorable electric field profile), V_{RF} can be estimated. Equation 7 then gives a starting point for optimum doping profile determination.

SECTION 5

RESULTS AT 30 GHz

As a first step, Equation 5 is evaluated for GaAs to obtain an estimate of the dc current density for operation at 30 GHz. For a one-sided GaAs Read structure with $\ell_a = 0.2$ μm and $\ell_d = 0.83$ μm (chosen so that $\theta = \pi$), it is found that $\alpha = 5 \times 10^4$ cm^{-1} and from the $\alpha(E)$ expression in Table 1, $E_a = 5.67 \times 10^5$ V/cm. Thus $\alpha' = 0.23$ V^{-1}, and evaluating Equation 5 at 30 GHz yields $J_o = 8.48 \times 10^3$ A/cm^2.

For Si and InP, Equation 5 is not applicable because the ionization rates for holes and electrons are not equal. However, for Si, if one performs the calculation first using the ionization rate expression for electrons and then the rate expression for holes in Table 2, one finds in both cases that J_o is substantially less than the J_o for GaAs; it is 2.65×10^3 A/cm^2 for electrons and 2.36×10^3 A/cm^2 for holes. Therefore, it is expected that the Si Read diode will operate at considerably lower current densities than the GaAs diode, mostly due to the larger slope of the ionization rates for Si.

For InP, Equation 5 is not applicable since the ionization rates for holes and electrons are quite different, and very different results are obtained for J_o depending on which is used.

Equation 7 can be used to estimate the optimum N_D needed to obtain the precollection mode for a GaAs double Read structure at 30 GHz. It has already been found that $E_a \approx 5.67 \times 10^5$ V/cm for an avalanche region width of 0.2 μm. If it is assumed that the

drift-region field is constant and equal to 2.6×10^5 V/cm and that the drift length is 0.67 μm long, a dc voltage of 46 V is estimated. Since the optimum V_{RF} is typically 0.65 V_{dc} for GaAs, the value V_{RF} = 30 V is used in Equation 7. When $v_{max} \cong 10^7$ cm/s and $w \cong 1.54$ μm, the value $N_D = 1.8 \times 10^{16}$ cm^{-3} is obtained.

Figure 1a shows a doping profile for a GaAs hybrid IMPATT that was simulated at 30 GHz, and Figure 1b shows the dc solution for J_{dc} = 9 kA/cm^2. Plots of the large-signal results obtained for this structure at T = 500°K are given in Figure 2. The maximum efficiency was 23.24 percent for J_{dc} = 9 kA/cm^2 and V_{RF} = 31.5 V. The maximum power density obtained was $P_{RF} = 1.216 \times 10^5$ W/cm^2 at J_{dc} = 17.1 kA/cm^2 and V_{RF} = 31.5 V.

Table 4 lists some of the large-signal results vs. J_{dc} plotted in Figure 2c. Also given in Table 4 are the dc, RF and dissipated powers in W that would result if the diode area is chosen so that the diode exhibits 1-Ω negative resistance. This value of area is given by

$$A = \frac{-G_D}{G_D^2 + B_D^2} \quad . \tag{8}$$

If the area were chosen larger, the negative resistance would be smaller than 1 Ω,and P_{RF} would be greater. However, since it is difficult to match the diode with a circuit whose resistance is below 1 Ω, the values in Table 4 are reasonable estimates of the maximum electronic power generating capabilities of the diode. These values can also be determined if the circuit load resistance for a particular circuit is known and is different from 1 Ω.

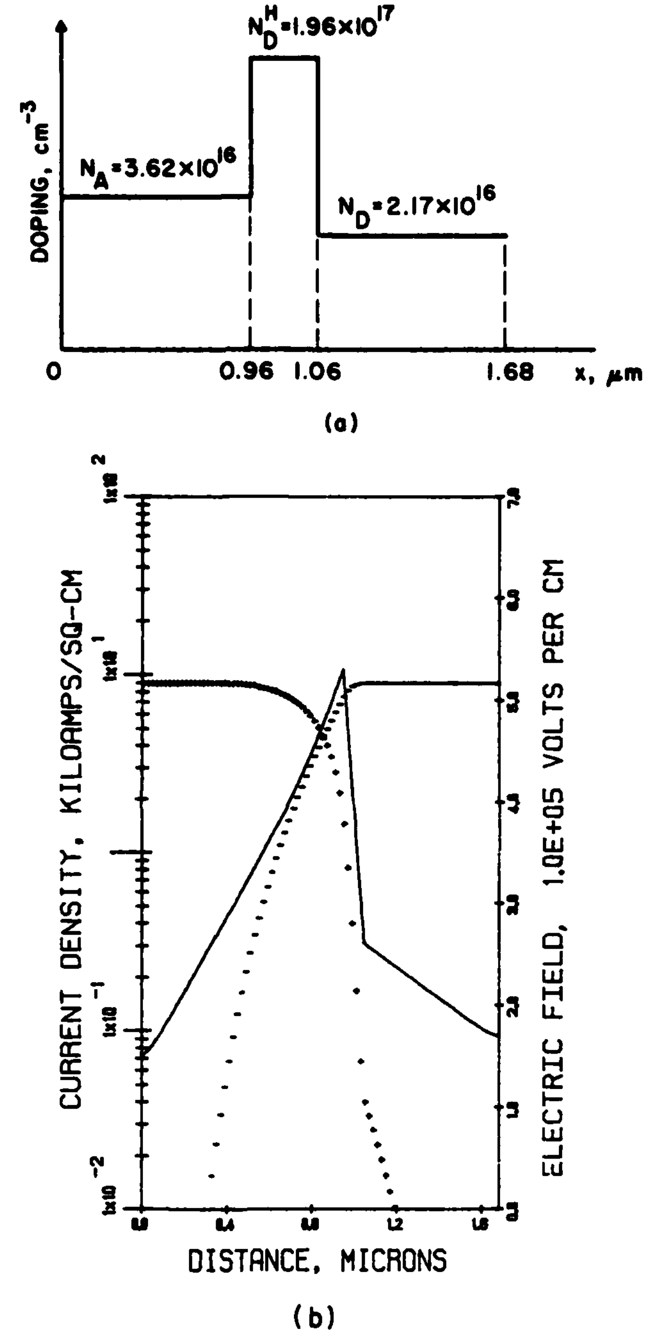

Figure 1. (a) GaAs Hybrid Profile for 30-GHz Operation and (b) Dc Solution at T = 500°K and J_{dc} = 9 kA/cm^2. (X_A = 0.44 μm, J_{dc} = 9 kA/cm^2, E_{max} = 5.31 x 10^5 V/cm, E_{LHS} = 1.52 x 10^5 V/cm, E_{to} = 2.61 x 10^5 V/cm and E_{RHS} = 1.71 x 10^5 V/cm)

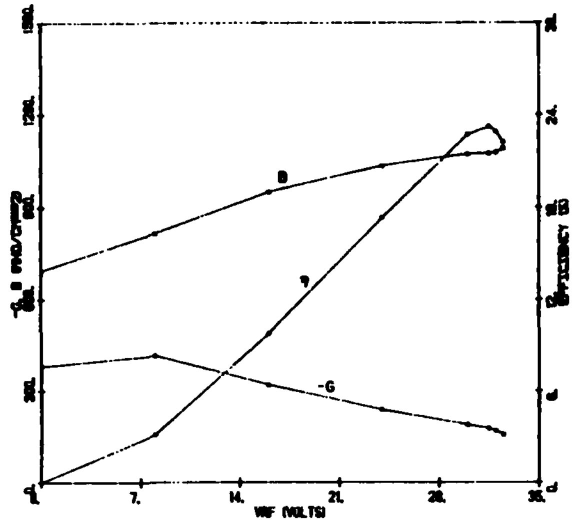

(a)

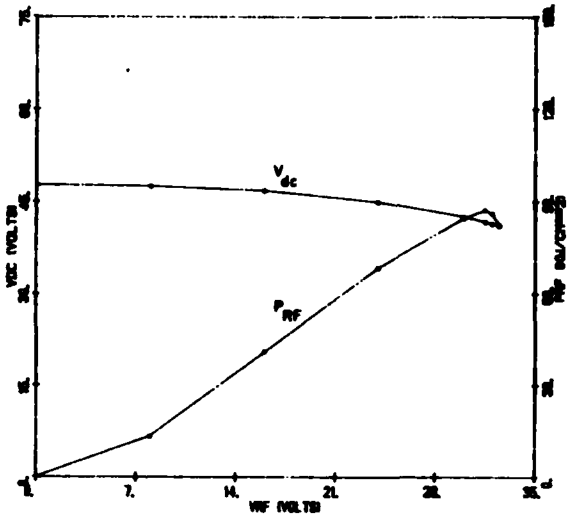

(b)

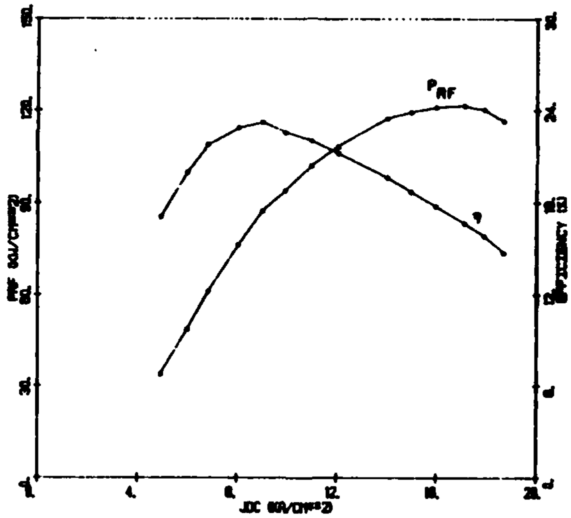

(c)

Figure 2. Large-Signal Results for the Profile of Figure 1a at $T = 500°K$, $f = 30$ GHz and (a and b) $J_{dc} \approx 9$ kA/cm^2, (c) $V_{RF} = 31.5$ V.

TABLE 4

LARGE-SIGNAL SIMULATION RESULTS FOR THE GaAs HYBRID PROFILE IN FIGURE 1a AND POWER LEVELS OBTAINED BY MATCHING TO 1-Ω RESISTANCE (f = 30 GHz, V_{RF} = 31.5 V)

J_{dc} (kA/cm²)	$-G_D$ (mho/cm²)	B_D (mho/cm²)	A x 10^{-4} (cm²)	I_{dc} (A)	V_{dc} (V)	η (Percent)	P_{dc} (W)	P_{RF} (W)	P_{diss} (W)	θ_R (°C/W)	D (mils)
4	38.4	1260	0.24	0.096	40	12.2	3.84	0.47	3.37	67	2.2
4.5	56.6	1236	0.37	0.17	40	15.6	6.8	1	5.8	39	2.7
5	68.2	1220	0.455	0.23	40	17	9.2	1.56	7.64	29	3
6.8	123	1146	0.92	0.62	41	21.8	25.4	5.53	19.8	11.3	4.26
8	154	1105	1.24	1.0	41	23	41	9.43	30.6	7	4.94
9	176	1074	1.48	1.3	42	23.2	54.6	12.7	41.9	5.4	5.4
10	190	1053	1.66	1.66	42	22.5	70	15.8	54	4	5.7
11	206	1023	1.89	2.0	42	22	84	18.5	65.5	3.4	6.5
14	237	945	2.5	3.5	43	20	150	30	120	1.8	7.4
16	244	895	2.8	4.5	43	18	193	35	158	1.4	7.8
17	245	862	3.0	5.1	43	17	220	37	183	1.2	8
18	242	836	3.2	5.7	43	16	245	39	206	1	8.2
18.7	235	820	3.2	5.9	43	14.7	253	37	216	1	8.2

The term "electronic" power means that thermal effects are ignored, and the diode is assumed to be at a constant temperature. These power levels may be achievable under very short (much lower than the device thermal-time constant) pulse conditions. θ_R is the thermal resistance which is required so that the diode temperature rise does not exceed 225°C above the ambient temperature. D is the diode diameter in mils corresponding to the area A in cm^2.

Of course, not all the P_{RF} values in Table 4 are achievable in practice under CW conditions. This is because for some values of diameter D the thermal resistance achievable in practice is larger than the required θ_R. Therefore, if the diode were operated at that power level, the temperature rise would exceed 225°C, and the diode would burn out. The achievable thermal resistance θ is calculated using Equation 1. As previously mentioned, the package/bonding term R_{PKG} is assumed to be zero, due mostly to lack of knowledge of this parameter. The buffer layer thickness ℓ_1 is assumed to be 0.5 μm, and the average buffer layer temperature T_1 is assumed to be 450°K. For this structure (see Figure 1a), the active layer thickness ℓ_2 is taken to be the p-layer thickness and is therefore 0.96 μm. The average temperature in the active layer T_2 is assumed to be 500°K.

Four different cases will be considered. The first case is for a single diode mesa on a copper heat sink. The thermal resistance for this case is denoted by $\theta(CM)$. Since the thermal conductivity for copper is 3.9 W/cm-°K, Equation 1 becomes

$$\theta(CM) = \frac{64.27}{d_m} + \frac{68.58}{d_m^2}, \qquad (9)$$

where d_m is the diameter in mils. For the case of a single mesa on a diamond heat sink, denoted by DM, evaluating Equation 1 using K_{hs} = 11.7 W/cm-°K for diamond yields

$$\theta(DM) = \frac{21.42}{d_m} + \frac{68.58}{d_m^2} \quad . \tag{10}$$

The remaining two cases use ring geometries instead of a single mesa. As explained in Reference 1, using an aspect ratio of 4 reduces the spreading term in Equation 1 by 0.55. If this aspect ratio is assumed, the thermal resistance for a ring geometry on a copper heat sink, denoted by $\theta(CR)$, is

$$\theta(CR) = \frac{35.35}{d_m} + \frac{68.58}{d_m^2} \quad , \tag{11}$$

where d_m is the equivalent diode diameter, i.e., $\pi d_m^2/4$ is the area of the diode annulus. For the case of a ring geometry on a diamond heat sink, the thermal resistance is

$$\theta(DR) = \frac{11.78}{d_m} + \frac{68.58}{d_m^2} \quad . \tag{12}$$

It is seen that for all these cases, the thermal resistance has the form

$$\theta = \frac{A}{d_m} + \frac{B}{d_m^2} \quad . \tag{13}$$

If it is required that the diode temperature rise not exceed 225°C, Equation 4 becomes

$$\left(\frac{A}{d_m} + \frac{B}{d_m^2}\right)(1 - \eta)V_{dc}J_{dc}\,\frac{\pi d_m^2(2.54 \times 10^{-3})^2}{4} \leqq 225 \quad , \tag{14}$$

where 2.54×10^{-3} is the conversion factor for mils to cm. Solving for d_m yields

$$d_m \leq \frac{1}{A}\left(\frac{4.44 \times 10^7}{(1 - \eta)V_{dc}J_{dc}} - B\right) . \qquad (15)$$

Therefore, the maximum achievable power from thermal considerations is calculated by taking the equality sign in Equation 15.

Therefore, two methods of calculating the maximum diode diameter and maximum power generated are now available. One is from matching considerations in Equation 8, where a minimum circuit resistance of 1 Ω is assumed. The second method is from thermal considerations in Equation 15. To estimate the maximum achievable power in practice, the procedure is to calculate the device diameter using both methods and then to choose the minimum of these two values.

This procedure has been carried out for the data of Table 4, and the results are given in Table 5. Results for each combination of diode geometry and heat-sink material are given. D is the minimum diameter for each case as discussed in the previous paragraph. θ is the corresponding achievable thermal resistance for this diameter as calculated from Equation 9 through 12. P_{RF} is the RF power corresponding to the given diameter; it is therefore the estimate for the maximum achievable CW RF power in practice.

It is seen from Table 5 that for low values of J_{dc}, the power generation is electronically limited. For higher J_{dc} values, the power output is thermally limited.

For pulsed operation, higher peak powers than those given in Table 5 are possible since the thermal limitation is relaxed.

TABLE 5

CW RESULTS FOR THE PROFILE IN FIGURE 1a AT 30 GHz TAKING INTO ACCOUNT

THE THERMAL-RESISTANCE EXPRESSIONS

D(CM) (mils)	θ(CM) (°C/W)	P_{RF}(CM) (W)	D(DM) (mils)	θ(DM) (°C/W)	P_{RF}(DM) (W)	D(CR) (mils)	θ(CR) (°C/W)	P_{RF}(CR) (W)	D(DR) (mils)	θ(DR) (°C/W)	P_{RF}(DR) (W)	J_{dc} (kA/cm²)
2.2	43.4	0.47	2.2	23.9	0.47	2.2	30.2	0.47	2.2	19.5	0.47	4
2.7	33.2	1	2.7	17.3	1	2.7	22.5	1	2.7	13.8	1	4.5
3	29	1.56	3	10	1.56	3	19.4	1.56	3	11.5	1.56	5
2.1	46	1.36	4.26	8.8	5.53	3.82	13.9	4.5	4.26	6.5	5.53	6.8
1.67	63	1.06	4.94	7.1	9.43	3.03	19.1	3.52	4.94	5.2	9.43	8
1.31	88	0.76	3.94	9.86	6.89	2.39	26.8	2.53	5.4	4.5	12.7	9
1.05	122	0.53	3.17	13.6	4.8	1.92	37	1.76	5.7	4.2	15.8	10
0.85	170	0.37	2.55	18.9	3.35	1.54	51.6	1.23	4.6	5.7	11.1	11
0.37	683	0.082	1.10	75.9	0.74	0.67	206	0.272	2	23	2.4	14
0.16	3173	0.016	0.47	352	0.14	0.29	960	0.051	0.86	107	0.46	16
0.072	1.43×10^4	3.2×10^{-3}	0.21	1588	0.029	0.13	4322	0.011	0.39	480	0.096	17
--	--	--	--	--	--	--	--	--	--	--	--	18
--	--	--	--	--	--	--	--	--	--	--	--	18.7

This depends on the pulse width relative to the thermal-time constant and the duty cycle.

The GaAs double Read structure of Figure 3a and b was simulated at 30 GHz. Large-signal results vs. V_{RF} at $J_{dc} = 9\ kA/cm^2$ are presented in Figure 4a and b. Figure 4c presents large-signal results vs. J_{dc} at $V_{RF} = 28$ V, the voltage at which maximum efficiency in Figure 4a was obtained. The maximum efficiency obtained for this structure was $\eta = 25.6$ percent at $V_{RF} = 28$ V and $J_{dc} = 7\ kA/cm^2$; the maximum power density was $P_{RF} = 94.6\ kW/cm^2$ at $V_{RF} = 28$ V and $J_{dc} = 11.14\ kA/cm^2$.

Table 6 presents large-signal results vs. J_{dc} at $V_{RF} = 28$ V, along with electronic powers obtainable if the diode is matched to 1-Ω resistance. Comparison with Table 4 shows that the electronic power for the hybrid structure is larger than for the double Read structure. This is because the doping on the p-side of the hybrid structure is larger than the p-doping in the double Read drift region, so that space-charge effects are not as severe for the hybrid, and it can operate at higher current densities than the double Read structure. Therefore, the hybrid structure is superior for pulsed applications where excessive heating is not a problem.

However, when thermal effects are included to evaluate CW performance, the double Read structure can generate more power than the hybrid. The thermal-resistance expressions for the double Read diode corresponding to Equations 9 through 12 and using $\ell_2 = 0.76\ \mu m$ from Figure 3a for the hybrid are

$$\theta(CM) = \frac{64.27}{d_m} + \frac{62}{d_m^2} , \qquad (16)$$

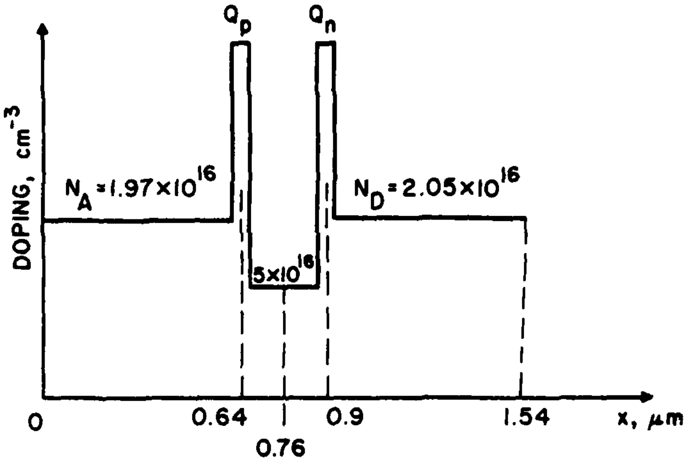

(a)

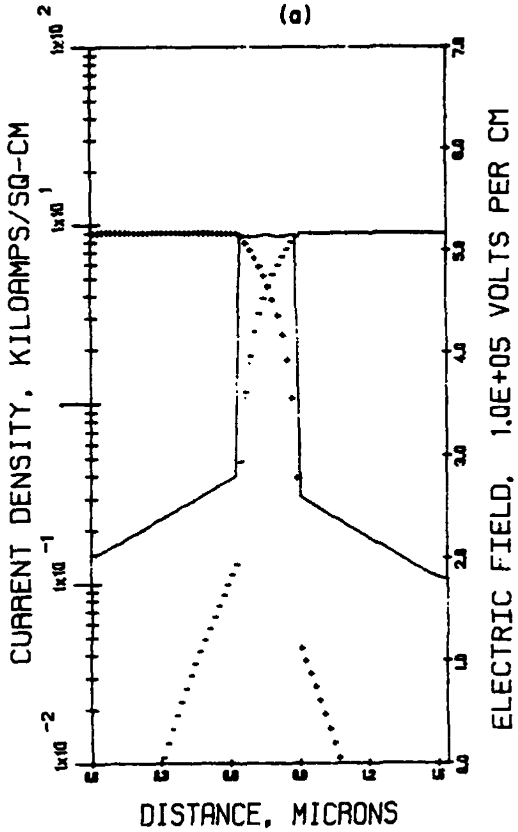

(b)

Figure 3. (a) GaAs Double-Read Profile for 30-GHz Operation and (b) Dc Solution at T = 500°K and J_{dc} = 9 kA/cm^2. (X_A = 0.26 μm, J_{dc} = 9 kA/cm^2, E(LHS) = 2.03 x 10^5 V/cm, E_{to}(LHS) = 2.8 x 10^5 V/cm, E_{max} = 5.16 x 10^5 V/cm, E_{to}(RHS) = 2.606 x 10^5 V/cm, E(RHS) = 1.81 x 10^5 V/cm, Integrated Doping Spike Q_p = 1.632 x 10^{12} cm^{-2} and Q_n = 1.78 x 10^{12} cm^{-2})

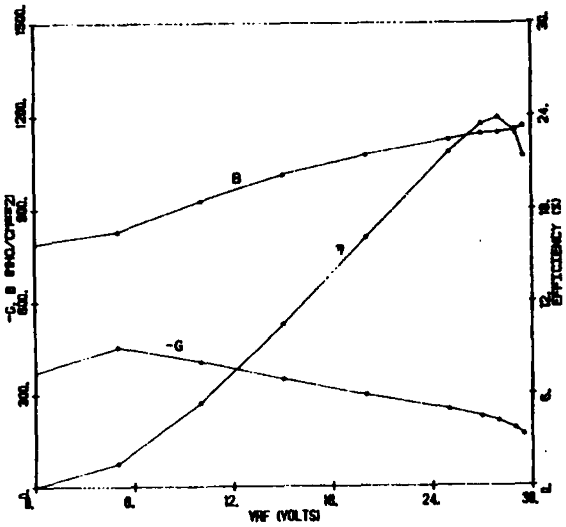

(a)

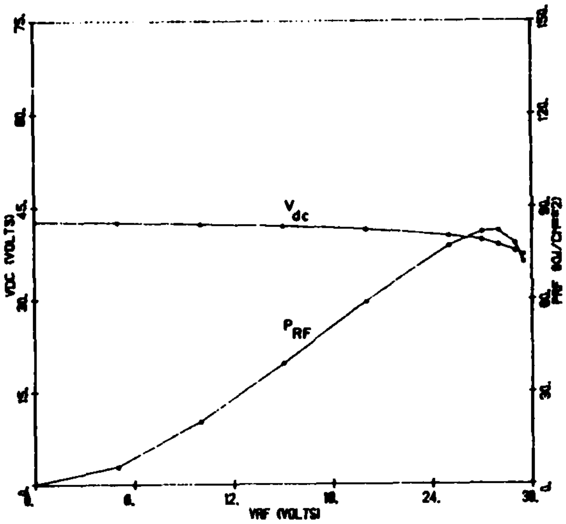

(b)

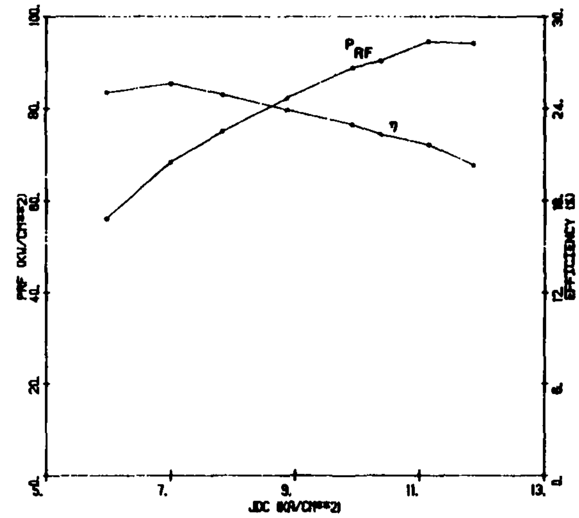

(c)

Figure 4. Large-Signal Results for the Profile of Figure 3a at $T = 500°K$, $f = 30$ GHz and (a and b) $J_{dc} = 9$ kA/cm^2, (c) $V_{RF} = 28$ V.

TABLE 6

LARGE-SIGNAL RESULTS FOR THE GaAs DOUBLE READ PROFILE IN FIGURE 3a AND

POWER LEVELS OBTAINED BY MATCHING TO 1-Ω RESISTANCE (f = 30 GHz, V_{RF} = 28 V)

J_{dc} (kA/cm²)	$-G_D$ (mho/cm²)	B_D (mho/cm²)	A x 10^{-4} (cm²)	I_{dc} (A)	V_{dc} (V)	η (Percent)	P_{dc} (W)	P_{RF} (W)	P_{diss} (W)	θ_R (°C/W)	D (mils)
4	77	1314	0.44	0.176	36	21.3	6.3	1.35	5	45	2.9
4.5	95	1292	0.57	0.26	36.7	22.6	9.5	2.15	8.4	27	3.3
5	110	1275	0.67	0.335	37	23.7	12.4	2.94	9.46	24	3.8
6	143	1235	0.93	0.56	37.5	25	21	5.25	15.75	14.3	4.2
7	174	1200	1.2	0.84	38	25.6	32	8.2	23.8	9.5	4.8
7.8	196	1176	1.35	1.05	38.4	25	40	10	30	7.5	5.1
9	210	1146	1.65	1.45	38.8	24	56	13.5	42.5	5.3	5.6
10	227	1110	1.77	1.77	39	23	69	16	53	4.2	5.8
11	241	1070	2.0	2.2	39	21.6	86	18.5	67.5	3.33	6.2
12	240	1047	2.0	2.4	39	20	94	18.7	75.3	3	6.2

$$\theta(DM) = \frac{21.42}{d_m} + \frac{62}{d_m^2} , \tag{17}$$

$$\theta(CR) = \frac{35.35}{d_m} + \frac{62}{d_m^2} \tag{18}$$

and

$$\theta(DR) = \frac{11.78}{d_m} + \frac{62}{d_m^2} . \tag{19}$$

Again restricting the maximum diode temperature rise to 225°C and evaluating Equations 13 through 15 gives the data presented in Table 7. As before, for low values of J_{dc} the power generation capability is electronically limited, and for higher values of J_{dc} it is thermally limited. For every geometry and heat-sink material, the double Read structure can generate more CW power than the hybrid at 30 GHz.

In addition to these GaAs structures, Si and InP hybrid profiles were simulated at 30 GHz. Figure 5a shows the Si hybrid profile used, and Figure 5b shows the dc solution at $T = 500°K$ and $J_{dc} = 3.5\ kA/cm^2$. Large-signal results vs. V_{RF} at $J_{dc} \cong 3.5\ kA/cm^2$ are plotted in Figure 6a and b. Figure 6c shows large-signal results vs. J_{dc} at $V_{RF} = 36$ V; both the maximum efficiency and power points appear in this curve. The maximum efficiency obtained was $\eta = 22.73$ percent at $J_{dc} = 2.5\ kA/cm^2$, and the maximum electronic power density was $79.3\ kW/cm^2$ at $J_{dc} = 7.9\ kA/cm^2$. It should be noted that Si hybrid operates at considerably lower current densities than the GaAs diodes, as was predicted from Equation 5 at the beginning of this section.

Large-signal results vs. J_{dc} at $V_{RF} = 36$ V are given in Table 8. To determine the thermal-resistance expressions, it is noted from Figure 5a that the length of the p-side is 1.68 μm;

TABLE 7

CW RESULTS FOR THE PROFILE IN FIGURE 3a AT 30 GHz TAKING INTO ACCOUNT

THE THERMAL-RESISTANCE EXPRESSIONS

D(CM) (mils)	θ(CM) (°C/W)	P_{RF}(CM) (W)	D(DM) (mils)	θ(DM) (°C/W)	P_{RF}(DM) (W)	D(CR) (mils)	θ(CR) (°C/W)	P_{RF}(CR) (W)	D(DR) (mils)	θ(DR) (°C/w)	P_{RF}(DR) (W)	J_{dc} (kA/cm^2)
2.9	29.5	1.35	2.9	14.8	1.35	2.9	19.6	1.35	2.9	11.4	1.35	4
3.3	25.2	2.15	3.3	11.8	2.15	3.3	16.4	2.15	3.3	9.26	2.15	4.5
3.8	21.2	2.94	3.8	9.93	2.94	3.8	13.6	2.94	3.8	7.39	2.94	5
3.1	26.9	2.79	4.2	8.6	5.25	4.2	11.9	5.25	4.2	6.32	5.25	6
2.5	35.2	2.2	4.8	7.15	8.2	4.59	10.6	7.28	4.8	5.14	8.2	7
2.1	44.4	1.69	5.1	6.58	10	3.84	13.4	5.59	5.1	4.69	10	7.8
1.6	62.3	1.14	4.9	6.92	10.3	2.98	18.8	3.77	5.6	4.08	13.5	9
1.3	82.8	0.811	4.0	9.2	7.3	2.43	25.1	2.68	5.8	3.87	16	10
1.1	111	0.557	3.3	12.4	5.0	1.98	33.6	1.84	5.94	3.74	16.6	11
0.88	153	0.368	2.6	17	3.3	1.6	46.3	1.22	4.8	5.14	10.9	12

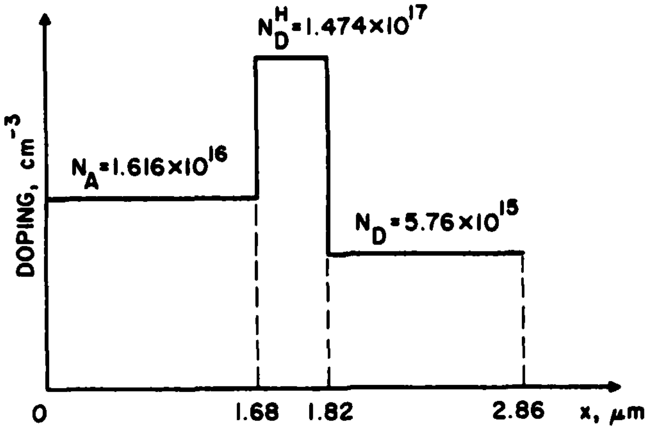

(a)

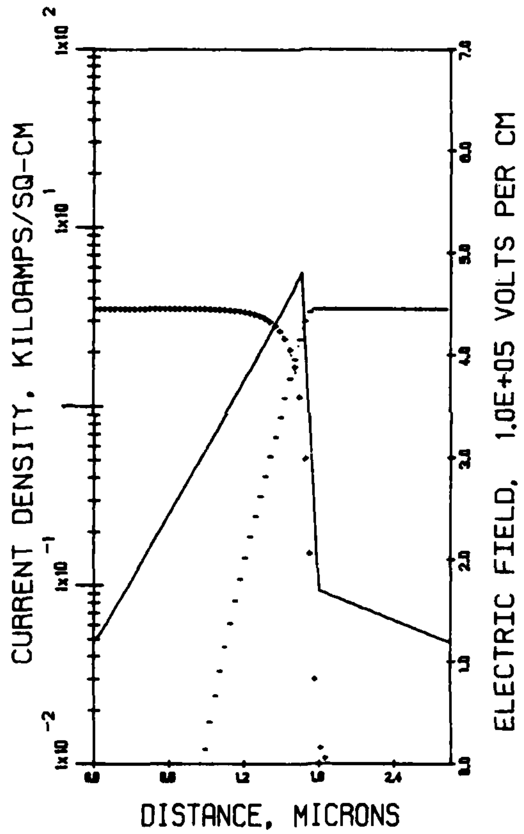

(b)

Figure 5. (a) Si Hybrid Profile for 30-GHz Operation and (b) Dc Solution at T = 500°K and J_{dc} = 3.5 kA/cm^2. (X_A = 0.5 μm, J_{dc} = 3.5 kA/cm^2, E(LHS) = 1.206 x 10^5 V/cm, E_{max} = 4.819 x 10^5 V/cm, E_{to} = 1.7 x 10^5 V/cm and E(RHS) = 1.203 x 10^5 V/cm)

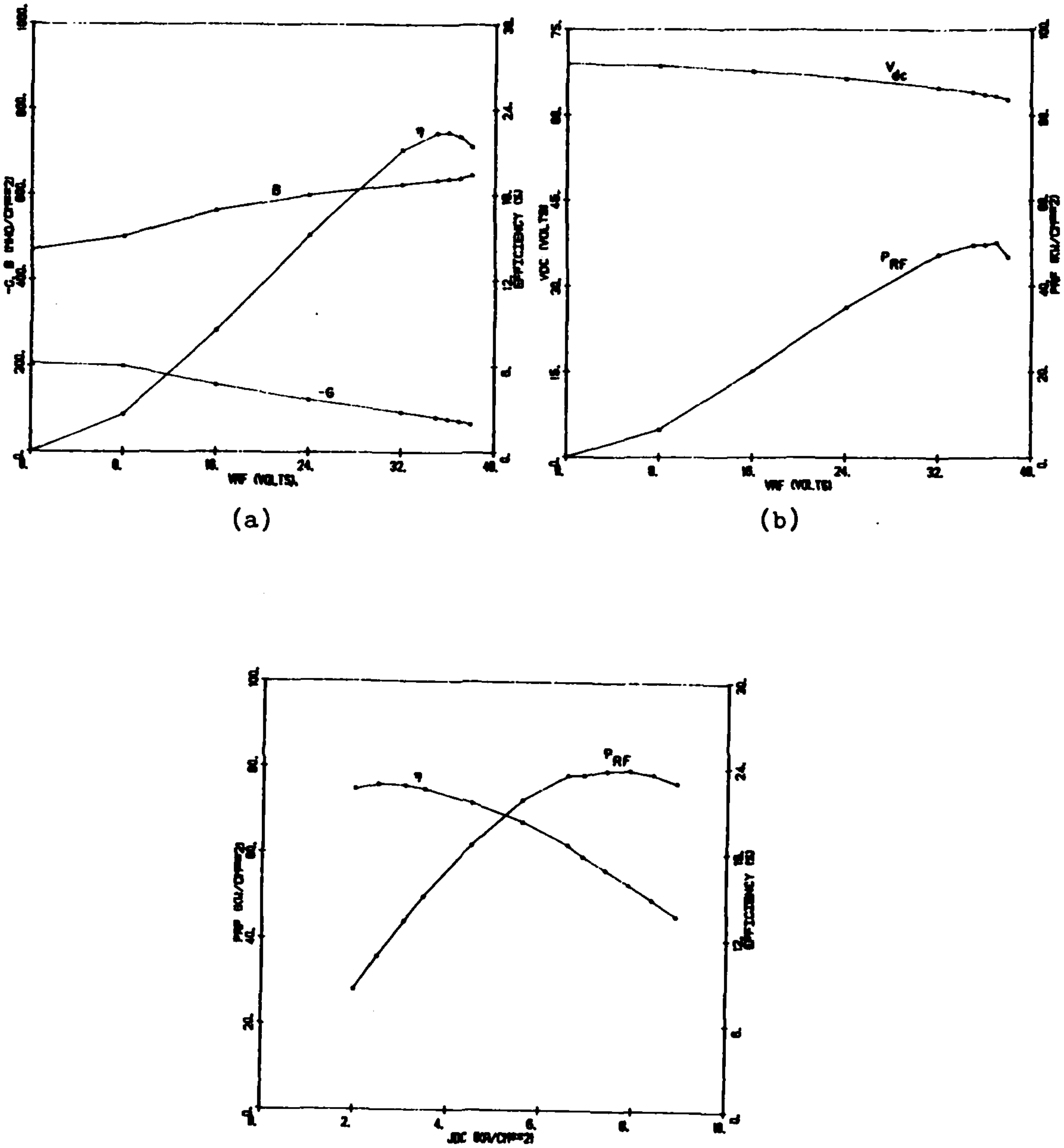

(a) (b)

(c)

Figure 6. Large-Signal Results for the Si Profile of Figure 5a at $f = 30$ GHz, $T = 500°K$ and (a and b) $J_{dc} \simeq 3.5\ kA/cm^2$, (c) $V_{RF} = 36$ V.

TABLE 8

LARGE-SIGNAL RESULTS FOR THE Si HYBRID PROFILE IN FIGURE 5a AND POWER LEVELS

OBTAINED BY MATCHING TO 1-Ω RESISTANCE (f = 30 GHz, V_{RF} = 36 V)

J_{dc} (kA/cm^2)	$-G_D$ (mho/cm^2)	B_D (mho/cm^2)	A x 10^{-4} (cm^2)	I_{dc} (A)	V_{dc} (V)	η (Percent)	P_{dc} (W)	P_{RF} (W)	P_{diss} (W)	θ_R (°C/W)	D (mils)
2	43.2	670	0.96	0.192	63	22.4	12.1	2.71	9.39	24	4.35
2.5	55	660	1.25	0.312	63.3	22.7	19.7	4.47	15.2	14.8	4.97
3	67.7	648	1.59	0.477	63.5	22.6	30.3	6.85	23.4	9.61	5.6
3.48	76.6	638	1.86	0.647	63.7	22.4	41.2	9.23	32.0	7	6.06
4.5	95.3	614	2.47	1.11	64	21.5	71.0	15.3	55.7	4	6.98
5.6	111	585	3.13	1.75	64.2	20.2	112	22.6	89.4	2.5	7.86
6.6	120.4	557	3.71	2.45	64	18.6	157	29.2	128	1.76	8.56
6.9	120.7	547	3.85	2.66	63.8	17.8	170	30.3	140	1.61	8.72
7.4	122.3	531	4.12	3.05	63.6	16.8	194	32.6	161	1.4	9.02
7.9	122.4	515	4.37	3.45	63.4	15.8	219	34.6	184	1.22	9.29
8.4	121	498	4.61	3.87	63.2	14.8	244	36.1	208	1.08	9.54
8.9	118	481	4.81	4.28	63	13.6	270	36.7	233	0.96	9.74

therefore $\ell_2 = 1.68 \times 10^{-4}$ cm is used in Equation 1. As before, it is assumed that $T_2 = 500°K$, $\ell_1 = 0.5 \times 10^{-4}$ cm and $T_1 = 450°K$. As was noted in Section 3, the thermal conductivity of Si is approximately 3 times that of GaAs; therefore the final two terms in Equation 1 are reduced by the factor 1/3. Then the expressions for thermal resistance of the Si hybrid are

$$\theta(CM) = \frac{64.27}{d_m} + \frac{30.78}{d_m^2} , \quad (20)$$

$$\theta(DM) = \frac{21.42}{d_m} + \frac{30.78}{d_m^2} , \quad (21)$$

$$\theta(CR) = \frac{35.35}{d_m} + \frac{30.78}{d_m^2} \quad (22)$$

and

$$\theta(DR) = \frac{11.78}{d_m} + \frac{30.78}{d_m^2} . \quad (23)$$

Evaluating Equations 13 through 15 along with the thermal-resistance expressions in Equations 20 through 23 gives the expected CW power levels in Table 9. Because of the lower thermal resistance for Si, the CW powers in Table 9 are greater than for either the GaAs hybrid structure or the GaAs double Read structure. The electronic powers in Table 8 are lower than for the GaAs hybrid in Table 4, indicating that the GaAs hybrid is capable of generating more power under pulsed conditions than the Si hybrid.

The final structure simulated at 30 GHz is the InP hybrid profile shown in Figure 7a. The dc solution for this profile at $T = 500°K$ and $J_{dc} = 7$ kA/cm^2 is shown in Figure 7b.

Large-signal results for the InP hybrid vs. V_{RF} are shown in Figure 8a and b, and results vs. J_{dc} at $V_{RF} = 42$ V are plotted

TABLE 9

CW RESULTS FOR THE PROFILE IN FIGURE 5a AT 30 GHz TAKING INTO ACCOUNT

THE THERMAL-RESISTANCE EXPRESSIONS

D(CM) (mils)	θ(CM) (°C/W)	P_{RF}(CM) (W)	D(DM) (mils)	θ(DM) (°C/W)	P_{RF}(DM) (W)	D(CR) (mils)	θ(CR) (°C/W)	P_{RF}(CR) (W)	D(DR) (mils)	θ(DR) (°C/W)	P_{RF}(DR) (W)	J_{dc} (kA/cm^2)
4.35	16.4	2.71	4.35	6.55	2.71	4.35	9.75	2.71	4.35	4.33	2.71	2
4.97	14.2	4.47	4.97	5.56	4.47	4.97	8.36	4.47	4.97	3.62	4.47	2.5
4.21	17	3.86	5.6	4.81	6.85	5.6	7.29	6.85	5.6	3.08	6.85	3
3.54	20.6	3.15	6.06	4.37	9.23	6.06	6.67	9.23	6.06	2.78	9.23	3.48
2.58	29.6	2.08	6.98	3.7	15.3	4.68	8.94	6.89	6.98	2.32	15.3	4.5
1.93	41.6	1.37	5.79	4.62	12.3	3.51	12.6	4.53	7.86	2.0	22.6	5.6
1.53	55.1	0.932	4.59	6.12	8.39	2.78	16.7	3.08	8.56	1.8	29.2	6.6
1.43	60	0.812	4.29	6.66	7.31	2.6	18.1	2.68	7.8	2.0	24.2	6.9
1.28	68.6	0.662	3.86	7.62	5.96	2.34	20.8	2.19	7.0	2.31	19.7	7.4
1.16	78.3	0.539	3.48	8.7	4.85	2.11	23.7	1.78	6.32	2.63	16	7.9
1.05	89.3	0.438	3.14	9.92	3.94	1.91	27.0	1.45	5.72	3.0	13	8.4
0.947	102	0.347	2.84	11.4	3.12	1.72	30.9	1.14	5.17	3.43	10.3	8.9

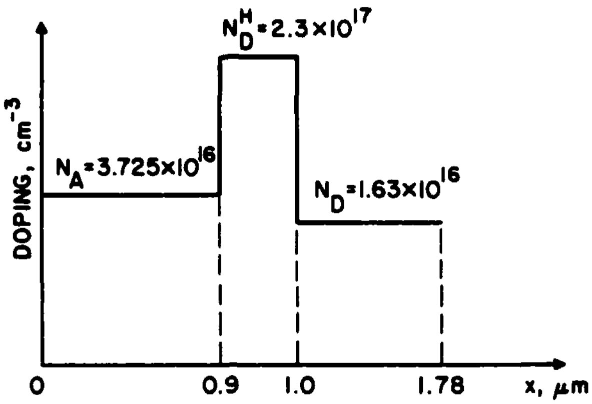

(a)

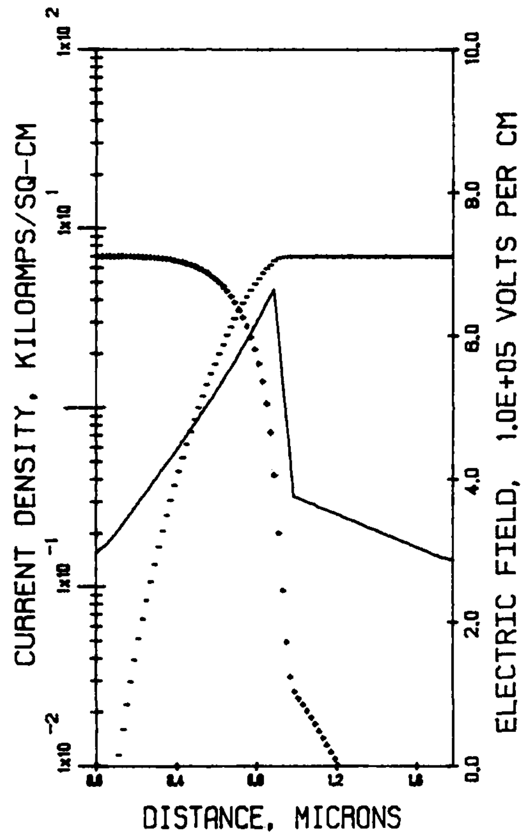

(b)

Figure 7. (a) InP Hybrid Profile for 30-GHz Operation and (b) Dc Solution at T = 500°K and J_{dc} = 7 kA/cm^2. (X_A = 0.54 μm, J_{dc} = 7 kA/cm^2, E(LHS) = 3.0 x 10^5 V/cm, E_{max} = 6.658 x 10^5 V/cm, E_{to} = 3.772 x 10^5 V/cm and E(RHS) = 2.89 x 10^5 V/cm)

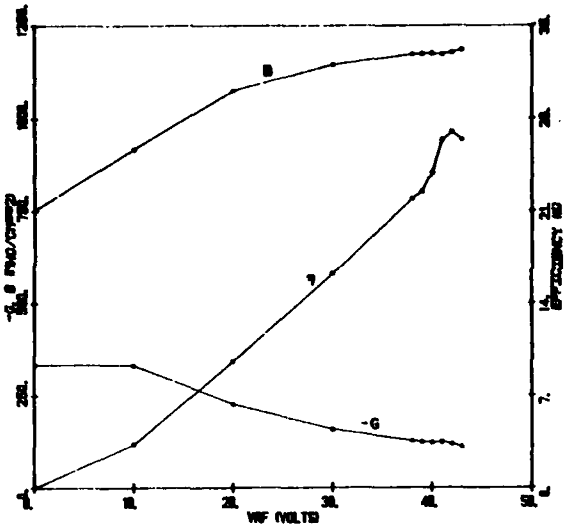

(a)

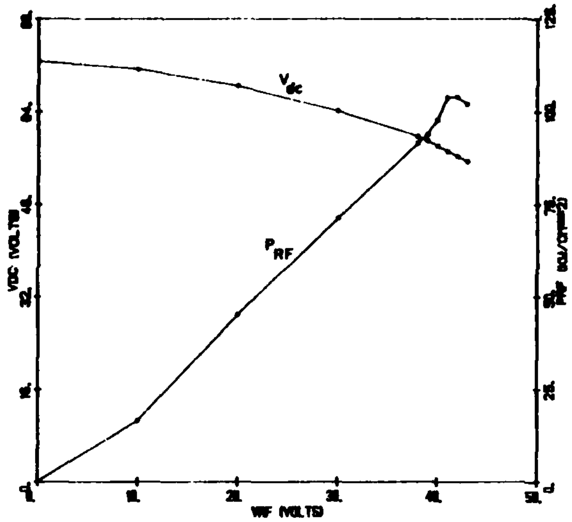

(b)

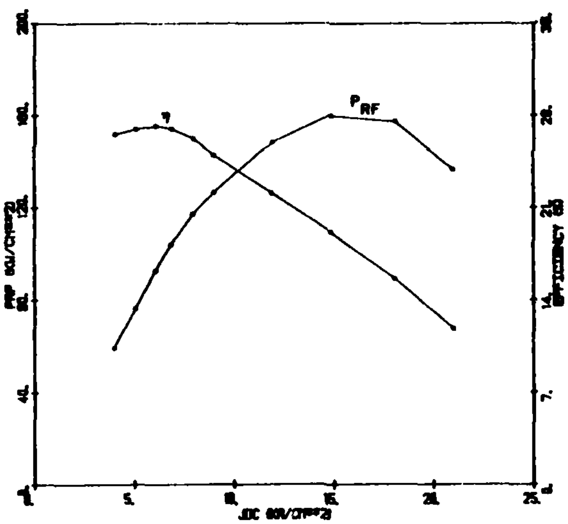

(c)

Figure 8. Large-Signal Results for the Profile of Figure 7a at $T = 500^{o}K$, $f = 30$ GHz and (a and b) $J_{dc} \approx 7\ kA/cm^2$, (c) $V_{RF} = 42$ V.

in Figure 8c. Table 10 presents large-signal results vs. J_{dc} and electronic powers obtained by matching the diode to 1-Ω resistance. The maximum efficiency obtained was 27.2 percent at J_{dc} = 6.06 kA/cm² and V_{RF} = 42 V, which is larger than the efficiencies obtained from any of the other structures simulated at 30 GHz. From Figure 7a, the active (p) layer width for thermal-resistance calculations is $\ell_2 = 0.9 \times 10^{-4}$ cm; also it is assumed as before that $\ell_1 = 0.5 \times 10^{-4}$ cm, T_1 = 450°K and T_2 = 500°K. As noted in Section 3, the thermal conductivity of InP is approximately 1.25 times that of GaAs; therefore the last two terms of Equation 1 are reduced by a factor of 0.8. Then the thermal resistances for the InP hybrid of Figure 7a are

$$\theta(CM) = \frac{64.27}{d_m} + \frac{53.28}{d_m^2} , \tag{24}$$

$$\theta(DM) = \frac{21.42}{d_m} + \frac{53.28}{d_m^2} , \tag{25}$$

$$\theta(CR) = \frac{35.35}{d_m} + \frac{53.28}{d_m^2} \tag{26}$$

and

$$\theta(DR) = \frac{11.78}{d_m} + \frac{53.28}{d_m^2} . \tag{27}$$

Evaluating Equations 13 through 15 together with the expressions in Equations 24 through 27 yields the CW powers in Table 11.

Although the maximum efficiency for the InP hybrid is large, the electronic power generated at the maximum efficiency point is less than for the GaAs structures. This is because the GaAs diodes, especially the hybrids, operate at higher current

TABLE 10

LARGE-SIGNAL RESULTS FOR THE InP HYBRID PROFILE IN FIGURE 7a AND

POWER LEVELS OBTAINED BY MATCHING TO 1-Ω RESISTANCE (f = 30 GHz, V_{RF} = 42 V)

J_{dc} (kA/cm^2)	$-G_D$ (mho/cm^2)	B_D (mho/cm^2)	A $\times 10^{-4}$ (cm^2)	I_{dc} (A)	V_{dc} (V)	η (Percent)	P_{dc} (W)	P_{RF} (W)	P_{diss} (W)	θ_R (°C/W)	D (mils)
4	67	1251	0.427	0.171	55.7	26.6	9.52	2.53	6.99	32.2	2.9
5.06	86.6	1222	0.577	0.292	56	27	16.4	4.43	12	18.8	3.37
6.06	105	1196	0.728	0.441	56.2	27.2	24.8	6.74	18.1	12.4	3.79
6.84	118	1178	0.842	0.576	56.3	27	32.4	8.75	23.6	9.53	4.08
7.93	133	1153	0.987	0.783	56.5	26.2	44.2	11.6	32.6	6.9	4.41
8.98	143	1132	1.10	0.988	56.4	25	55.7	13.9	41.8	5.38	4.66
11.9	168	1070	1.43	1.70	56.5	22.1	96	21.2	74.8	3	5.31
14.8	181	1004	1.74	2.58	56.3	19.1	145	27.7	117	1.92	5.86
18.1	178	935	1.96	3.55	55.8	15.6	198	30.9	167	1.35	6.22
21.0	155	874	1.97	4.14	55.1	11.8	228	26.9	201	1.12	6.24

TABLE 11

CW RESULTS FOR THE PROFILE IN FIGURE 7a AT 30 GHz

TAKING INTO ACCOUNT THE THERMAL-RESISTANCE EXPRESSIONS

D(CM) (mils)	θ(CM) (°C/W)	P_{RF}(CM) (W)	D(DM) (mils)	θ(DM) (°C/W)	P_{RF}(DM) (W)	D(CR) (mils)	θ(CR) (°C/W)	P_{RF}(CR) (W)	D(DR) (mils)	θ(DR) (°C/W)	P_{RF}(DR) (W)	J_{dc} (kA/cm^2)
2.9	28.5	2.53	2.9	13.7	2.53	2.9	18.5	2.53	2.9	10.4	2.53	4
2.51	34	2.44	3.37	11	4.43	3.37	15.2	4.43	3.37	8.19	4.43	5.06
1.96	46.7	1.8	3.79	9.36	6.74	3.56	14.1	5.94	3.79	6.82	6.74	6.06
1.63	59.6	1.4	4.08	8.45	8.75	2.96	18	4.62	4.08	6.09	8.75	6.84
1.26	84.5	0.945	3.78	9.39	8.5	2.29	25.6	3.12	4.41	5.41	11.6	7.93
0.99	119	0.628	2.97	13.3	5.66	1.8	36.1	2.08	4.66	4.98	13.9	8.98
0.49	353	0.181	1.47	39.2	1.63	0.891	107	0.60	2.67	11.9	5.38	11.9
0.196	1719	0.031	0.587	191	0.278	0.356	520	0.102	1.07	57.8	0.92	14.8
--	--	--	--	--	--	--	--	--	--	--	--	18.1
--	--	--	--	--	--	--	--	--	--	--	--	21

densities than the InP hybrids. This power is greater than for the Si hybrid, since the Si hybrid operates at a lower current density than the InP hybrid at the maximum efficiency point. At the maximum electronic power points, both the Si hybrid and the GaAs hybrid generate more power than the InP hybrid.

In summary, the simulations at 30 GHz show that for CW operation, the Si hybrid is capable of generating the most RF power due to its high thermal conductivity. Another advantage of Si is that diodes of larger area can be matched to 1-Ω circuit resistance since the diode susceptance is more nearly equal in magnitude to the diode conductance (see Equation 8).

For pulsed applications where excessive heating is not a problem, the uniformly doped GaAs hybrid structure was found to generate the most RF power.

SECTION 6.

RESULTS AT 40 GHz

The use of Equations 5 for GaAs with $\ell_a = 0.2$ μm and $\ell_d = 0.625$ μm predicts from the simplified analysis that maximum small-signal negative conductance for a Read structure at 40 GHz is obtained for $J_{dc} = 15.4$ kA/cm^2. Also, Equation 7 is evaluated to estimate the doping needed to obtain the precollection mode in GaAs at 40 GHz. Of course, the validity of Equation 7 at 40 GHz is suspect since it is questionable whether the standard precollection mode can be obtained at this frequency. This can only be determined by carrying out energy and momentum conserving IMPATT simulations for GaAs, which will be done in the course of the program. It is found that V_{dc} for the GaAs double-drift structures for 40-GHz operation is typically approximately 36 V. When $V_{RF} = 0.65\ V_{dc}$ and w = 1.2 μm in Equation 7, the value $N_D = 2.39 \times 10^{16}$ cm^{-3} is obtained.

Figure 9a shows a GaAs hybrid doping profile simulated at 40 GHz; the dc solution at T = 500°K and $J_{dc} = 10$ kA/cm^2 is shown in Figure 9b. Figure 10a and b shows plots of the large-signal results vs. V_{RF} at T = 500°K, f = 40 GHz, $J_{dc} \approx 11$ kA/cm^2, and Figure 10c shows large-signal results vs. J_{dc} at T = 500°K and $V_{RF} = 26$ V. The best efficiency obtained for the GaAs hybrid was $\eta = 20.5$ percent at $J_{dc} = 11$ kA/cm^2 and $V_{RF} = 26$ V, and the maximum electronic RF power density was $P_{RF} = 131.3$ kW/cm^2 at $J_{dc} = 26$ kA/cm^2 and $V_{RF} = 26$ V. Table 12 shows the large-signal results vs. J_{dc} at f = 40 GHz and $V_{RF} = 26$ V. When it is noted

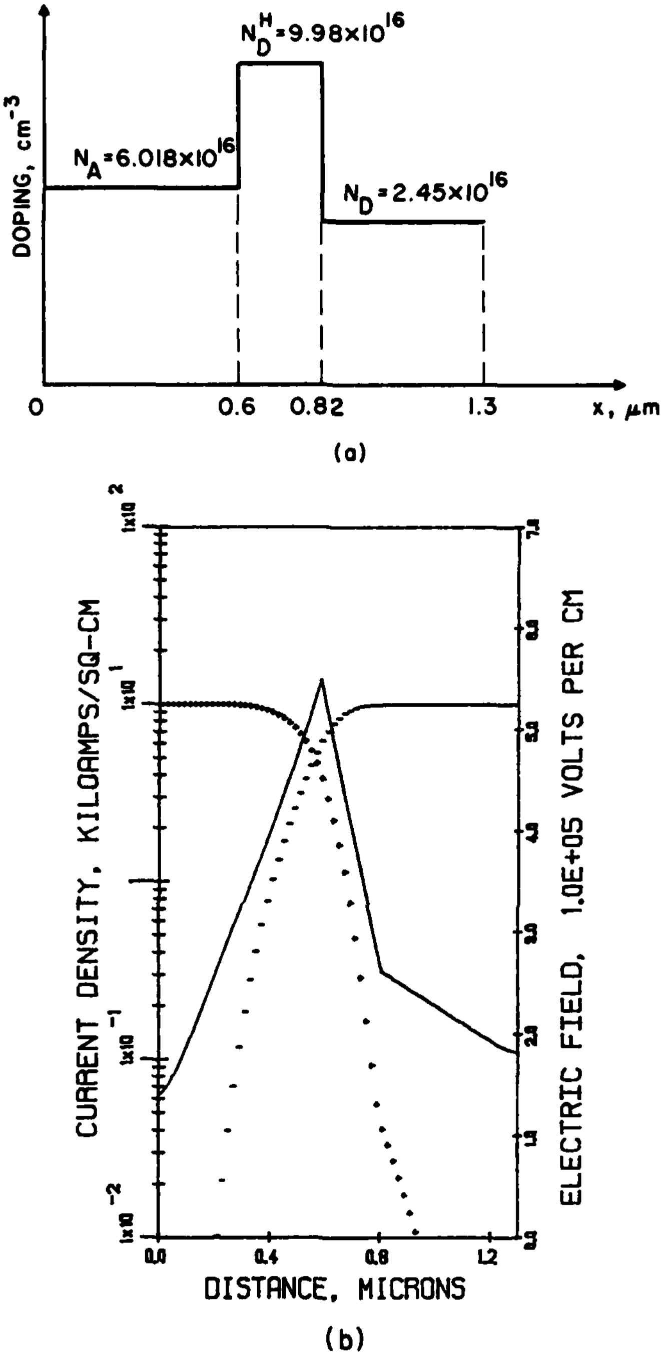

Figure 9. (a) GaAs Hybrid Profile for 40-GHz Operation and (b) Dc Solution at T = 500°K and J_{dc} = 10 kA/cm^2. (X_A = 0.36 μm, J_{dc} = 10 kA/cm^2, E(LHS) = 1.41 x 10^5 V/cm, E_{max} = 5.495 x 10^5 V/cm, E_{to} = 2.616 x 10^5 V/cm and E(RHS) = 1.83 x 10^5 V/cm)

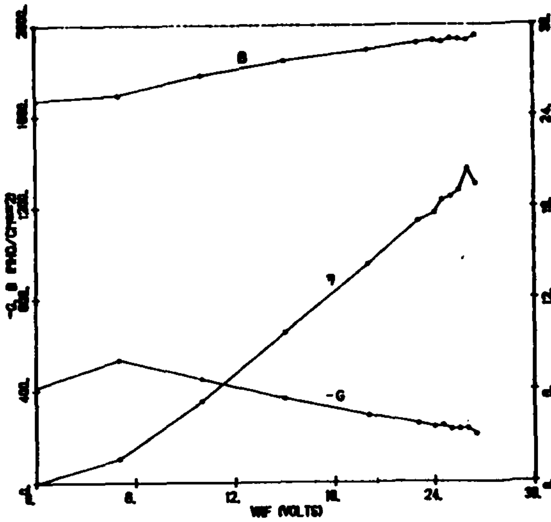

(a)

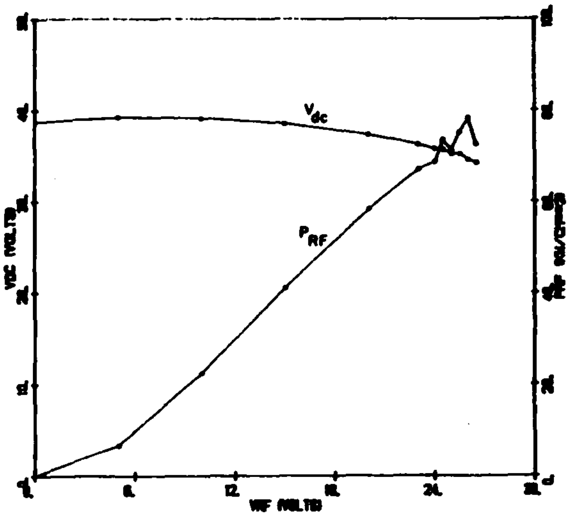

(b)

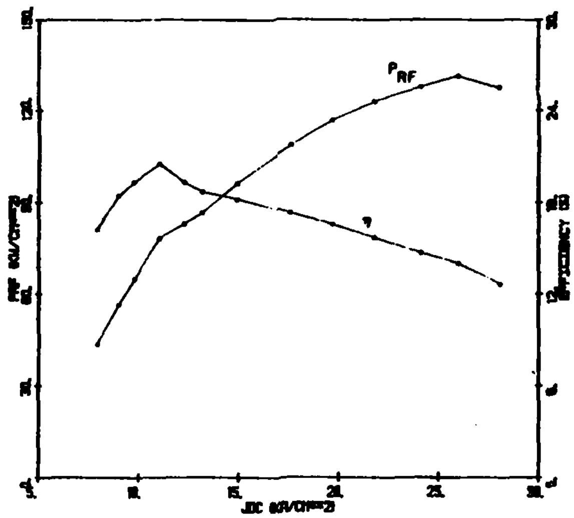

(c)

Figure 10. Large-Signal Results for the Profile of Figure 9a at $T = 500°K$, $f = 40$ GHz and (a and b) $J_{dc} = 11\ kA/cm^2$, (c) $V_{RF} = 26$ V.

TABLE 12

LARGE-SIGNAL RESULTS FOR THE GaAs HYBRID PROFILE OF FIGURE 9a AND POWER LEVELS

OBTAINED BY MATCHING TO 1-Ω RESISTANCE (f = 40 GHz, V_{RF} = 26 V)

J_{dc} (kA/cm^2)	$-G_D$ (mho/cm^2)	B_D (mho/cm^2)	A x 10^{-4} (cm^2)	I_{dc} (A)	V_{dc} (V)	η (Percent)	P_{dc} (W)	P_{RF} (W)	P_{diss} (W)	θ_R (°C/W)	D (mils)
7.93	129	2057	0.304	0.241	33.8	16.2	8.14	1.32	6.82	33	2.45
9	167	2007	0.412	0.371	34.1	18.4	12.6	2.32	10.3	21.8	2.85
9.78	192	1978	0.486	0.475	34.3	19.3	16.3	3.14	13.2	17	3.1
11	232	1932	0.613	0.674	34.6	20.5	23.3	4.78	18.5	12.2	3.48
12.3	245	1911	0.66	0.812	35	19.3	28.4	5.48	22.9	9.82	3.61
13.2	256	1891	0.703	0.928	35.2	18.7	32.7	6.11	26.6	8.46	3.72
14.9	285	1845	0.818	1.22	35.4	18.2	43.2	7.86	35.3	6.37	4.02
17.6	321	1772	0.99	1.74	35.7	17.3	62.1	10.7	51.4	4.38	4.42
19.6	346	1715	1.13	2.21	35.9	16.5	79.3	13.1	66.2	3.4	4.72
21.8	364	1658	1.26	2.75	36	15.7	99	15.5	83.5	3.69	4.99
24.1	378	1598	1.4	3.37	36.2	14.6	122	17.8	104	2.16	5.26
26	388	1536	1.54	4.0	36.2	14	145	20.3	125	1.8	5.51
28	378	1490	1.6	4.48	36	12.6	161	20.3	141	1.6	5.62

from Figure 9a that the p-region width is $\ell_2 = 0.6 \times 10^{-4}$ cm and $\ell_1 = 0.5 \times 10^{-4}$ cm, as before, for the buffer-layer thickness, the thermal-resistance expressions for this structure become

$$\theta(CM) = \frac{64.27}{d_m} + \frac{56.74}{d_m^2} , \quad (28)$$

$$\theta(DM) = \frac{21.42}{d_m} + \frac{56.74}{d_m^2} , \quad (29)$$

$$\theta(CR) = \frac{35.35}{d_m} + \frac{56.74}{d_m^2} \quad (30)$$

and

$$\theta(DR) = \frac{11.78}{d_m} + \frac{56.74}{d_m^2} . \quad (31)$$

Evaluating Equations 13 through 15 together with the expressions in Equations 28 through 31 yields the CW power data given in Table 13. It should be noted that for the CM case (copper heat sink, single mesa), the CW power levels are all thermally limited. For the other cases, as before, for low values of J_{dc} the power is electronically limited, and for higher values of J_{dc} the power is thermally limited.

Figure 11a shows a double Read GaAs profile simulated at 40 GHz. The dc solution for this profile is shown in Figure 11b. Large-signal results vs. V_{RF} at T = 500°K, f = 40 GHz and $J_{dc} \approx 9$ kA/cm² are plotted in Figure 12a and b, and results vs. J_{dc} at V_{RF} = 23 V are plotted in Figure 12c. The maximum efficiency was η = 20.83 percent at J_{dc} = 6.02 kA/cm² and V_{RF} = 23 V, and the maximum electronic RF power density was P_{RF} = 86.16 kW/cm² at J_{dc} = 16 kA/cm² and V_{RF} = 23 V. Table 14 lists the large-signal results vs. J_{dc} along with the electronic power generated when the device exhibits 1-Ω negative resistance. In Figure 11a it is seen that

TABLE 13

CW RESULTS FOR THE PROFILE IN FIGURE 9a AT 40 GHz TAKING INTO

ACCOUNT THE THERMAL-RESISTANCE EXPRESSIONS

D(CM) (mils)	θ(CM) (°C/W)	P_{RF}(CM) (W)	D(DM) (mils)	θ(DM) (°C/W)	P_{RF}(DM) (W)	D(CR) (mils)	θ(CR) (°C/W)	P_{RF}(CR) (W)	D(DR) (mils)	θ(DR) (°C/W)	P_{RF}(DR) (W)	J_{dc} (kA/cm^2)
2.19	41.1	1.06	2.45	18.2	1.32	2.45	23.9	1.32	2.45	14.3	1.32	7.93
1.88	50.4	1.01	2.85	14.5	2.32	2.85	19.4	2.32	2.85	11.1	2.32	9
1.67	58.9	0.914	3.1	12.8	3.14	3.03	17.8	3.02	3.1	9.7	3.14	9.78
1.4	74.8	0.775	3.48	10.8	4.78	2.55	22.6	2.56	3.48	8.07	4.78	11
1.1	104	0.515	3.32	11.6	4.63	2.01	31.6	1.7	3.61	7.62	5.48	12.3
0.946	131	0.394	2.84	14.6	3.55	1.72	39.7	1.3	3.72	7.27	6.11	13.2
0.718	199	0.251	2.16	22.2	2.26	1.31	60.3	0.83	3.92	6.7	7.47	14.9
0.447	428	0.11	1.34	47.6	0.989	0.812	130	0.363	2.44	14.4	3.27	17.6
0.293	880	0.05	0.879	97.8	0.454	0.533	266	0.167	1.6	29.6	1.5	19.6
0.161	2580	0.016	0.484	286	0.146	0.293	779	0.054	0.88	86.6	0.484	21.8
0.044	3020	0.0013	0.133	3360	0.011	0.081	9136	0.0042	0.242	1015	0.038	24.1
--	--	--	--	--		--	--	--	--	--	--	26
--	--	--	--	--		--	--	--	--	--	--	28

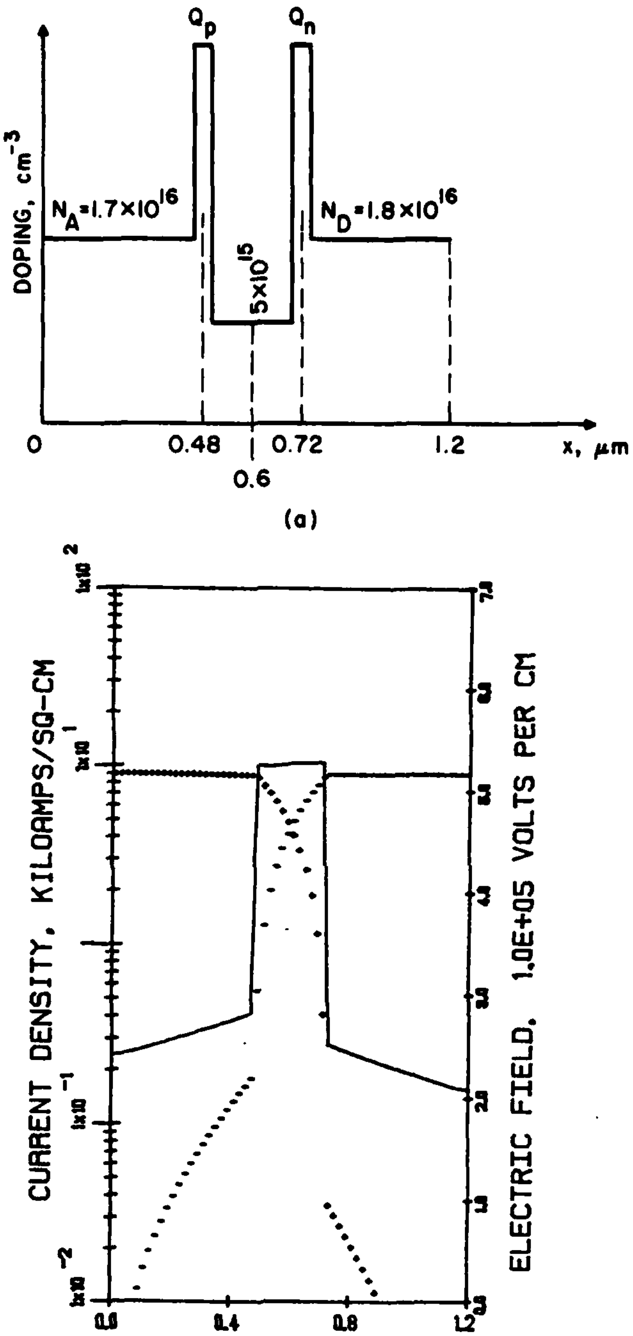

Figure 11. (a) GaAs Double-Read Profile for 40-GHz Operation and (b) Dc Solution at T = 500°K and J_{dc} = 9 kA/cm^2. (X_A = 0.24 μm, J_{dc} = 9 kA/cm^2, E_{max} = 5.283 x 10^5 V/cm, Integrated Doping Spike Q_p = 1.7 x 10^{12} cm^{-2} and Q_n = 1.93 x 10^{12} cm^{-2})

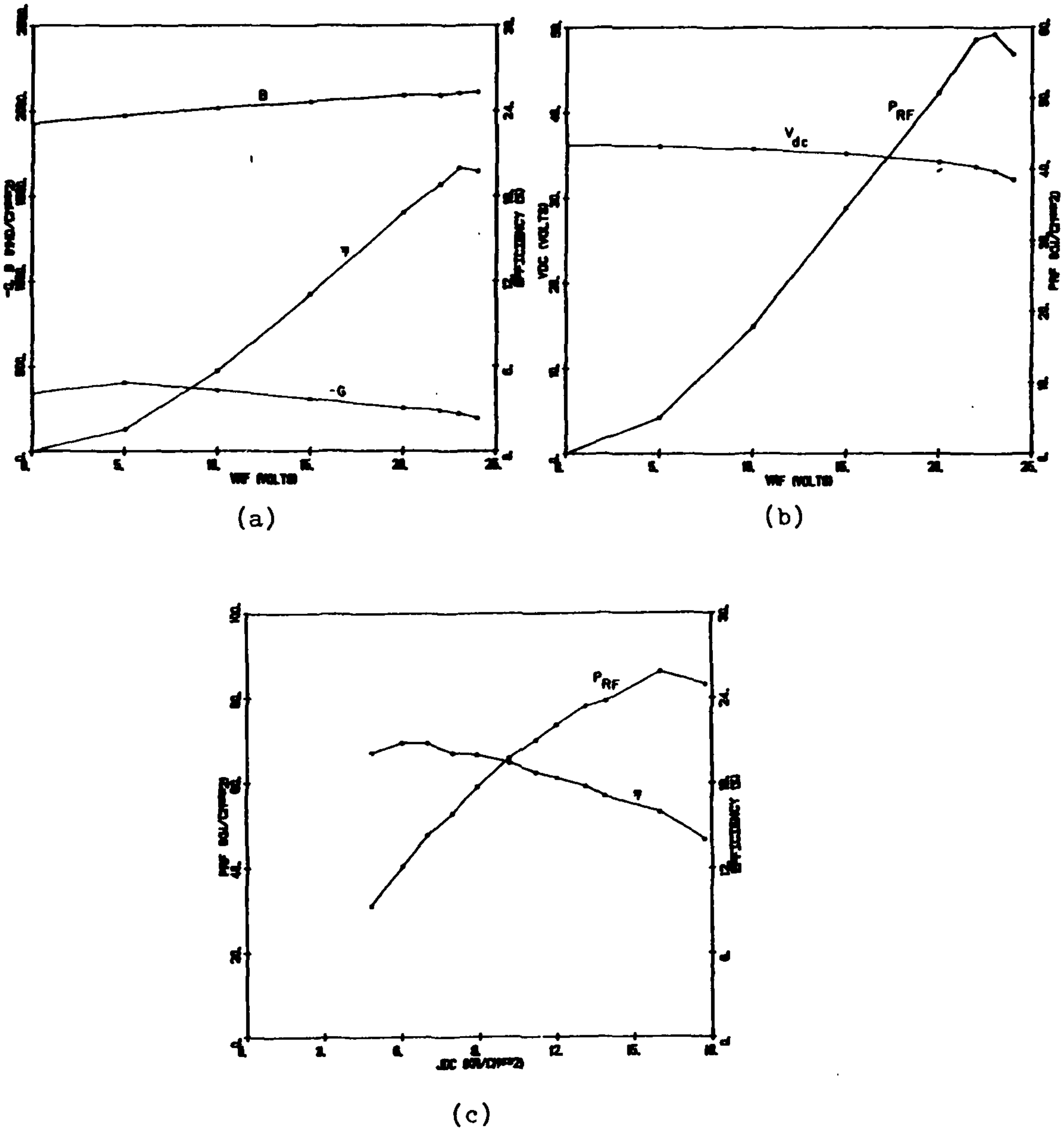

Figure 12. Large-Signal Results for the Profile of Figure 11a at $T = 500°K$, $f = 40$ GHz and (a and b) $J_{dc} \approx 9$ kA/cm^2, (c) $V_{RF} = 23$ V.

TABLE 14

LARGE-SIGNAL RESULTS FOR THE GaAs DOUBLE READ PROFILE IN FIGURE 11a AND POWER LEVELS

OBTAINED BY MATCHING TO 1-Ω RESISTANCE (f = 40 GHz, V_{RF} = 23 V)

J_{dc} (kA/cm²)	$-G_D$ (mho/cm²)	B_D (mho/cm²)	A x 10^{-4} (cm²)	I_{dc} (A)	V_{dc} (V)	η (Percent)	P_{dc} (W)	P_{RF} (W)	P_{diss} (W)	θ_R (°C/W)	D (mils)
4.84	118	2220	0.239	0.116	31.9	20.1	3.7	0.744	2.96	76	2.17
6.02	153	2181	0.32	0.193	32.2	20.83	6.21	1.29	4.92	45.7	2.51
7.01	180	2154	0.385	0.27	32.7	20.8	8.83	1.84	6.99	32.2	2.76
7.98	200	2132	0.436	0.348	32.9	20.1	11.4	2.29	9.11	24.7	2.93
8.92	223	2102	0.5	0.446	33.1	20	14.8	2.96	11.8	19.1	3.14
10.2	249	2067	0.574	0.585	33.4	19.4	19.5	3.78	15.7	14.3	3.36
11.2	264	2038	0.625	0.7	33.4	18.7	23.4	4.37	19	11.8	3.51
12	278	2009	0.676	0.811	33.4	18.3	27.1	4.96	22.1	10.2	3.65
13.1	295	1974	0.74	0.969	33.6	17.7	32.6	5.77	26.8	8.4	3.82
13.9	299	1949	0.769	1.07	33.5	17	35.8	6.09	29.7	7.58	3.9
16	326	1880	0.895	1.43	33.7	15.9	48.2	7.66	40.5	5.56	4.2
17.7	314	1838	0.903	1.6	33.5	14	53.6	7.5	46.1	4.88	4.22

the width of the p-type region is 0.6 μm, the same as for the hybrid structure previously considered. Therefore, the thermal-resistance expressions given in Equations 28 through 31 are also applicable to the double Read structure. Solving Equations 13 through 15 for this case yields the data given in Table 15. Comparisons with the data in Table 13 for the hybrid shows that for the single mesa cases, the double Read is capable of generating more CW power than the hybrid structure.

In addition to the GaAs double-drift structures simulated at 40 GHz, a single-drift GaAs Read structure was simulated. Figure 13a shows the doping profile, and Figure 13b is the dc solution at $T = 500°K$ and $J_{dc} = 8\ kA/cm^2$. Large-signal results at $T = 500°K$, $f = 40$ GHz and $J_{dc} = 8\ kA/cm^2$ are plotted in Figure 14a and b, and results vs. J_{dc} at $V_{RF} = 13.5$ V are given in Figure 14c. Table 16 presents the data for large-signal runs vs. J_{dc}. The maximum efficiency obtained for this structure was $\eta = 18.1$ percent at $J_{dc} = 7.02\ kA/cm^2$ and $V_{RF} = 13.5$ V, and the maximum RF power density was $P_{RF} = 33.6\ kW/cm^2$ at $J_{dc} = 12.1\ kA/cm^2$ and $V_{RF} = 13.5$ V. When $\ell_2 = 0$ in Equation 1 and $\ell_1 = 0.5$ μm as before, the thermally limited RF powers were calculated for this device by solving Equations 13 through 15. However, for every geometry and heat-sink material combination, the resulting diode diameter was larger than the corresponding diameter given in Table 16. Therefore, for all cases this device is electronically limited.

The doping profile for the Si hybrid structure simulated at 40 GHz is given in Figure 15a, and the dc solution at $T = 500°K$ and $J_{dc} = 7.5\ kA/cm^2$ is shown in Figure 15b. Figure 16a and b shows

TABLE 15

CW RESULTS FOR THE PROFILE IN FIGURE 11a AT 40 GHz TAKING INTO ACCOUNT

THE THERMAL-RESISTANCE EXPRESSIONS

D(CM) (mils)	θ(CM) (°C/W)	P_{RF}(CM) (W)	D(DM) (mils)	θ(DM) (°C/W)	P_{RF}(DM) (W)	D(CR) (mils)	θ(CR) (°C/W)	P_{RF}(CR) (W)	D(DR) (mils)	θ(DR) (°C/W)	P_{RF}(DR) (W)	J_{dc} (kA/cm²)
2.17	41.7	0.744	2.17	21.9	0.744	2.17	28.3	0.744	2.17	17.5	0.744	4.84
2.51	34.6	1.29	2.51	17.5	1.29	2.51	23.1	1.29	2.51	13.7	1.29	6.02
2.76	30.7	1.84	2.76	15.2	1.84	2.76	20.2	1.84	2.76	11.7	1.84	7.01
2.41	36.4	1.55	2.93	13.9	2.29	2.93	18.7	2.29	2.93	10.6	2.29	7.98
2.04	45.1	1.25	3.14	12.6	2.96	3.14	17	2.96	3.14	9.51	2.96	8.92
1.63	60.6	0.893	3.36	11.4	3.78	2.97	18.3	2.95	3.36	8.53	3.78	10.2
1.39	75.7	0.684	3.51	10.7	4.37	2.52	22.9	2.26	3.51	7.96	4.37	11.2
1.23	90.1	0.56	3.65	10.1	4.96	2.23	27.2	1.85	3.65	7.49	4.96	12
1.02	117	0.414	3.07	13	3.73	1.86	35.3	1.37	3.82	6.97	5.77	13.1
0.905	140	0.328	2.71	15.6	2.95	1.64	42.4	1.08	3.9	6.75	6.09	13.9
0.641	238	0.178	1.92	26.5	1.6	1.16	72.2	0.589	3.49	8.02	5.3	16
0.472	391	0.094	1.42	43.4	0.843	0.858	118	0.31	2.57	13.1	2.79	17.7

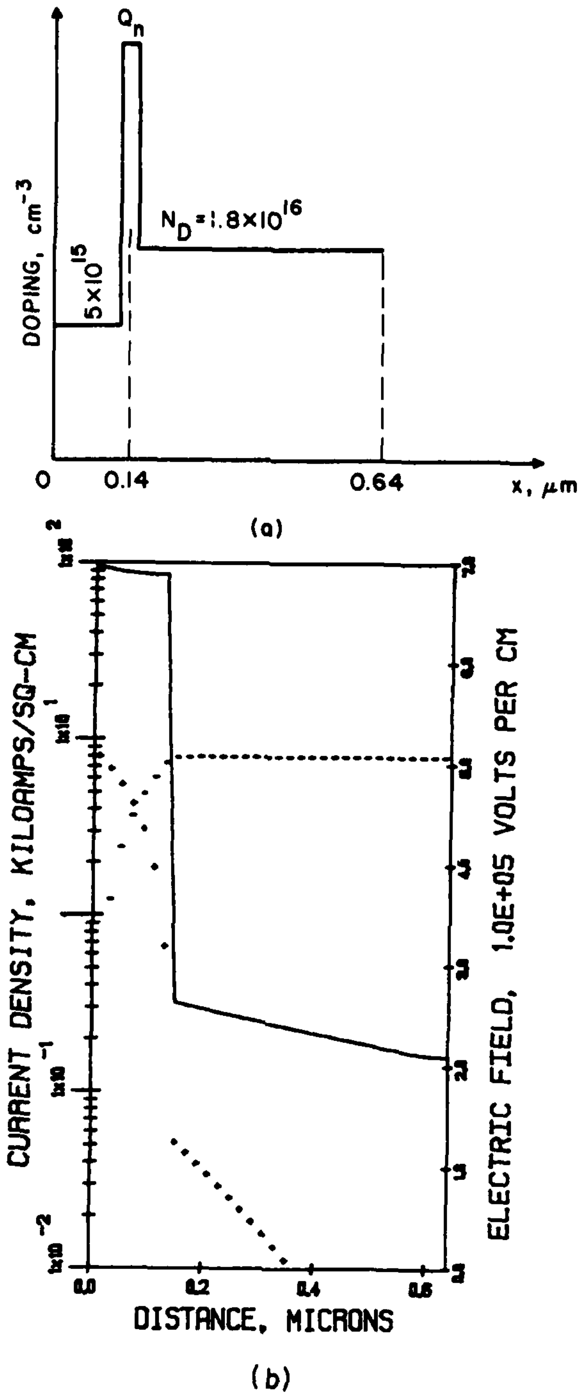

Figure 13. (a) Single-Drift GaAs Read Structure for 40-GHz Operation and (b) Dc Solution at $T = 500°K$ and $J_{dc} = 8\ kA/cm^2$. ($X_A = 0.14\ \mu m$, $T = 500°K$, $J_{dc} = 8\ kA/cm^2$, $E_{max} = 6.96 \times 10^5$ V/cm, $E_{to} = 2.637 \times 10^5$ V/cm, E(RHS) $= 2.101 \times 10^5$ V/cm, and Integrated Doping Spike $Q_n = 2.95 \times 10^{12}\ cm^{-2}$)

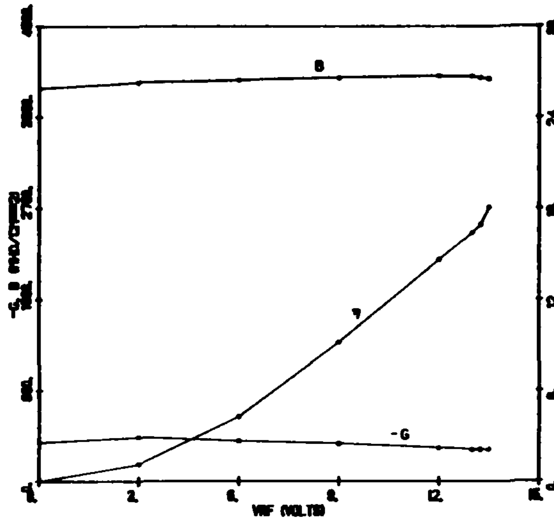

(a)

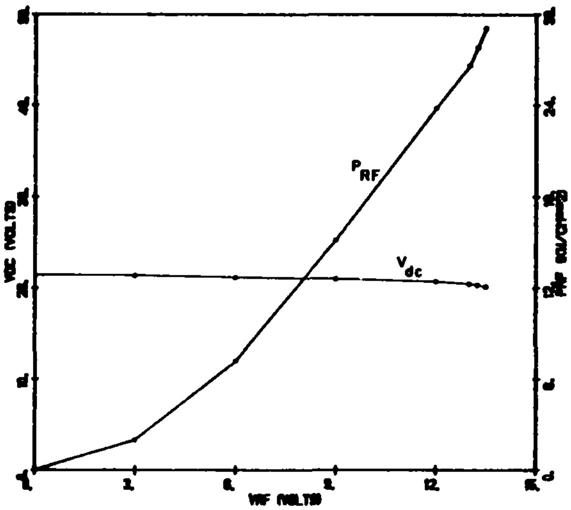

(b)

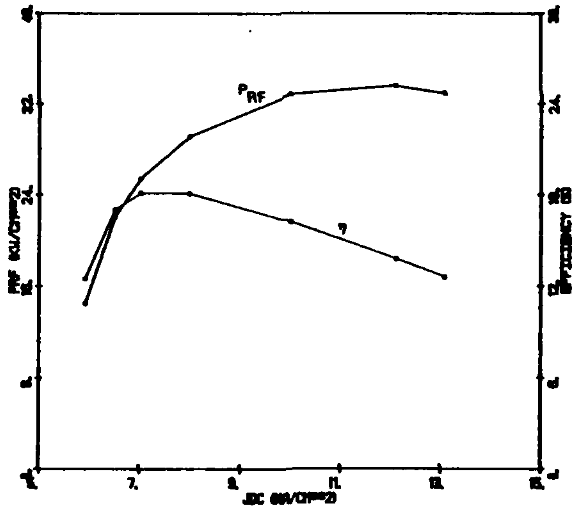

(c)

Figure 14. Large-Signal Results for the Profile of Figure 13a at f = 40 GHz, T = 500°K and (a and b) $J_{dc} \approx 8$ kA/cm^2, (c) V_{RF} = 13.5 V.

TABLE 16

LARGE-SIGNAL RESULTS FOR THE GaAs SINGLE-DRIFT READ PROFILE IN FIGURE 13a AND POWER LEVELS

OBTAINED BY MATCHING TO 1-Ω RESISTANCE (f = 40 GHz, V_{RF} = 13.5 V)

J_{dc} (kA/cm^2)	$-G_D$ (mho/cm^2)	B_D (mho/cm^2)	A x 10^{-4} (cm^2)	I_{dc} (A)	V_{dc} (V)	η (Percent)	P_{dc} (W)	P_{RF} (W)	P_{diss} (W)	θ_R (°C/W)	D (mils)
5.92	159	4156	0.0919	0.0544	19.5	12.5	1.06	0.132	0.928	242	1.35
6.52	242	4076	0.145	0.0945	19.9	17	1.88	0.32	1.56	144	1.69
7.02	279	4034	0.171	0.12	20	18.1	2.4	0.434	1.97	114	1.84
8.0	319	3980	0.2	0.16	20.1	18	3.22	0.58	2.64	85.2	1.99
10	360	3879	0.237	0.237	20.2	16.2	4.79	0.776	4.01	56.1	2.16
12.1	368	3771	0.256	0.31	20.1	13.8	6.23	0.86	5.37	41.9	2.25
13.1	361	3715	0.259	0.339	20	12.6	6.78	0.854	5.93	37.9	2.26

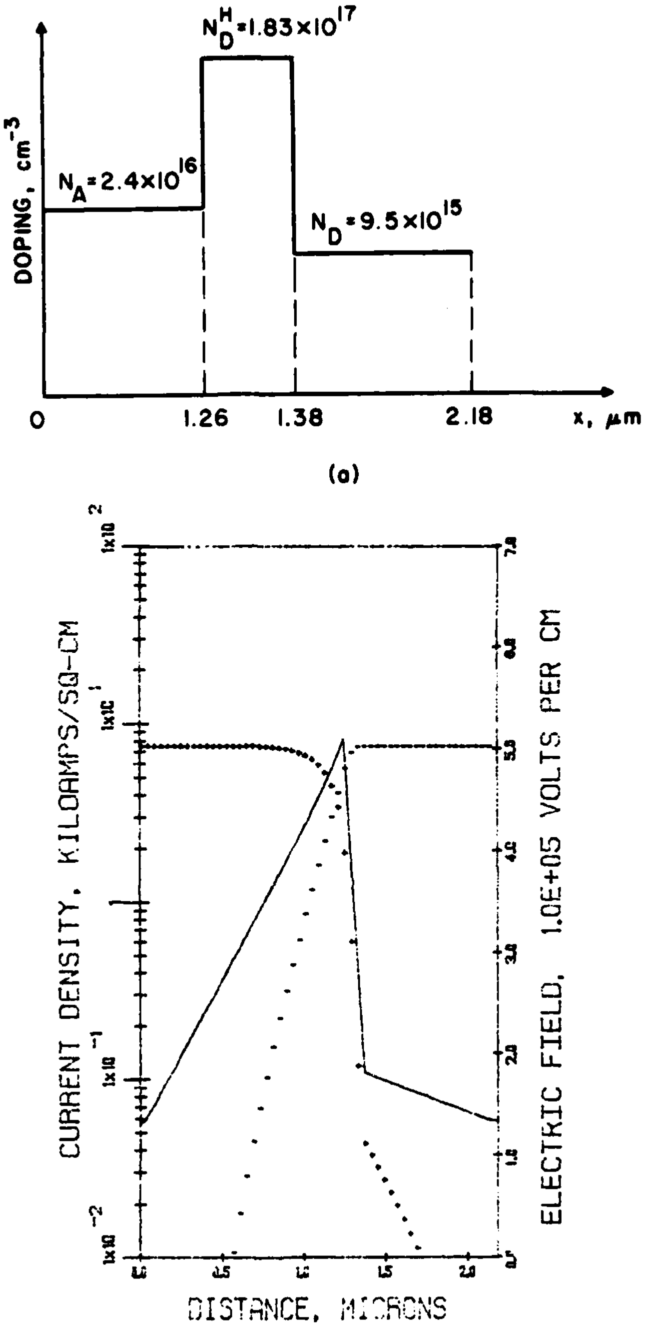

Figure 15. (a) Si Hybrid Profile for 40-GHz Operation and (b) Dc Solution at T = 500°K and J_{dc} = 7.5 kA/cm^2. (X_A = 0.4 μm, J_{dc} = 7.5 kA/cm^2, E(LHS) = 1.32 x 10^5 V/cm, E_{max} = 5.1 x 10^5 V/cm, E_{to} = 1.82 x 10^5 V/cm and E(RHS) = 1.34 x 10^5 V/cm)

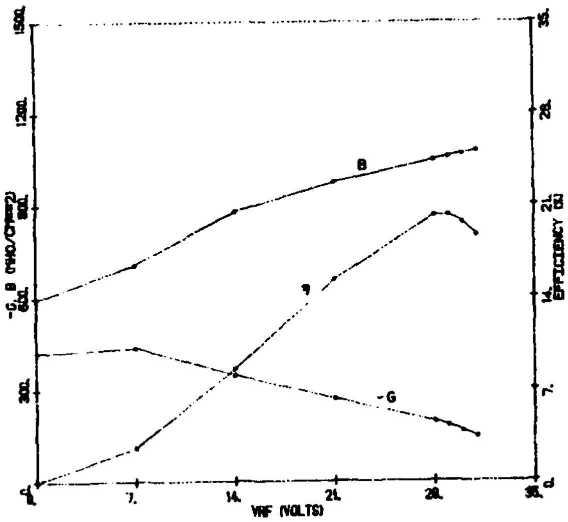

(a)

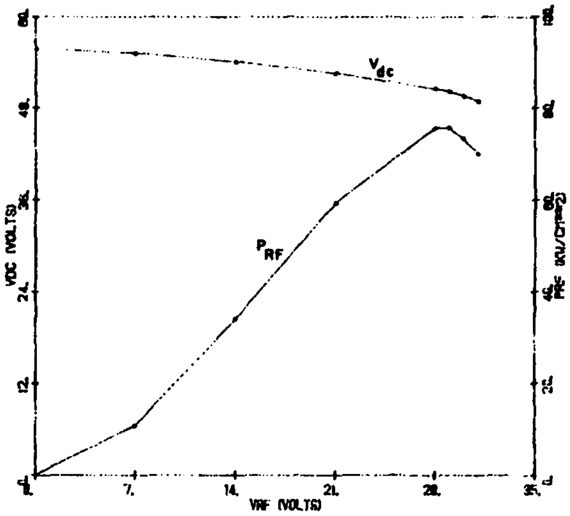

(b)

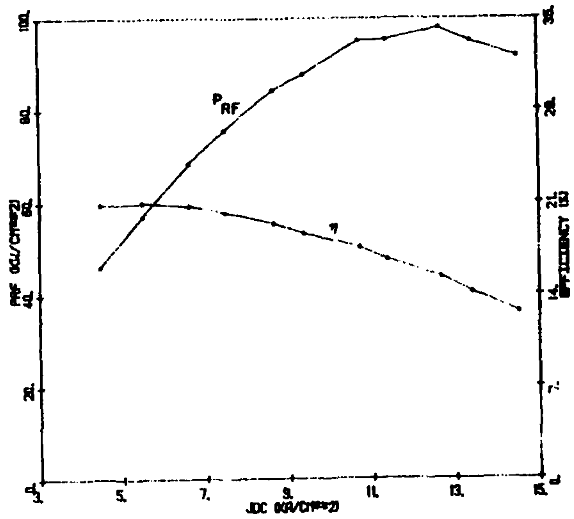

(c)

Figure 16. Large-Signal Results for the Profile of Figure 15a at f = 40 GHz, T = 500°K and (a and b) $J_{dc} \approx 7.5$ kA/cm^2, (c) V_{RF} = 29 V.

the large-signal results vs. V_{RF} at 40 GHz, and Figure 16c shows large-signal results vs. J_{dc}. The maximum efficiency was η = 21.0 percent at J_{dc} = 5.47 kA/cm^2 and V_{RF} = 29 V, and the maximum electronic RF power density was P_{RF} = 97.8 kW/cm^2 at J_{dc} = 12.6 kA/cm^2 and V_{RF} = 29 V. Table 17 presents the large-signal results vs. J_{dc}. From Figure 15a it is seen that $\ell_2 = 1.26 \times 10^{-4}$ cm. Using $\ell_1 = 0.5 \times 10^{-4}$ cm as before and reducing the last two terms of Equation 1 by 1/3 due to the higher thermal conductivity of Si gives the following thermal-resistance expressions:

$$\theta(CM) = \frac{64.27}{d_m} + \frac{26.17}{d_m^2} , \tag{32}$$

$$\theta(DM) = \frac{21.42}{d_m} + \frac{26.17}{d_m^2} , \tag{33}$$

$$\theta(CR) = \frac{35.35}{d_m} + \frac{26.17}{d_m^2} \tag{34}$$

and

$$\theta(DR) = \frac{11.78}{d_m} + \frac{26.17}{d_m^2} . \tag{35}$$

Solving Equations 13 through 15 and 32 through 35 yields the CW data of Table 18 for the Si hybrid. Again due to the higher thermal conductivity of Si, the Si hybrid structure is capable of generating more CW RF power than the GaAs structure.

Figure 17a gives the doping profile of an InP hybrid simulated at 40 GHz; Figure 17b gives the dc solution at T = 500°K and J_{dc} = 10 kA/cm^2. Large-signal results vs. V_{RF} at T = 500°K and f = 40 GHz are plotted in Figure 18a and b, and Figure 18c shows the results vs. J_{dc}. The maximum efficiency obtained was η = 24.8 percent at J_{dc} = 9.87 kA/cm^2 and V_{RF} = 33 V, and the maximum RF power density

TABLE 17

LARGE-SIGNAL RESULTS FOR THE Si HYBRID PROFILE IN FIGURE 15a AND POWER LEVELS

OBTAINED BY MATCHING TO 1-Ω RESISTANCE (f = 40 GHz, V_{RF} = 29 V)

J_{dc} (kA/cm²)	$-G_D$ (mho/cm²)	B_D (mho/cm²)	A x 10^{-4} (cm²)	I_{dc} (A)	V_{dc} (V)	η (Percent)	P_{dc} (W)	P_{RF} (W)	P_{diss} (W)	θ_R (°C/W)	D (mils)
4.47	109	1144	0.825	0.369	49.4	20.9	18.2	3.8	14.4	15.6	4.04
5.47	135	1116	1.07	0.585	49.6	21	29	6.09	22.9	9.82	4.59
6.6	162	1082	1.35	0.891	50	20.7	44.6	9.23	35.4	6.36	5.16
7.45	180	1056	1.57	1.17	50.1	20.2	58.6	11.8	46.8	4.81	5.57
8.63	200	1018	1.86	1.6	50.3	19.4	80.5	15.6	64.9	3.47	6.06
9.36	208	993	2.02	1.89	50.2	18.6	94.9	17.6	77.3	2.91	6.31
10.7	226	945	2.39	2.56	50.4	17.6	129	22.7	106	2.12	6.87
11.4	226	920	2.52	2.87	50.3	16.6	144	23.9	120	1.88	7.05
12.6	232	870	2.86	3.6	50.3	15.3	181	27.7	153	1.47	7.51
13.4	226	841	2.98	3.99	50.1	14.2	200	28.4	172	1.31	7.67
14.5	218	796	3.2	4.64	50	12.6	232	29.2	203	1.11	7.95

TABLE 18

CW RESULTS FOR THE PROFILE IN FIGURE 15a AT 40 GHz TAKING

INTO ACCOUNT THE THERMAL-RESISTANCE EXPRESSIONS

D(CM) (mils)	θ(CM) (°C/W)	P_{RF}(CM) (W)	D(DM) (mils)	θ(DM) (°C/W)	P_{RF}(DM) (W)	D(CR) (mils)	θ(CR) (°C/W)	P_{RF}(CR) (W)	D(DR) (mils)	θ(DR) (°C/W)	P_{RF}(DR) (W)	J_{dc} (kA/cm^2)
3.55	20.2	2.94	4.04	6.9	3.8	4.04	10.4	3.8	4.04	4.52	3.8	4.47
2.82	26.1	2.29	4.59	5.91	6.09	4.59	8.94	6.09	4.59	3.81	6.09	5.47
2.23	34	1.72	5.16	5.13	9.23	4.06	10.3	5.7	5.16	3.26	9.23	6.6
1.91	40.8	1.4	5.57	4.69	11.8	3.48	12.3	4.62	5.57	2.96	11.8	7.45
1.57	51.6	1.05	4.7	5.74	9.43	2.85	15.6	3.46	6.06	2.66	15.6	8.63
1.4	59.3	0.867	4.2	6.59	7.8	2.54	17.9	2.86	6.31	2.52	17.6	9.36
1.15	75.9	0.633	3.44	8.43	5.7	2.09	23	2.09	6.26	2.55	18.8	10.7
1.04	86.3	0.519	3.11	9.58	4.67	1.89	26.1	1.72	5.66	2.9	15.4	11.4
0.88	107	0.38	2.64	11.9	3.42	1.6	32.3	1.26	4.8	3.59	11.3	12.6
0.792	123	0.303	2.38	13.6	2.73	1.44	37.2	1.0	4.32	4.13	9.02	13.4
0.683	150	0.216	2.05	16.7	1.94	1.24	45.4	0.714	3.72	5.05	6.42	14.5

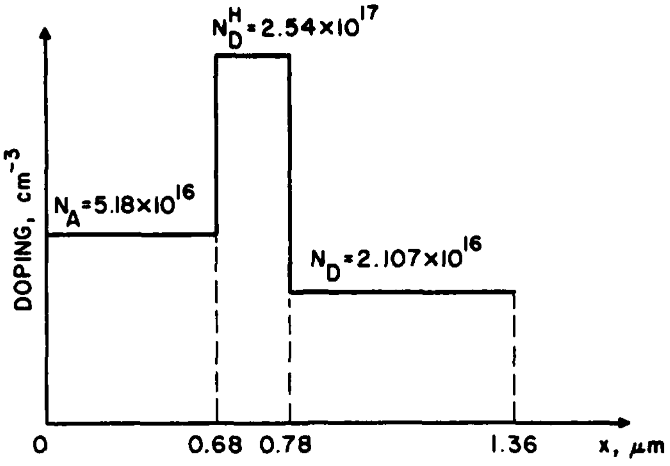

(a)

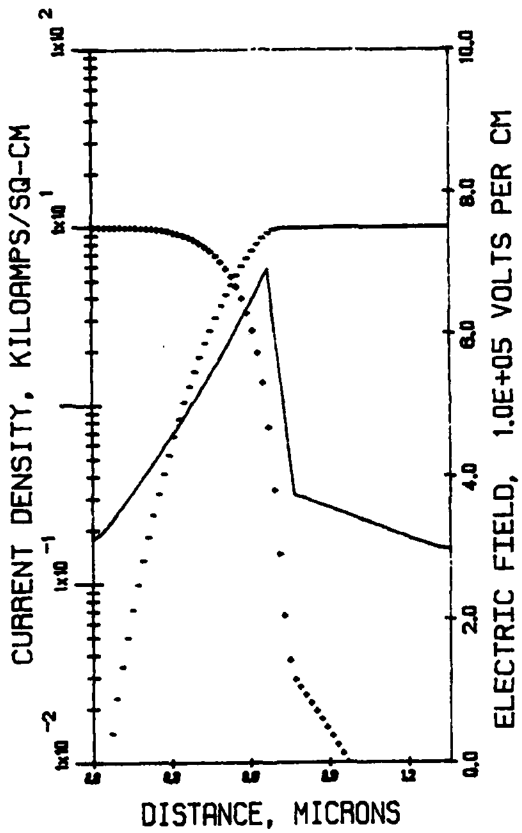

(b)

Figure 17. (a) InP Hybrid Profile for 40-GHz Operation and (b) Dc Solution at T = 500°K and J_{dc} = 10 kA/cm^2. (X_A = 0.42 μm, J_{dc} = 10 kA/cm^2, E(LHS) = 3.15 x 10^5 V/cm, E_{max} = 6.916 x 10^5 V/cm, E_{to} = 3.755 x 10^5 V/cm and E(RHS) = 2.99 x 10^5 V/cm)

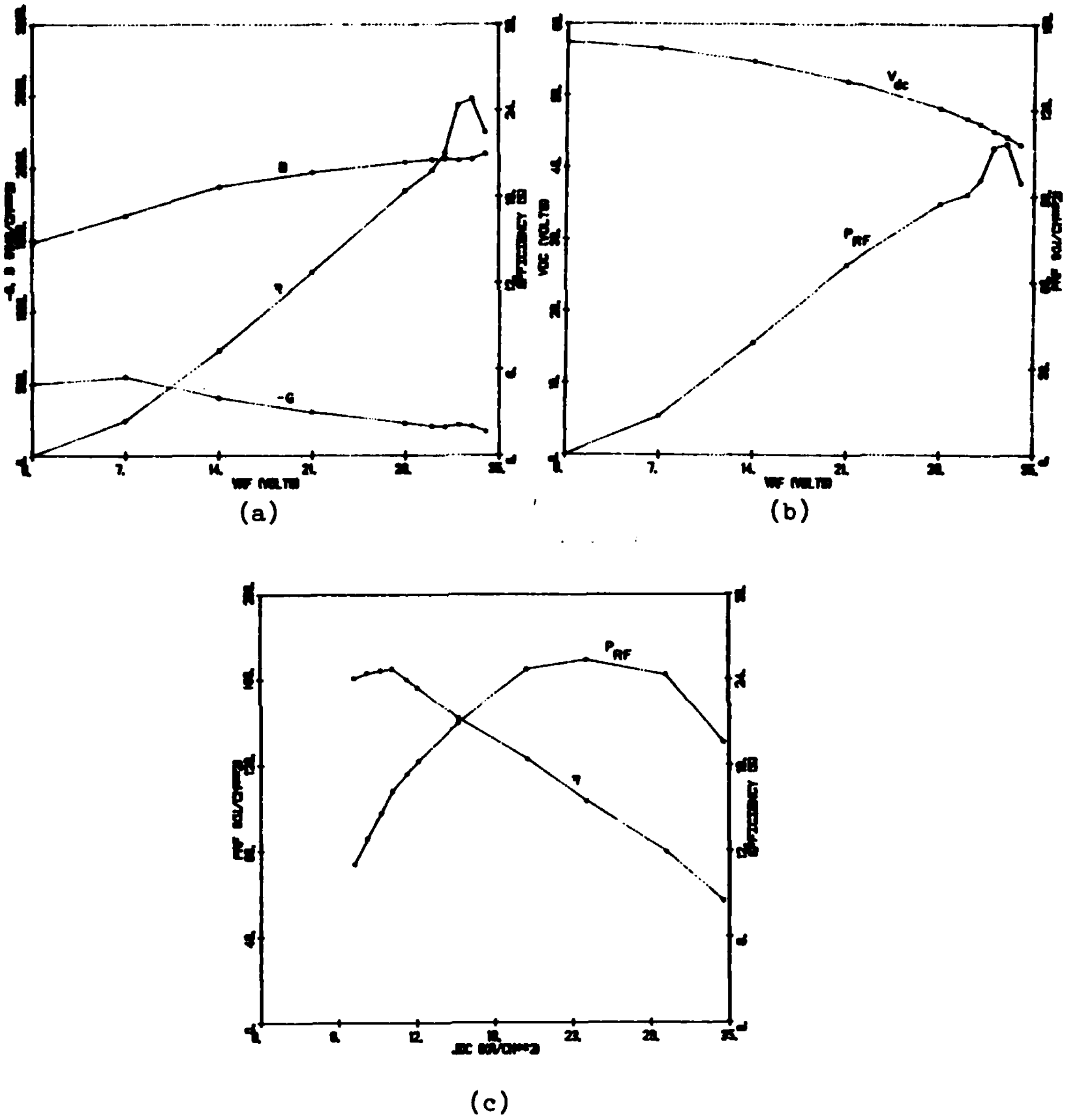

Figure 18. Large-Signal Results for the Profile of Figure 17a at $T = 500°K$, $f = 40$ GHz and (a and b) $J_{dc} = 10$ kA/cm², $V_{RF} = 33$ V.

was P_{RF} = 169 kW/cm^2 at J_{dc} = 24.3 kA/cm^2 and V_{RF} = 33 V. Table 19 lists the large-signal results vs. J_{dc} and the electronic RF powers obtained by matching the diode negative resistance to 1 Ω.

From Figure 17a, the p-region width is $\ell_2 = 0.68 \times 10^{-4}$ cm. As before, when $\ell_1 = 0.5 \times 10^{-4}$ cm and the final two terms in Equation 1 are reduced by 0.8 due to the higher thermal conductivity of InP (relative to GaAs), the following thermal-resistance expressions are obtained:

$$\theta(CM) = \frac{64.27}{d_m} + \frac{47.5}{d_m^2} , \qquad (36)$$

$$\theta(DM) = \frac{21.42}{d_m} + \frac{47.5}{d_m^2} , \qquad (37)$$

$$\theta(CR) = \frac{35.35}{d_m} + \frac{47.5}{d_m^2} \qquad (38)$$

and

$$\theta(DR) = \frac{11.78}{d_m} + \frac{47.5}{d_m^2} . \qquad (39)$$

Solving Equations 13 through 15 and 36 through 39 yields the CW powers given in Table 20 for the InP hybrid structure.

Summarizing the 40-GHz results given in Tables 12 through 20 shows that the Si hybrid generates more CW power than any of the GaAs or InP structures for all combinations of geometry and heat-sink material. In addition, the Si hybrid generated more electronic RF power (matching into 1-Ω resistance) than any other 40-GHz structure. This is due to the fact that for the Si structure, the susceptance is much nearer to the magnitude of the conductance than for the other structures (G = - 218, B = 796 mho/cm^2 for Si;

TABLE 19

LARGE-SIGNAL RESULTS FOR THE InP HYBRID PROFILE IN FIGURE 17a AND POWER LEVELS

OBTAINED BY MATCHING TO 1-Ω RESISTANCE (f = 40 GHz, V_{RF} = 33 V)

J_{dc} (kA/cm^2)	$-G_D$ (mho/cm^2)	B_D (mho/cm^2)	A $\times 10^{-4}$ (cm^2)	I_{dc} (A)	V_{dc} (V)	η (Percent)	P_{dc} (W)	P_{RF} (W)	P_{diss} (W)	θ_R (°C/W)	D (mils)
7.02	136	2151	0.293	0.206	43.7	24.1	9	2.17	6.83	32.9	2.4
8	158	2117	0.35	0.28	43.9	24.5	12.3	3.01	9.29	24.2	2.63
9.02	180	2086	0.411	0.371	44	24.6	16.3	4.01	12.3	18.3	2.85
9.87	198	2058	0.463	0.457	44.2	24.8	20.2	5.01	15.2	14.8	3.02
10.9	213	2030	0.511	0.557	44.2	24	24.6	5.9	18.7	12	3.18
11.8	224	2010	0.548	0.647	44.2	23.4	28.6	6.69	21.9	10.3	3.29
14.7	257	1937	0.673	0.989	44.5	21.3	44	9.37	34.6	6.5	3.64
19.9	302	1804	0.903	1.8	44.9	18.4	80.8	14.9	65.9	3.41	4.22
24.3	311	1692	1.05	2.55	44.8	15.5	114	17.7	96.3	2.34	4.55
30.3	298	1542	1.21	3.67	44.8	11.9	164	19.5	144	1.56	4.89
34.6	240	1441	1.12	3.88	44.3	8.54	172	14.7	157	1.43	4.7

TABLE 20

CW RESULTS FOR THE PROFILE IN FIGURE 17a AT 40 GHz TAKING INTO

ACCOUNT THE THERMAL-RESISTANCE EXPRESSIONS

D(CM) (mils)	θ(CM) (°C/W)	P_{RF}(CM) (W)	D(DM) (mils)	θ(DM) (°C/W)	P_{RF}(DM) (W)	D(CR) (mils)	θ(CR) (°C/W)	P_{RF}(CR) (W)	D(DR) (mils)	θ(DR) (°C/W)	P_{RF}(DR) (W)	J_{dc} (kA/cm^2)
2.23	38.4	1.86	2.4	17.2	2.17	2.4	23	2.17	2.4	13.2	2.17	7.02
1.87	48.1	1.52	2.63	15	3.01	2.63	20.3	3.01	2.63	11.3	3.01	8
1.57	60.2	1.22	2.85	13.4	4.01	2.85	18.2	4.01	2.85	9.98	4.01	9.02
1.37	72.4	1.02	3.02	12.3	5.01	2.48	21.9	3.38	3.02	9.11	5.01	9.87
1.15	92	0.772	3.18	11.4	5.9	2.09	27.8	2.55	3.18	8.4	5.9	10.9
0.99	113	0.606	2.97	12.6	5.46	1.8	34.3	2	3.29	7.97	6.69	11.8
0.603	237	0.257	1.81	26.4	2.31	1.1	71.8	0.848	3.29	7.97	7.64	14.7
0.208	1400	0.0362	0.626	156	0.326	0.379	424	0.12	1.14	47.1	1.08	19.9
0.012	3.36×10^{5}	1.23×10^{-4}	0.036	3.74×10^{4}	1.1×10^{-3}	0.0218	1.02×10^{5}	4.06×10^{-3}	0.065	1.13×10^{4}	3.6×10^{-3}	24.3
--	--	--	--	--	--	--	--	--	--	--	--	30.3
--	--	--	--	--	--	--	--	--	--	--	--	34.6

$G = -298$, $B = 1441$ mho/cm^2 for InP). As a result, when the Si diode is matched to 1-Ω resistance, the resulting diode size is larger for Si, and a higher peak P_{RF} is obtained.

The InP hybrid structure had the best efficiency, $\eta = 24.8$ percent, of any of the 40-GHz structures.

SECTION 7

RESULTS AT 60 GHz

Figure 19a shows the doping profile for the single-drift GaAs Read structure simulated at 60 GHz, and Figure 19b shows the solution at $T = 500°K$ and $J_{dc} = 15\ kA/cm^2$. Large-signal results for this structure at $f = 60$ GHz, $T = 500°K$ and $J_{dc} = 15\ kA/cm^2$ are plotted in Figure 20a and b, and large-signal results vs. J_{dc} at $V_{RF} = 10$ V are shown in Figure 20c. The maximum efficiency obtained was $\eta = 11.1$ percent at $J_{dc} = 15.2\ kA/cm^2$ and $V_{RF} = 10$ V; the maximum electronic RF power density was $P_{RF} = 38\ kW/cm^2$ at $J_{dc} = 26.5\ kA/cm^2$ and $V_{RF} = 10$ V.

Table 21 presents large-signal results vs. J_{dc} for this structure and RF powers obtained by matching to 1-Ω resistance. Setting $\ell_2 = 0$ and $\ell_1 = 0.5 \times 10^{-4}$ cm, as before, gives the following thermal-resistance expressions from Equation 1:

$$\theta(CM) = \frac{64.27}{d_m} + \frac{14.8}{d_m^2} , \tag{40}$$

$$\theta(DM) = \frac{21.42}{d_m} + \frac{14.8}{d_m^2} , \tag{41}$$

$$\theta(CR) = \frac{35.35}{d_m} + \frac{14.8}{d_m^2} \tag{42}$$

and

$$\theta(DR) = \frac{11.78}{d_m} + \frac{14.8}{d_m^2} . \tag{43}$$

Solving Equations 13 through 15 and 40 through 43 yields the CW powers listed in Table 22. The only case which becomes

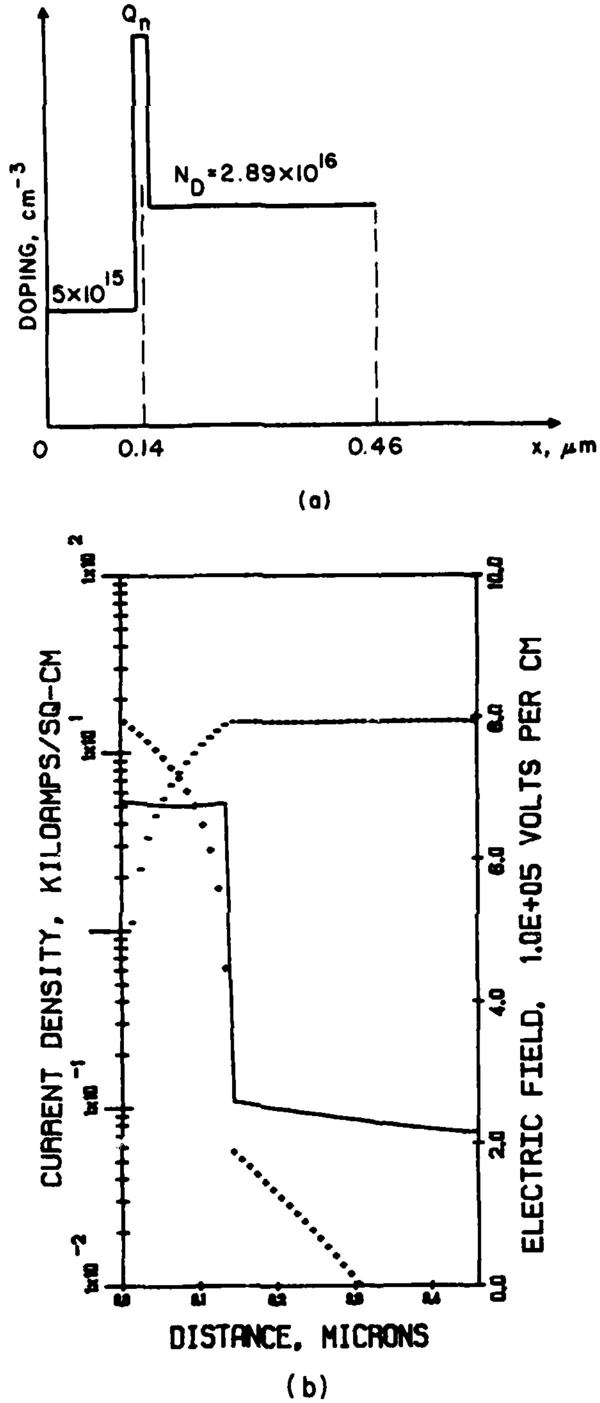

Figure 19. (a) Single-Drift GaAs Read Structure for 60-GHz Operation and (b) Dc Solution at T = 500°K and J_{dc} = 15 kA/cm^2. (X_A = 0.14 μm, T = 500°K, J_{dc} = 15 kA/cm^2, E_{max} = 6.82 x 10^5 V/cm, E_{to} = 2.59 x 10^5 V/cm, E(RHS) = 2.16 x 10^5 V/cm and Integrated Doping Spike Q_n = 2.91 x 10^{12} cm^{-2})

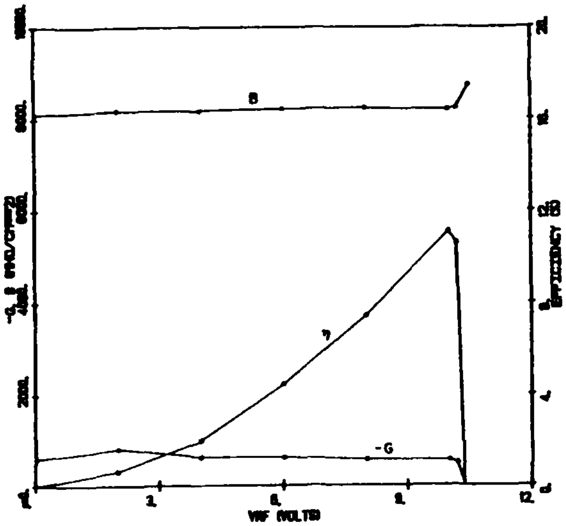

(a)

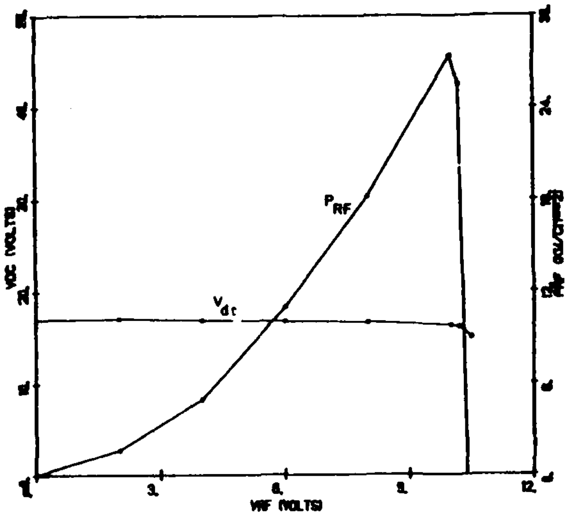

(b)

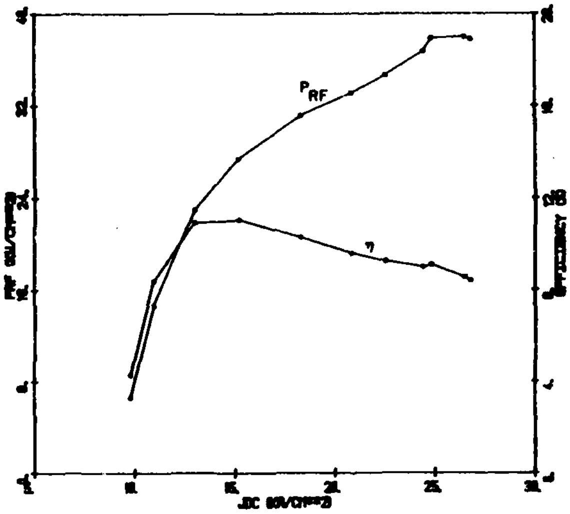

(c)

Figure 20. Large-Signal Results for the Profile of Figure 19a at $T = 500^{o}K$, $f = 60$ GHz and (a and b) $J_{dc} = 15$ kA/cm^2, (c) $V_{RF} = 10$ V.

TABLE 21

LARGE-SIGNAL RESULTS FOR THE GaAs SINGLE-DRIFT READ PROFILE OF FIGURE 19a AND POWER LEVELS

OBTAINED BY MATCHING TO 1-Ω RESISTANCE (f = 60 GHz, V_{RF} = 10 V)

J_{dc} (kA/cm²)	$-G_D$ (mho/cm²)	B_d (mho/cm²)	A x 10^{-4} (cm²)	I_{dc} (A)	V_{dc} (V)	η (Percent)	P_{dc} (W)	P_{RF} (W)	P_{diss} (W)	θ_R (°C/W)	D (mils)
9.78	132	8750	0.0172	0.0168	15.8	4.28	0.265	0.0113	0.254	886	0.583
10.9	293	8570	0.0398	0.0434	16	8.38	0.694	0.0581	0.636	354	0.886
13	459	8350	0.0656	0.0853	16.2	10.9	1.38	0.15	1.23	183	1.14
15.2	548	8200	0.0811	0.123	16.3	11.1	2	0.222	1.78	126	1.26
18.3	623	8010	0.0965	0.176	16.5	10.3	2.9	0.299	2.6	86.5	1.38
20.8	662	7840	0.107	0.222	16.5	9.6	3.66	0.351	3.31	68	1.45
22.5	693	7730	0.115	0.259	16.6	9.26	4.3	0.398	3.9	57.7	1.51
24.4	734	7600	0.126	0.307	16.7	9	5.13	0.462	4.67	48.2	1.58
24.8	757	7560	0.131	0.325	16.7	9.11	5.43	0.495	4.94	45.5	1.61
26.5	759	7440	0.136	0.36	16.7	8.56	6.01	0.514	5.5	40.9	1.64
26.8	755	7430	0.135	0.362	16.7	8.42	6.04	0.508	5.53	40.7	1.63

TABLE 22

CW RESULTS FOR THE PROFILE IN FIGURE 19a AT 60 GHz TAKING INTO

ACCOUNT THE THERMAL-RESISTANCE EXPRESSIONS

D(CM) (mils)	θ(CM) (°C/W)	P_{RF}(CM) (W)	D(DM) (mils)	θ(DM) (°C/W)	P_{RF}(DM) (W)	D(CR) (mils)	θ(CR) (°C/W)	P_{RF}(CR) (W)	D(DR) (mils)	θ(DR) (°C/W)	P_{RF}(DR) (W)	J_{dc} (kA/cm^2)
0.583	154	0.0113	0.583	80.3	0.0113	0.583	104	0.0113	0.583	63.7	0.0113	9.78
0.886	91.4	0.0581	0.886	43	0.0581	0.886	58.8	0.0581	0.886	32.1	0.0581	10.9
1.14	67.8	0.15	1.14	30.2	0.15	1.14	42.4	0.15	1.14	21.7	0.15	13
1.26	60.3	0.222	1.26	26.3	0.222	1.26	37.4	0.222	1.26	18.7	0.222	15.2
1.38	54.3	0.299	1.38	23.3	0.299	1.38	33.4	0.299	1.38	16.3	0.299	18.3
1.45	51.4	0.351	1.45	21.8	0.351	1.45	31.4	0.351	1.45	15.2	0.351	20.8
1.46	61.2	0.375	1.51	20.7	0.398	1.51	29.9	0.398	1.51	14.3	0.398	22.5
1.29	72.2	0.308	1.58	19.5	0.462	1.58	28.3	0.462	1.58	13.4	0.462	24.4
1.26	74.3	0.303	1.61	19	0.495	1.61	27.7	0.495	1.61	13	0.495	24.8
1.13	85.7	0.246	1.64	18.6	0.514	1.64	27	0.514	1.64	12.7	0.514	26.5
1.11	88	0.235	1.63	18.7	0.508	1.63	27.2	0.508	1.63	12.8	0.508	26.8

thermally limited is the single mesa, copper heat-sink case starting at J_{dc} = 22.5 kA/cm². The other cases are electronically limited.

Figure 21a shows the hybrid GaAs double-drift profile simulated at 60 GHz, and the dc solution at T = 500°K and J_{dc} = 18 kA/cm² is shown in Figure 21b. Large-signal results vs. V_{RF} at T = 500°K, f = 60 GHz and J_{dc} = 18 kA/cm² are plotted in Figure 22a and b, and large-signal results vs. J_{dc} are plotted in Figure 22c. The maximum efficiency obtained was η = 14.2 percent at J_{dc} = 17.7 kA/cm², and the maximum electronic RF power density was P_{RF} = 132 kW/cm² at J_{dc} = 54.8 kA/cm² and V_{RF} = 18 V. Large-signal results vs. J_{dc} are listed in Table 23 along with electronic RF power obtained by matching to 1-Ω resistance. When it is noted from Figure 21a that the p-region width is $\ell_2 = 0.4 \times 10^{-4}$ cm, and when $\ell_1 = 0.5 \times 10^{-4}$ cm as before, the thermal-resistance expressions become

$$\theta(CM) = \frac{64.27}{d_m} + \frac{50.16}{d_m^2} , \qquad (44)$$

$$\theta(DM) = \frac{21.42}{d_m} + \frac{50.16}{d_m^2} , \qquad (45)$$

$$\theta(CR) = \frac{35.35}{d_m} + \frac{50.16}{d_m^2} \qquad (46)$$

and

$$\theta(DR) = \frac{11.78}{d_m} + \frac{50.16}{d_m^2} . \qquad (47)$$

Solving Equations 13 through 15 and 44 through 47 yields the CW powers listed in Table 24. The case of a single mesa on a copper heat sink is thermally limited at all the current densities

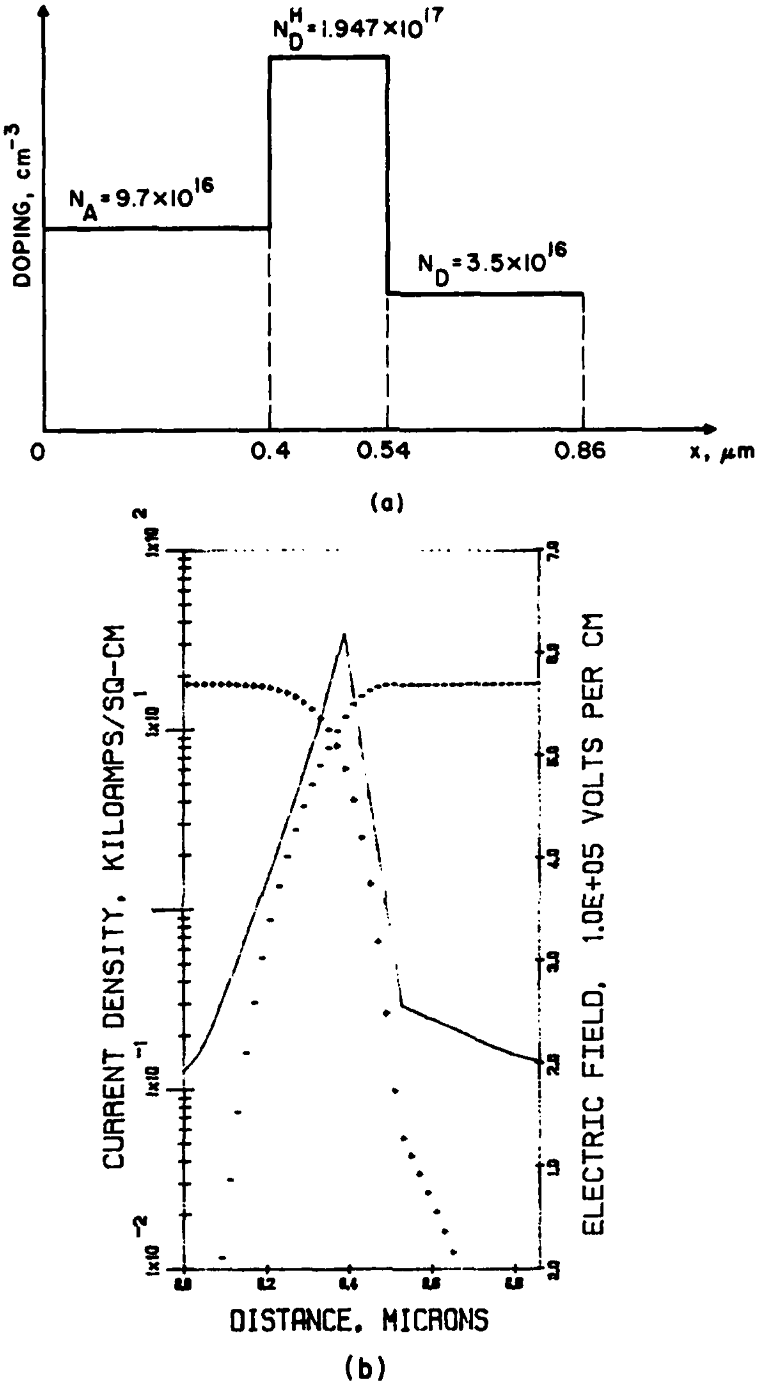

Figure 21. (a) GaAs Hybrid Double-Drift Profile for 60-GHz Operation and (b) Dc Solution at T = 500°K and J_{dc} = 18 kA/cm². (X_A = 0.26 μm, J_{dc} = 18 kA/cm², E(LHS) = 1.97 x 10^5 V/cm, E_{max} = 6.18 x 10^5 V/cm, E_{to} = 2.57 x 10^5 V/cm and E(RHS) = 2.04 x 10^5 V/cm)

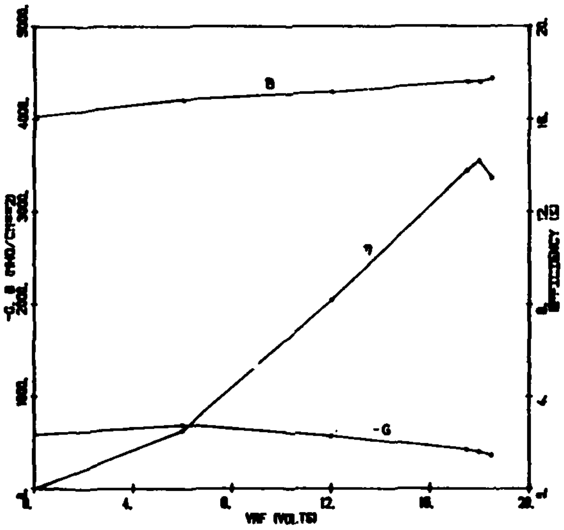

(a)

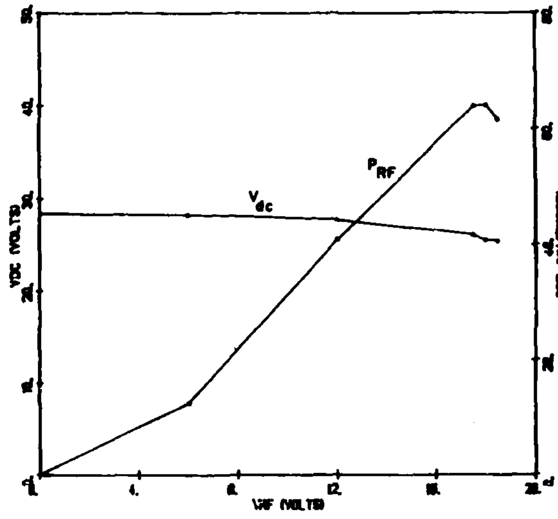

(b)

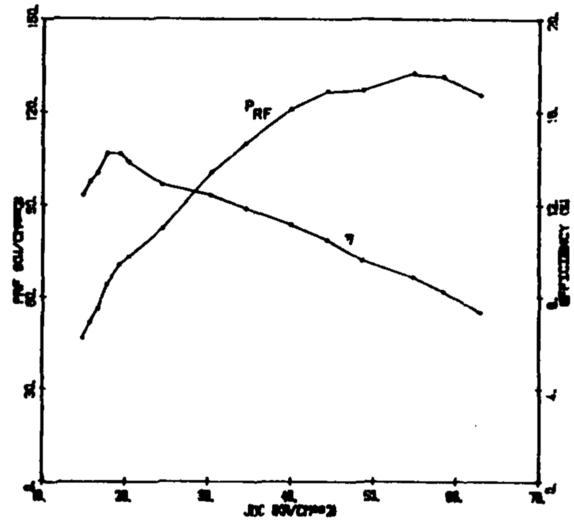

(c)

Figure 22. Large-Signal Results for the Profile of Figure 21a at $f = 60$ GHz, $T = 500°K$ and (a and b) $J_{dc} = 18$ kA/cm^2, (c) $V_{RF} = 18$ V.

TABLE 23

LARGE-SIGNAL RESULTS FOR THE GaAs HYBRID PROFILE IN FIGURE 21a AND POWER LEVELS

OBTAINED BY MATCHING TO 1-Ω RESISTANCE (f = 60 GHz, V_{RF} = 18 V)

J_{dc} (kA/cm^2)	$-G_D$ (mho/cm^2)	B_D (mho/cm^2)	A $\times 10^{-4}$ (cm^2)	I_{dc} (A)	V_{dc} (V)	η (Percent)	P_{dc} (W)	P_{RF} (W)	P_{diss} (W)	θ_R (°C/W)	D (mils)
14.9	288	4540	0.139	0.207	25.2	12.4	5.22	0.647	4.57	49.2	1.66
15.7	319	4500	0.157	0.246	25.3	13	6.22	0.809	5.41	41.6	1.76
16.6	347	4460	0.173	0.287	25.4	13.4	7.29	0.977	6.31	35.6	1.85
17.7	396	4400	0.203	0.359	25.5	14.2	9.15	1.3	7.85	28.7	2
19.3	436	4360	0.227	0.438	25.9	14.2	11.3	1.6	9.7	23.2	2.12
20.4	452	4330	0.238	0.485	26	13.8	12.6	1.74	10.9	20.6	2.17
24.5	508	4210	0.282	0.691	26.2	12.8	18.1	2.32	15.8	14.2	2.36
30.4	619	4020	0.374	1.14	26.7	12.4	30.4	3.77	26.6	8.46	2.72
34.5	676	3880	0.436	1.5	26.9	11.8	40.4	4.77	35.6	6.32	2.93
40	746	3700	0.524	2.1	27.1	11.1	56.9	6.32	50.6	4.45	3.22
44.4	782	3540	0.595	2.64	27.2	10.5	71.8	7.54	64.3	3.5	3.43
48.6	784	3400	0.644	3.13	27.2	9.6	85.1	8.17	76.9	2.92	3.56

Cont.

Table 23, Cont.

J_{dc} (kA/cm^2)	$-G_D$ (mho/cm^2)	B_D (mho/cm^2)	A x 10^{-4} (cm^2)	I_{dc} (A)	V_{dc} (V)	η (Percent)	P_{dc} (W)	P_{RF} (W)	P_{diss} (W)	θ_R (°C/W)	D (mils)
54.8	817	3200	0.749	4.1	27.3	8.85	112	9.91	102	2.2	3.84
58.4	810	3060	0.808	4.72	27.2	8.25	128	10.6	117	1.92	3.99
62.9	774	2920	0.848	5.33	27.1	7.35	144	10.6	133	1.69	4.09

TABLE 24

CW RESULTS FOR THE PROFILE IN FIGURE 21a AT 60 GHz TAKING INTO ACCOUNT THE THERMAL-RESISTANCE EXPRESSIONS

D(CM) (mils)	θ(CM) (°C/W)	P_{RF}(CM) (W)	D(DM) (mils)	θ(DM) (°C/W)	P_{RF}(DM) (W)	D(CR) (mils)	θ(CR) (°C/W)	P_{RF}(CR) (W)	D(DR) (mils)	θ(DR) (°C/W)	P_{RF}(DR) (W)	J_{dc} (kA/cm^2)
1.32	77.5	0.411	1.66	31.1	0.647	1.66	39.5	0.647	1.66	25.3	0.647	14.9
1.22	86.5	0.389	1.76	28.4	0.809	1.76	36.3	0.809	1.76	22.9	0.809	15.7
1.11	98.4	0.354	1.85	26.2	0.977	1.85	33.8	0.977	1.85	21	0.977	16.6
1	114	0.327	2	23.2	1.3	1.82	34.4	1.08	2	18.4	1.3	17.7
0.83	150	0.248	2.12	21.3	1.6	1.51	45.4	0.82	2.12	16.7	1.6	19.3
0.73	182	0.198	2.17	20.5	1.74	1.33	55	0.654	2.17	16.1	1.74	20.4
0.454	385	0.0857	1.36	42.8	0.772	0.825	116	0.283	2.36	14	2.32	24.5
0.191	1710	0.0186	0.573	190	0.168	0.348	517	0.0616	1.04	57.4	0.554	30.4
0.0635	1.34×10^4	0.0022	0.19	1490	0.0202	0.115	4070	0.0074	0.346	452	0.067	34.5
--	--	--	--	--	--	--	--	--	--	--	--	40

used in the simulations. For the other cases, the CW power is electronically limited at low values of J_{dc} and thermally limited at higher values of J_{dc}. It should be noted that it is not possible to obtain CW power for any configuration above 35 kA/cm^2.

Next, a uniformly doped GaAs double-drift structure is considered. The doping profile is shown in Figure 23a, and the dc solution at T = 500°K and J_{dc} = 18 kA/cm^2 is shown in Figure 23b. Large-signal results vs. V_{RF} at f = 60 GHz and J_{dc} = 18 kA/cm^2 are plotted in Figure 24a and b, and large-signal results vs. J_{dc} at V_{RF} = 17 V are plotted in Figure 24c. The maximum efficiency obtained for this structure was η = 12.1 percent at J_{dc} = 29.6 kA/cm^2 and V_{RF} = 17 V, and the maximum RF power density was P_{RF} = 174.8 kW/cm^2 at J_{dc} = 78.8 kA/cm^2. Large-signal results vs. J_{dc} are listed in Table 25. From Figure 23a it is seen that $\ell_2 = 0.43 \times 10^{-4}$ cm, and when $\ell_1 = 0.5 \times 10^{-4}$ cm is used as before, the thermal resistance expressions for the uniform double-drift diode are

$$\theta(CM) = \frac{64.27}{d_m} + \frac{51.15}{d_m^2} , \qquad (48)$$

$$\theta(DM) = \frac{21.42}{d_m} + \frac{51.15}{d_m^2} , \qquad (49)$$

$$\theta(CR) = \frac{35.35}{d_m} + \frac{51.15}{d_m^2} \qquad (50)$$

and

$$\theta(DR) = \frac{11.78}{d_m} + \frac{51.15}{d_m^2} . \qquad (51)$$

Solving Equations 13 through 15 and 48 through 51 yields the CW power data given in Table 26. CW operation is only possible for

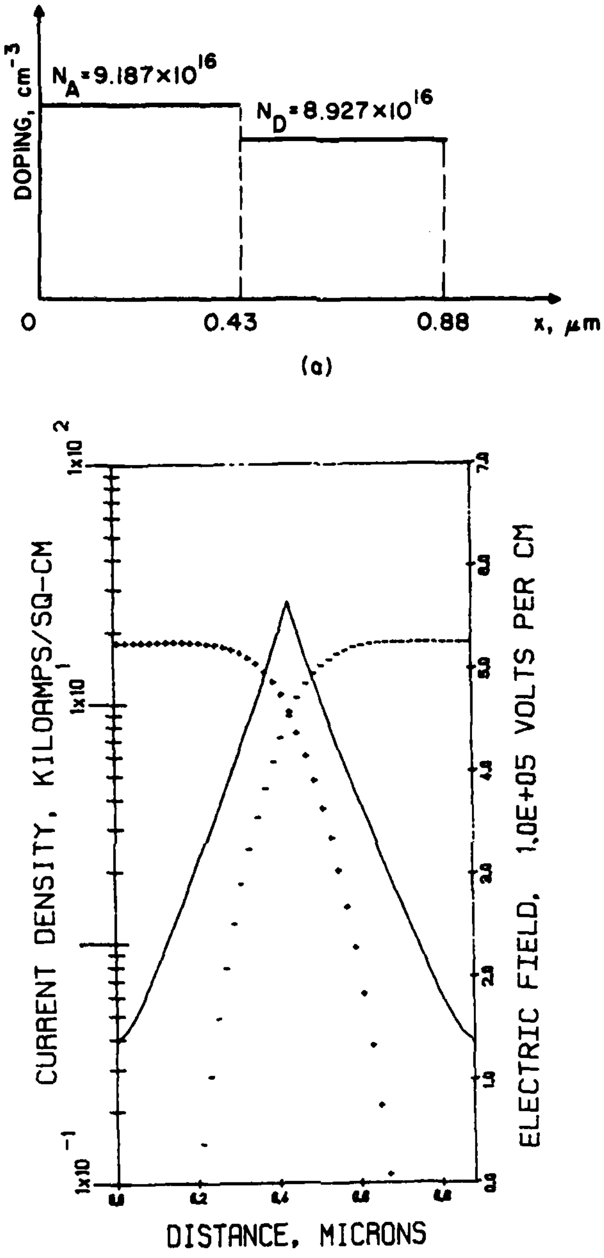

(b)

Figure 23. (a) Uniform GaAs Double-Drift Doping Profile for 60-GHz Operation and (b) Dc Solution at T = 500°K and J_{dc} = 18 kA/cm^2. (X_A = 0.34 μm, J_{dc} = 18 kA/cm^2, E(LHS) = 1.413 x 10^5 V/cm, E_{max} = 5.658 x 10^5 V/cm and E(RHS) = 1.412 x 10^5 V/cm)

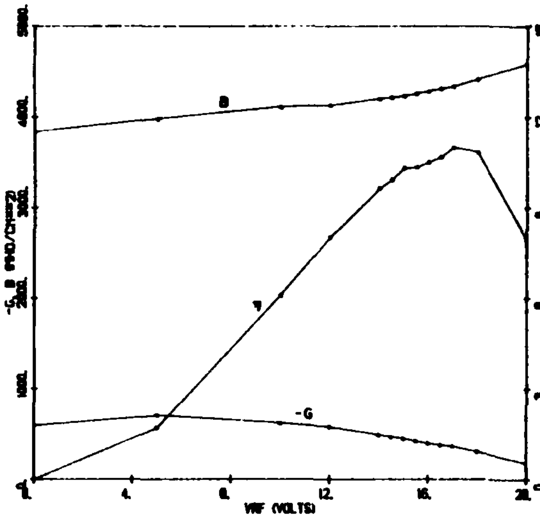

(a)

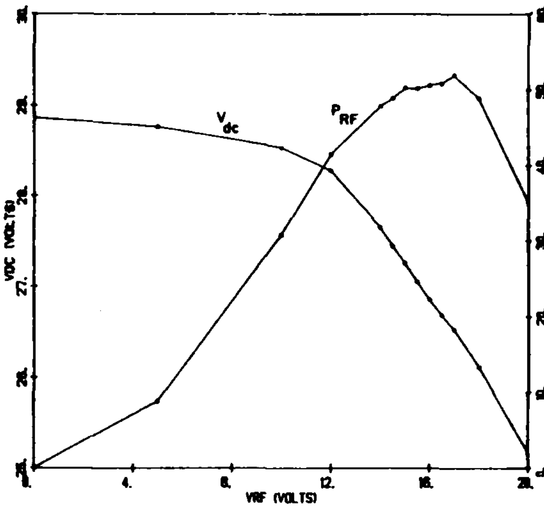

(b)

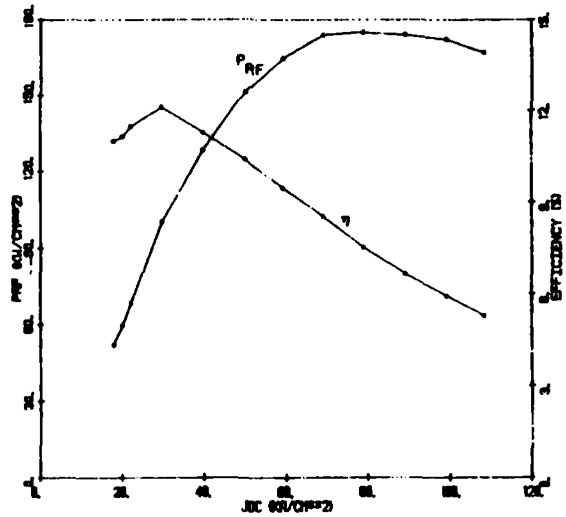

(c)

Figure 24. Large-Signal Results for the Profile of Figure 23a at $f = 60$ GHz, $T = 500°K$ and (a and b) $J_{dc} = 18$ kA/cm^2, (c) $V_{RF} = 17$ V.

TABLE 25

LARGE-SIGNAL RESULTS FOR THE GaAs UNIFORM DOUBLE-DRIFT PROFILE IN FIGURE 23a AND POWER LEVELS OBTAINED BY MATCHING TO 1-Ω RESISTANCE (f = 60 GHz, V_{RF} = 17 V)

J_{dc} (kA/cm^2)	$-G_D$ (mho/cm^2)	B_D (mho/cm^2)	A x10^{-4}(cm^2)	I_{dc} (A)	V_{dc} (V)	η (Percent)	P_{dc} (W)	P_{RF} (W)	P_{diss} (W)	θ_R (°C/W)	D (mils)
17.8	360	4340	0.19	0.338	26.5	11	8.96	0.986	7.97	28.2	1.94
20	412	4240	0.227	0.454	26.7	11.1	12.1	1.34	10.8	20.8	2.12
22.2	474	4150	0.272	0.604	26.9	11.5	16.2	1.86	14.3	15.7	2.32
29.6	694	3870	0.449	1.33	28	12.1	37.2	4.5	32.7	6.88	2.98
39.8	888	3500	0.681	2.71	28.6	11.3	77.5	8.76	68.7	3.28	3.66
49.9	1040	3130	0.956	4.77	29.1	10.4	139	14.4	125	1.8	4.34
59.1	1140	2790	1.25	7.39	29.4	9.46	217	20.5	196	1.15	4.97
69	1220	2440	1.64	11.3	29.5	8.53	333	28.4	305	0.738	5.69
78.8	1210	2110	2.04	16.1	29.5	7.53	475	35.8	439	0.512	6.34
89	1200	1780	2.6	23.1	29.4	6.65	679	45.2	634	0.355	7.16
99	1190	1490	3.27	32.4	29.3	5.92	949	56.2	893	0.252	8.03
108	1150	1260	3.95	42.7	29.1	5.28	1242	65.6	1180	0.191	8.83

Cont.

Table 25 Cont.

J_{dc} (kA/cm^2)	$-G_D$ (mho/cm^2)	B_D (mho/cm^2)	A x10^{-4}(cm^2)	I_{dc} (A)	V_{dc} (V)	η (Percent)	P_{dc} (W)	P_{RF} (W)	P_{diss} (W)	θ_R (°C/W)	D (mils)
125	975.1	914.9	5.45	68.1	28.3	4.01	1928	76.8	1851	0.122	10.4
163	250	182.8	26.1	425	25.4	0.87	1.08 x 10^4	94.2	1.07 x 10^4	0.021	22.7
171	137	64.23	59.8	1023	24.9	0.46	2.55 x 10^4	118	2.54 x 10^4	8.87 x 10^{-3}	34.4
172	87.8	37.8	96.1	1653	24.8	0.30	4.1 x 10^4	122	4.09 x 10^4	5.5 x 10^{-3}	43.5

AD-A123 380 CAPABILITIES AND POTENTIAL OF MILLIMETER-WAVE IMPATT DEVICES(U) MICHIGAN UNIV ANN ARBOR ELECTRON PHYSICS LAB R K MAINS ET AL. NOV 82 TR-159 AFWAL-TR-82-1141 2/2

UNCLASSIFIED F33615-81-K-1429 F/G 9/1 NL

END

FILMED

DTIC

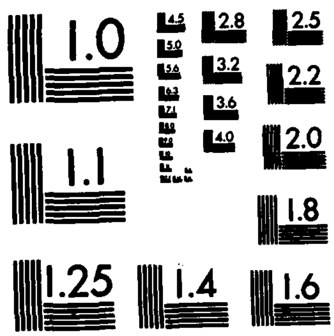
1.0
4.5
5.0
5.6
6.3
7.1
2.8
3.2
3.6
4.0
2.5
2.2
2.0
1.1
1.8
1.25
1.4
1.6

TABLE 26

CW RESULTS FOR THE PROFILE IN FIGURE 23a AT 60 GHz TAKING INTO ACCOUNT THE THERMAL-RESISTANCE EXPRESSIONS

D(CM) (mils)	θ(CM) (°C/W)	P_{RF}(CM) (W)	D(DM) (mils)	θ(DM) (°C/W)	P_{RF}(DM) (W)	D(CR) (mils)	θ(CR) (°C/W)	P_{RF}(CR) (W)	D(DR) (mils)	θ(DR) (°C/W)	P_{RF}(DR) (W)	J_{dc} (kA/cm^2)
0.85	146	0.19	1.94	24.6	0.986	1.54	44.3	0.628	1.94	19.7	0.986	17.8
0.659	215	0.131	1.98	23.9	1.18	1.2	65	0.432	2.12	16.9	1.34	20
0.511	321	0.091	1.53	35.7	0.819	0.93	97.2	0.301	2.32	14.6	1.8	22.2
0.152	2620	0.0118	0.457	291	0.106	0.277	793	0.039	0.832	88.1	0.351	29.6

low values of dc current density. Comparison with the hybrid double-drift CW powers in Table 24 shows that the hybrid is capable of generating considerably more power than the uniform double-drift at 60 GHz. However, comparison of electronic RF powers indicates that the uniform double-drift can generate more power in pulsed operation.

The next structure considered is the GaAs double Read profile of Figure 25a. The dc solution for this structure at $T = 500°K$ and $J_{dc} = 15$ kA/cm^2 is given in Figure 25b. Large-signal results at $f = 60$ GHz and $J_{dc} = 15$ kA/cm^2 are plotted in Figure 26a and b, and results vs. J_{dc} at $V_{RF} = 17.5$ V are plotted in Figure 26c. The best efficiency obtained was $\eta = 13.85$ percent at $J_{dc} = 14.8$ kA/cm^2 and $V_{RF} = 17.5$ V; the maximum electronic RF power density was $P_{RF} = 82.8$ kW/cm^2 at $J_{dc} = 30.9$ kA/cm^2 and $V_{RF} = 17.5$ V. Table 27 presents large-signal results vs. J_{dc} and powers obtained when the diode is matched to 1 Ω. If $\ell_2 = 0.42 \times 10^{-4}$ cm from Figure 25a and $\ell_1 = 0.5 \times 10^{-4}$ cm, then the thermal-resistance expressions are

$$\theta(CM) = \frac{64.27}{d_m} + \frac{50.82}{d_m^2} , \tag{52}$$

$$\theta(DM) = \frac{21.42}{d_m} + \frac{50.82}{d_m^2} , \tag{53}$$

$$\theta(CR) = \frac{35.35}{d_m} + \frac{50.82}{d_m^2} \tag{54}$$

and

$$\theta(DR) = \frac{11.78}{d_m} + \frac{50.82}{d_m^2} . \tag{55}$$

Solving Equations 13 through 15 and 52 through 55 yields the CW powers listed in Table 28. Comparing these powers with the

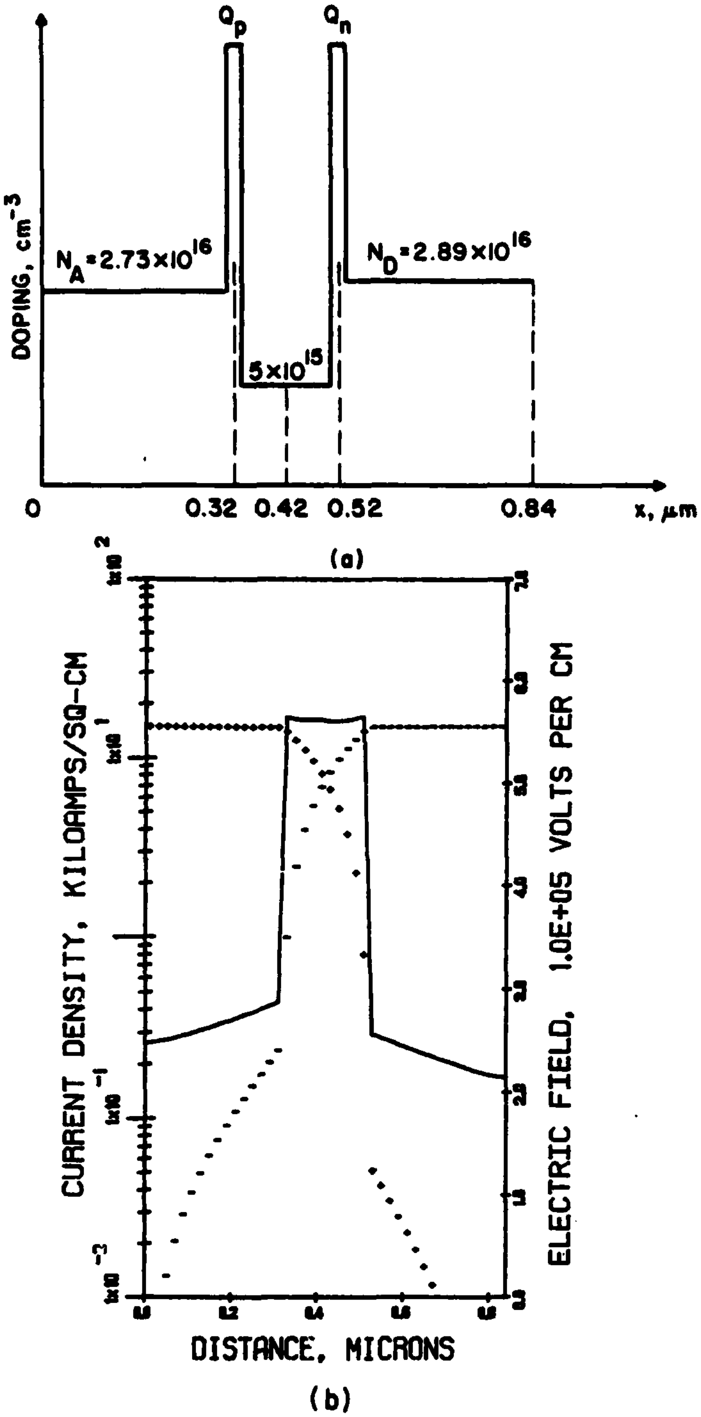

Figure 25. (a) Double-Read GaAs Doping Profile for 60-GHz Operation and (b) Dc Solution at T = 500°K and J_{dc} = 15 kA/cm². (X_A = 0.22 μm, J_{dc} = 15 kA/cm², E(LHS) = 2.48 x 10^5 V/cm, E_{to}(LHS) = 2.87 x 10^5 V/cm, E_{max} = 5.649 x 10^5 V/cm, E_{to}(RHS) = 2.57 x 10^5 V/cm, E(RHS) = 2.158 x 10^5 V/cm, Q_n = 2.16 x 10^{12} cm^{-2} and Q_p = 1.948 x 10^{12} cm^{-2})

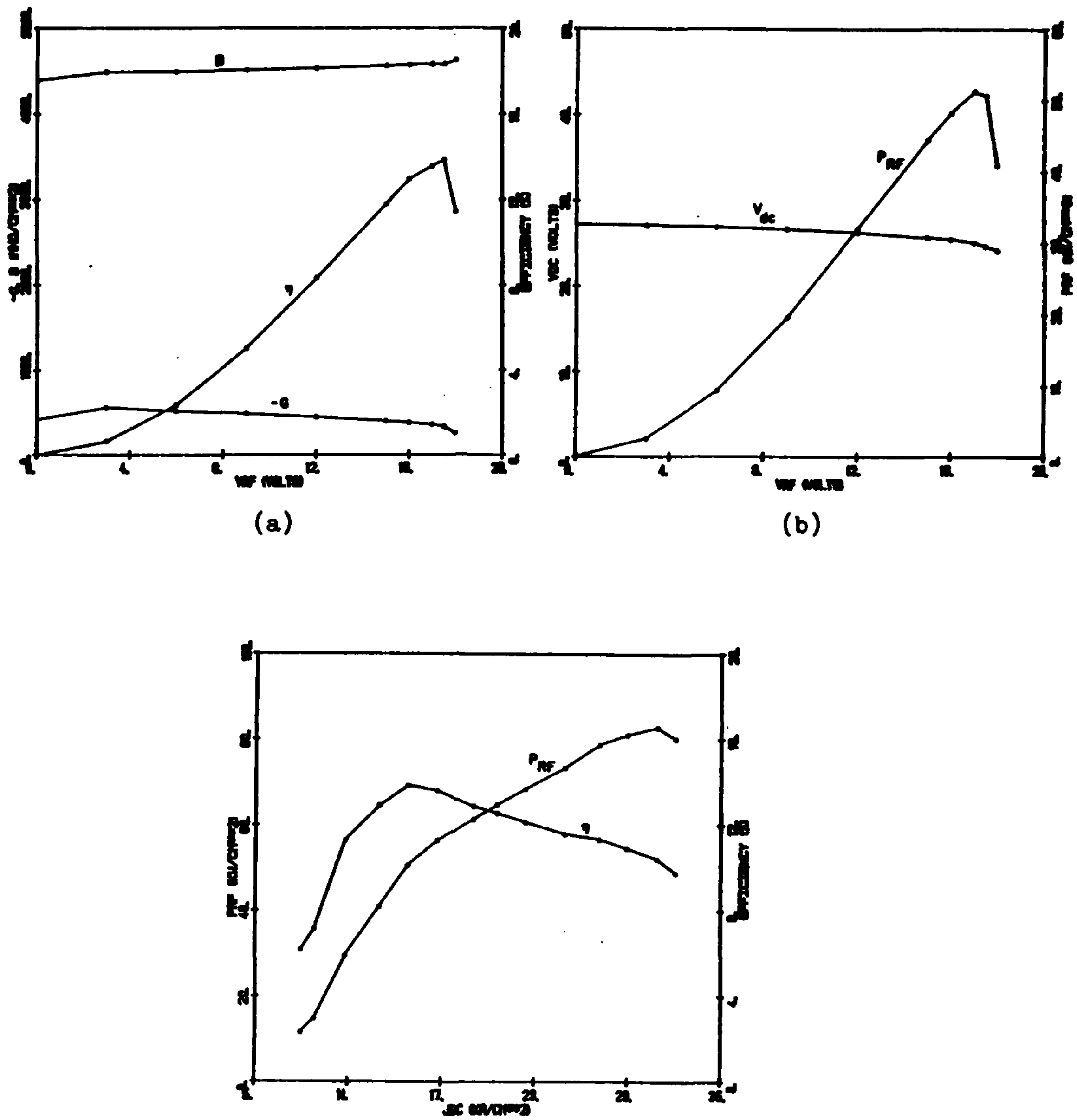

(a) (b)

(c)

Figure 26. Large-Signal Results for the Profile of Figure 25a at $f = 60$ GHz, $T = 500°K$ and (a and b) $J_{dc} = 15$ kA/cm^2, (c) $V_{RF} = 17.5$ V.

TABLE 27

LARGE-SIGNAL RESULTS FOR THE DOUBLE READ GaAs PROFILE IN FIGURE 25a AND POWER LEVELS

OBTAINED BY MATCHING TO 1-Ω RESISTANCE (f = 60 GHz, V_{RF} = 17.5 V)

J_{dc} (kA/cm^2)	$-G_D$ (mho/cm^2)	B_D (mho/cm^2)	A $\times 10^{-4}$ (cm^2)	I_{dc} (A)	V_{dc} (V)	η (Percent)	P_{dc} (W)	P_{RF} (W)	P_{diss} (W)	θ_R (°C/W)	D (mils)
7.92	75.6	4890	0.0316	0.025	23.6	6.17	0.59	0.0364	0.554	406	0.79
8.77	97	4860	0.041	0.036	23.7	7.15	0.853	0.061	0.792	284	0.9
10.8	192	4740	0.0853	0.0921	24.1	11.3	2.22	0.251	1.97	114	1.3
13	268	4650	0.124	0.161	24.4	12.9	3.93	0.507	3.42	65.8	1.56
14.8	331	4580	0.157	0.232	24.7	13.8	5.73	0.791	4.94	45.5	1.76
16.7	369	4520	0.179	0.299	24.8	13.6	7.42	1.01	6.41	35.1	1.88
19	401	4460	0.20	0.38	25	12.9	9.5	1.22	8.28	27.2	1.99
20.6	423	4400	0.216	0.445	25.1	12.6	11.2	1.41	9.79	23	2.06
22.4	447	4350	0.234	0.524	25.2	12.2	13.2	1.61	11.6	19.4	2.15
24.9	479	4270	0.259	0.645	25.4	11.6	16.4	1.9	14.5	15.5	2.26
27.2	515	4200	0.288	0.783	25.5	11.4	20	2.28	17.7	12.7	2.38
29	530	4140	0.304	0.882	25.6	10.9	22.6	2.46	20.1	11.2	2.45

Cont.

Table 27 Cont.

J_{dc} (kA/cm^2)	$-G_D$ (mho/cm^2)	B_D (mho/cm^2)	A x 10^{-4} (cm^2)	I_{dc} (A)	V_{dc} (V)	η (Percent)	P_{dc} (W)	P_{RF} (W)	P_{diss} (W)	θ_R (°C/W)	D (mils)
30.9	541	4070	0.321	0.992	25.6	10.4	25.4	2.64	22.8	9.87	2.52
32.1	524	4040	0.316	1.01	25.5	9.79	25.8	2.52	23.3	9.66	2.5

TABLE 28

CW RESULTS FOR THE PROFILE IN FIGURE 25a AT 60 GHz TAKING INTO ACCOUNT THE THERMAL-RESISTANCE EXPRESSIONS

D(CM) (mils)	θ(CM) (°C/W)	P_{RF}(CM) (W)	D(DM) (mils)	θ(DM) (°C/W)	P_{RF}(DM) (W)	D(CR) (mils)	θ(CR) (°C/W)	P_{RF}(CR) (W)	D(DR) (mils)	θ(DR) (°C/W)	P_{RF}(DR) (W)	J_{dc} (kA/cm^2)
0.79	163	0.0364	0.79	108	0.0364	0.79	126	0.0364	0.79	96.3	0.0364	7.92
0.9	134	0.061	0.9	86.5	0.061	0.9	102	0.061	0.9	75.8	0.061	8.77
1.3	79.5	0.251	1.3	46.5	0.251	1.3	57.3	0.251	1.3	39.1	0.251	10.8
1.56	62.1	0.507	1.56	34.6	0.507	1.56	43.5	0.507	1.56	28.4	0.507	13
1.4	71.7	0.502	1.76	28.6	0.791	1.76	36.5	0.791	1.76	23.1	0.791	14.8
1.14	95.5	0.371	1.88	25.8	1.01	1.88	33.2	1.01	1.88	20.6	1.01	16.7
0.879	139	0.24	1.99	23.6	1.22	1.6	42	0.793	1.99	18.8	1.22	19
0.738	180	0.18	2.06	22.4	1.41	1.34	54.6	0.594	2.06	17.7	1.41	20.6
0.603	246	0.127	1.81	27.4	1.14	1.1	74.5	0.42	2.15	16.5	1.61	22.4
0.445	401	0.0736	1.33	44.6	0.662	0.809	121	0.243	2.26	15.2	1.9	24.9
0.333	650	0.0446	1	72.2	0.401	0.606	196	0.147	1.82	21.8	1.32	27.2
0.254	1040	0.0264	0.761	116	0.238	0.461	315	0.0872	1.38	35	0.785	29
0.184	1850	0.0141	0.552	206	0.127	0.334	560	0.0466	1	62.2	0.42	30.9
0.145	2860	0.0085	0.435	318	0.0767	0.263	866	0.0282	0.79	96.3	0.254	32.1

expected CW powers for the GaAs hybrid in Table 24 shows that the CW power levels are comparable. Furthermore, since the hybrid can generate higher peak electronic powers, there is no advantage to fabricating a double Read structure instead of the hybrid structure at 60 GHz.

Figure 27a shows an InP hybrid structure simulated at 60 GHz, and Figure 27b shows the dc solution at T = 500°K and J_{dc} = 18 kA/cm^2. Large-signal results vs. V_{RF} at 40 GHz are plotted in Figure 28a and b, and results vs. J_{dc} at V_{RF} = 23 V are plotted in Figure 28c. The best efficiency obtained was η = 19.31 percent at J_{dc} = 15.8 kA/cm^2 and V_{RF} = 23 V, and the maximum RF power density was P_{RF} = 173 kW/cm^2 at J_{dc} = 50.4 kA/cm^2 and V_{RF} = 23 V. Table 29 lists the large-signal results vs. J_{dc}. From Figure 27a, ℓ_2 equals 0.46 x 10^{-4} cm. Using ℓ_1 = 0.5 x 10^{-4} cm as before and reducing the last two terms in Equation 1 by the factor 0.8 to account for the higher thermal conductivity of InP obtains the following thermal-resistance expressions:

$$\theta(CM) = \frac{64.27}{d_m} + \frac{41.71}{d_m^2} , \qquad (56)$$

$$\theta(DM) = \frac{21.42}{d_m} + \frac{41.71}{d_m^2} , \qquad (57)$$

$$\theta(CR) = \frac{35.35}{d_m} + \frac{41.71}{d_m^2} \qquad (58)$$

and

$$\theta(DR) = \frac{11.78}{d_m} + \frac{41.71}{d_m^2} . \qquad (59)$$

Solving Equations 13 through 15 and 56 through 59 yields the expected CW powers given in Table 30 for the hybrid InP structure.

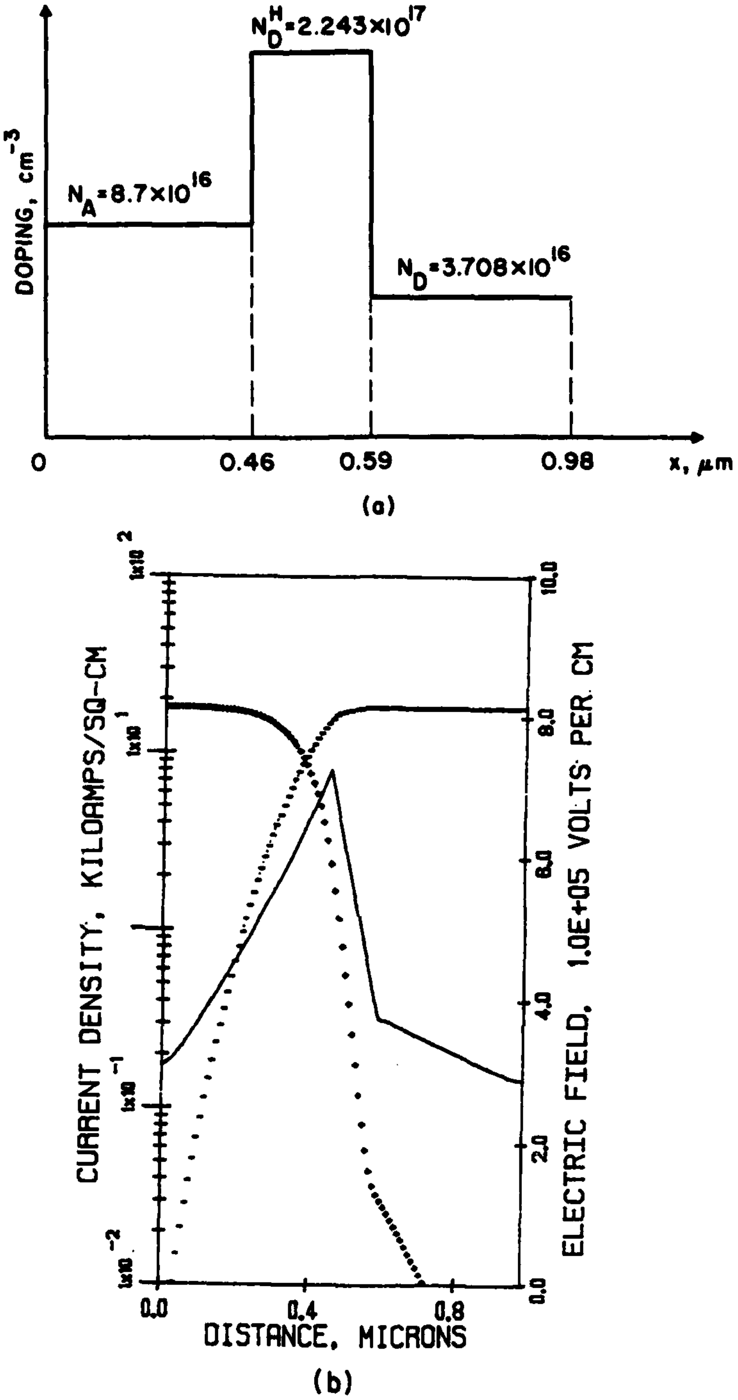

Figure 27. (a) InP Hybrid Doping Profile for 60-GHz Operation and (b) Dc Solution at T = 500°K and J_{dc} = 18 kA/cm². (X_A = 0.28 µm, J_{dc} = 18 kA/cm², E(LHS) = 3.12 x 10^5 V/cm, E_{max} = 7.26 x 10^5 V/cm, E_{to} = 3.77 x 10^5 V/cm and E(RHS) = 2.905 x 10^5 V/cm)

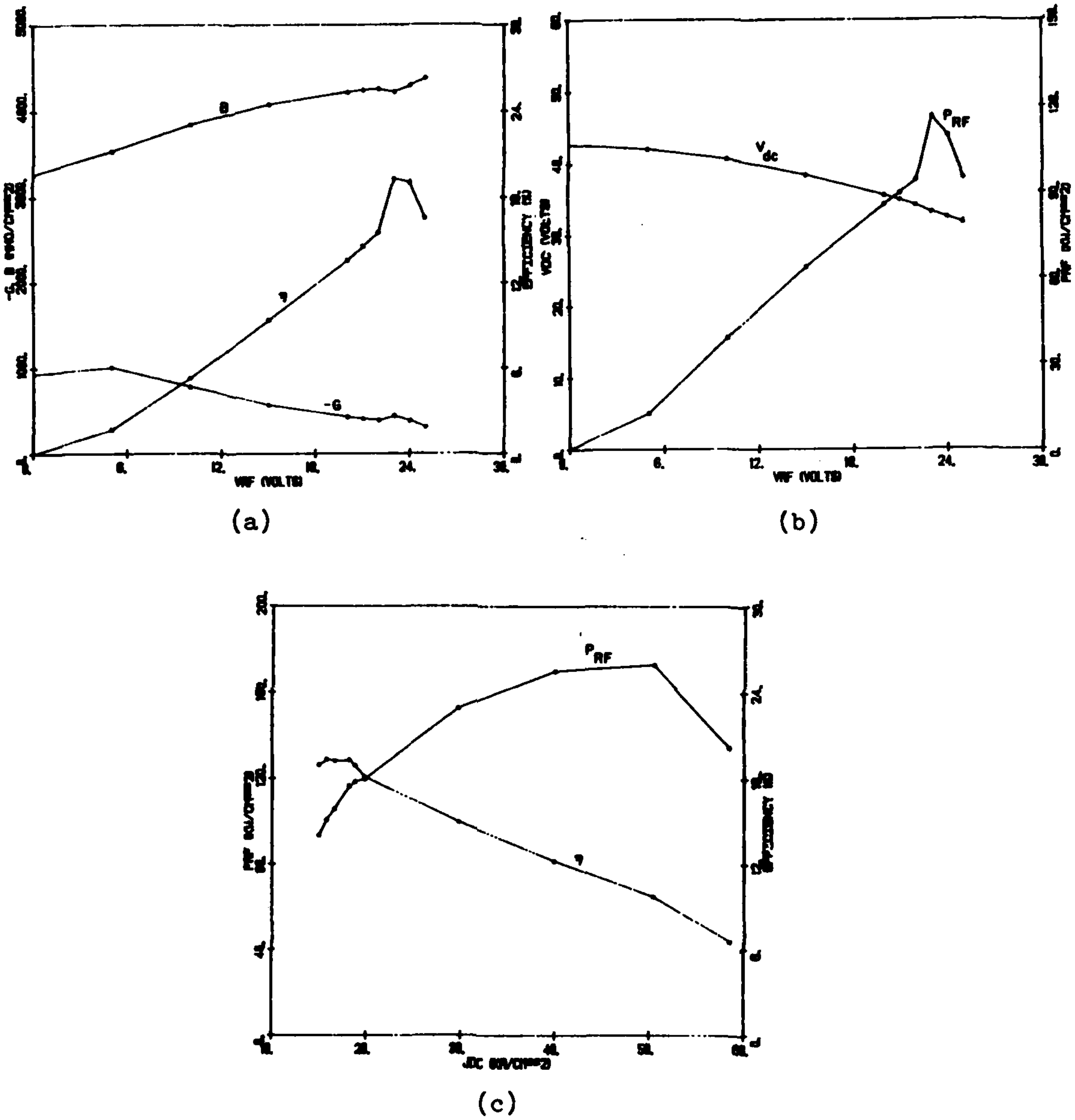

Figure 28. Large-Signal Results for the Profile of Figure 27a at $f = 60$ GHz, $T = 500°K$ and (a and b) $J_{dc} = 18$ kA/cm^2, (c) $V_{RF} = 23$ V.

TABLE 29

LARGE-SIGNAL RESULTS FOR THE InP HYBRID PROFILE IN FIGURE 27a AND POWER LEVELS

OBTAINED BY MATCHING TO 1-Ω RESISTANCE (f = 60 GHz, V_{RF} = 23 V)

J_{dc} (kA/cm^2)	$-G_D$ (mho/cm^2)	B_D (mho/cm^2)	A $\times 10^{-4}$ (cm^2)	I_{dc} (A)	V_{dc} (V)	η (Percent)	P_{dc} (W)	P_{RF} (W)	P_{diss} (W)	θ_R (°C/W)	D (mils)
15	352	4350	0.185	0.278	32.9	18.9	9.15	1.73	7.42	30.3	1.91
15.8	381	4310	0.204	0.322	33	19.3	10.6	2.04	8.56	26.3	2.01
16.6	399	4280	0.216	0.358	33.1	19.2	11.8	2.26	9.54	23.6	2.06
18.2	440	4230	0.243	0.442	33.2	19.3	14.7	2.84	11.9	18.9	2.19
18.8	448	4210	0.25	0.47	33.4	18.9	15.7	2.97	12.7	17.7	2.22
19.8	453	4190	0.255	0.505	33.4	18.1	16.9	3.06	13.8	16.3	2.24
29.8	577	3880	0.375	1.12	34.3	14.9	38.4	5.72	32.7	6.88	2.72
39.9	642	3540	0.496	1.98	34.9	12.2	69.1	8.43	60.7	3.71	3.13
50.4	653	3180	0.62	3.12	35.3	9.69	110	10.6	99.4	2.26	3.5
58.4	509	2930	0.576	3.36	35.1			7.73	110	2.04	3.37

TABLE 30

CW RESULTS FOR THE PROFILE IN FIGURE 27a AT 60 GHz TAKING INTO ACCOUNT THE THERMAL-RESISTANCE EXPRESSIONS

D(CM) (mils)	θ(CM) (°C/W)	P_{RF}(CM) (W)	D(DM) (mils)	θ(DM) (°C/W)	P_{RF}(DM) (W)	D(CR) (mils)	θ(CR) (°C/W)	P_{RF}(CR) (W)	D(DR) (mils)	θ(DR) (°C/W)	P_{RF}(DR) (W)	J_{dc} (kA/cm^2)
1.08	95.6	0.548	1.91	22.6	1.73	1.91	29.9	1.73	1.91	17.6	1.73	15
0.993	107	0.503	2.01	21	2.04	1.8	32.4	1.66	2.01	16.2	2.04	15.8
0.907	122	0.44	2.06	20.2	2.26	1.65	36.8	1.45	2.06	15.5	2.26	16.6
0.768	154	0.348	2.19	18.5	2.84	1.4	46.7	1.15	2.19	14.1	2.84	18.2
0.708	174	0.301	2.12	19.3	2.71	1.29	52.7	0.996	2.22	13.8	2.97	18.8
0.626	209	0.238	1.88	23.2	2.14	1.14	63.2	0.787	2.24	13.6	3.06	19.8
0.145	2420	0.0163	0.436	269	0.146	0.264	732	0.0538	0.792	81.3	0.485	29.8
--	--	--	--	--	--	--	--	--	--	--	--	39.9
--	--	--	--	--	--	--	--	--	--	--	--	50.4
--	--	--	--	--	--	--	--	--	--	--	--	58.4

Comparison with the CW results for the GaAs hybrid in Table 24 shows that the InP hybrid is expected to have better performance at 60 GHz.

Figure 29a shows the Si hybrid doping profile that was simulated at 60 GHz, and Figure 29b gives the dc solution at $T = 500°K$ and $J_{dc} = 18\ kA/cm^2$. Large-signal results vs. V_{RF} at $f = 60$ GHz and $J_{dc} = 18\ kA/cm^2$ are plotted in Figure 30a and b; results vs. J_{dc} at $V_{RF} = 22$ V are plotted in Figure 30c. Large-signal results vs. J_{dc} are listed in Table 31 along with electronic RF powers obtained by matching the device to 1-Ω resistance. The best efficiency obtained was $\eta = 18.3$ percent at $J_{dc} = 14.1\ kA/cm^2$ and $V_{RF} = 22$ V, and the best RF power density was $P_{RF} = 128\ kW/cm^2$ at $J_{dc} = 24.8\ kA/cm^2$ and $V_{RF} = 22$ V. Using $\ell_2 = 0.84 \times 10^{-4}$ cm and $\ell_1 = 0.5 \times 10^{-4}$ cm as before and reducing the final two terms in Equation 1 by the factor 1/3 due to the higher thermal conductivity of Si obtains the following thermal-resistance expressions:

$$\theta(CM) = \frac{64.27}{d_m} + \frac{21.57}{d_m^2} , \tag{60}$$

$$\theta(DM) = \frac{21.42}{d_m} + \frac{21.57}{d_m^2} , \tag{61}$$

$$\theta(CR) = \frac{35.35}{d_m} + \frac{21.57}{d_m^2} \tag{62}$$

and

$$\theta(DR) = \frac{11.78}{d_m} + \frac{21.57}{d_m^2} . \tag{63}$$

Solving Equations 13 through 15 and 60 through 63 yields the CW powers listed in Table 32 for the Si hybrid diode. The Si hybrid can generate more CW power than GaAs and InP due to

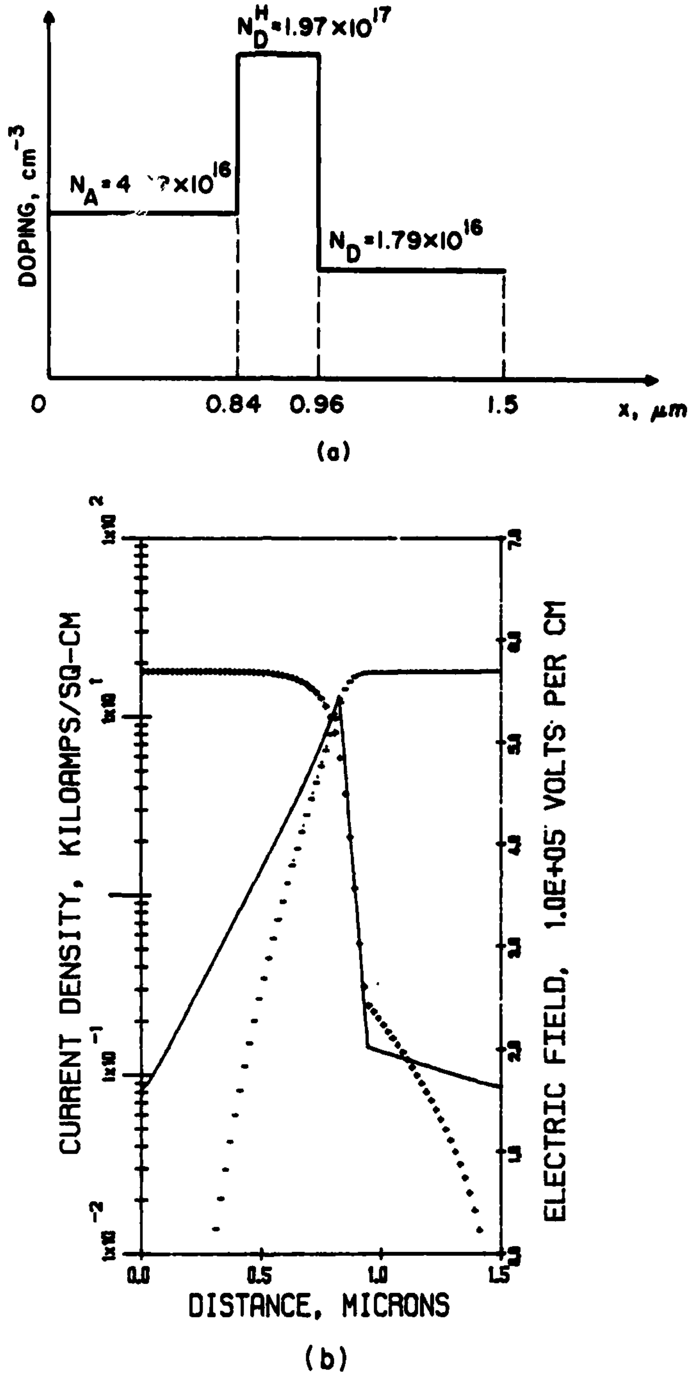

Figure 29. (a) Si Hybrid Doping Profile for 60-GHz Operation and (b) Dc Solution at T = 500°K and J_{dc} = 18 kA/cm². (X_A = 0.34 μm, J_{dc} = 18 kA/cm², E(LHS) = 1.62 x 10^5 V/cm, E_{max} = 5.46 x 10^5 V/cm, E_{to} = 2.02 x 10^5 V/cm and E(RHS) = 1.64 x 10^5 V/cm)

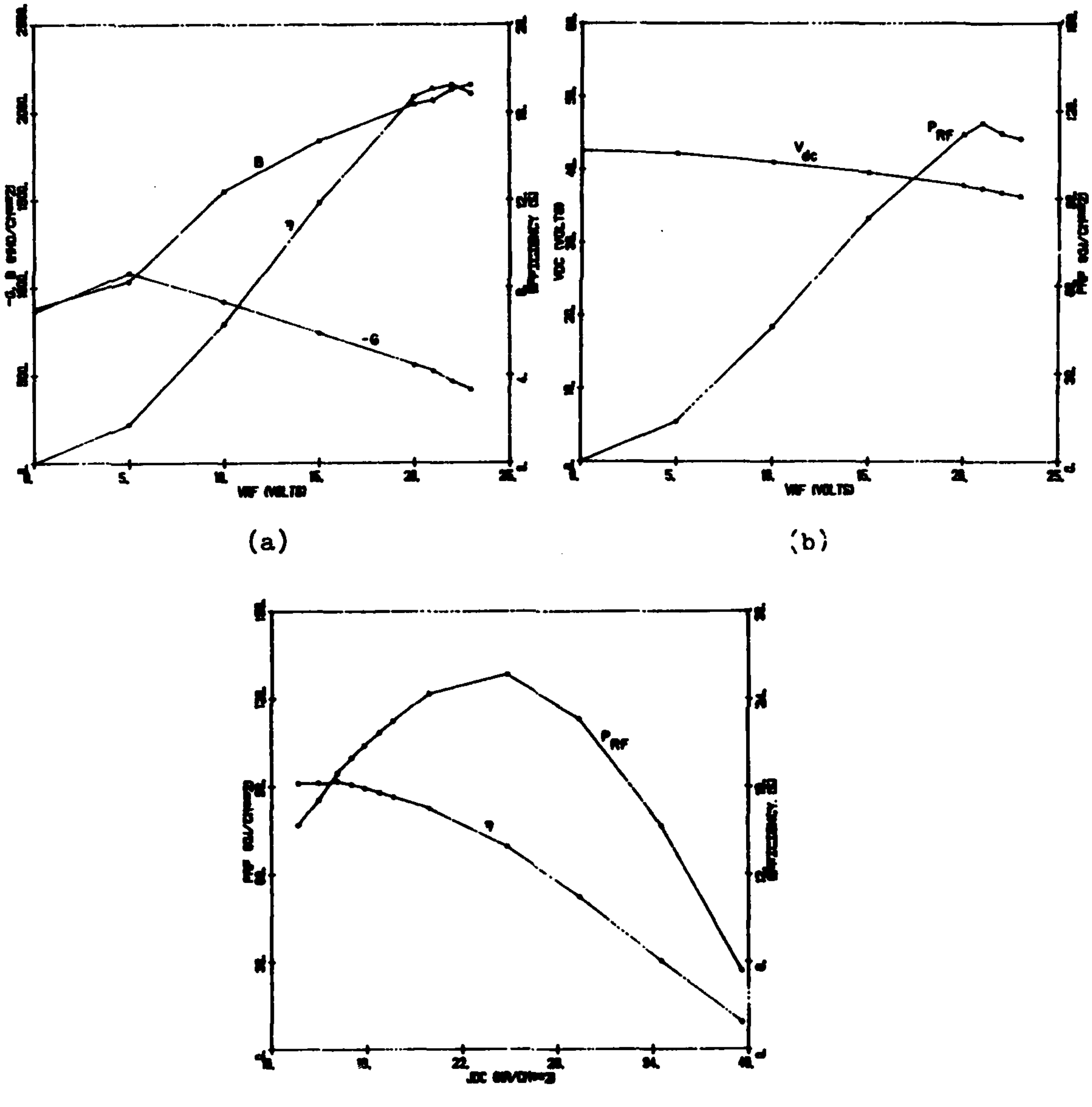

Figure 30. Large-Signal Results for the Profile of Figure 29a at $T = 500^{\circ}K$, $f = 60$ GHz and (a and b) $J_{dc} = 18$ kA/cm^2, (c) $V_{RF} = 22$ V.

TABLE 31

LARGE-SIGNAL RESULTS FOR THE Si HYBRID PROFILE IN FIGURE 29a AND POWER LEVELS

OBTAINED BY MATCHING TO 1-Ω RESISTANCE (f = 60 GHz, V_{RF} = 22 V)

J_{dc} (kA/cm²)	$-G_D$ (mho/cm²)	B_D (mho/cm²)	A x 10^{-4} (cm²)	I_{dc} (A)	V_{dc} (V)	η (Percent)	P_{dc} (W)	P_{RF} (W)	P_{diss} (W)	θ_R (°C/W)	D (mils)
7.82	185	2540	0.285	0.223	35.4	16.1	7.89	1.27	6.62	34	2.37
8.46	209	2510	0.329	0.278	35.5	16.8	9.87	1.66	8.21	27.4	2.55
9.06	233	2490	0.372	0.337	35.7	17.4	12	2.09	9.91	22.7	2.71
10.9	294	2410	0.499	0.544	35.9	18.1	19.5	3.53	16	14.1	3.41
11.3	306	2390	0.527	0.596	36	18.2	21.4	3.89	17.5	12.8	3.22
11.5	314	2380	0.545	0.627	36	18.3	22.6	4.14	18.5	12.2	3.28
11.7	317	2380	0.55	0.644	36.1	18.2	23.2	4.22	19	11.8	3.29
12.9	352	2330	0.634	0.818	36.2	18.2	29.6	5.39	24.2	9.3	3.54
14.1	391	2280	0.731	1.03	36.5	18.3	37.6	6.88	30.7	7.33	3.8
15	412	2240	0.794	1.19	36.6	18.1	43.6	7.89	35.7	6.3	3.96
15.8	429	2210	0.846	1.34	36.6	17.9	49	8.77	40.2	5.6	4.09
16.8	448	2170	0.912	1.53	36.7	17.6	56.2	9.89	46.3	4.86	4.24

Cont.

Table 31 Cont.

J_{dc} (kA/cm^2)	$-G_D$ (mho/cm^2)	B_D (mho/cm^2)	A x 10^{-4} (cm^2)	I_{dc} (A)	V_{dc} (V)	η (Percent)	P_{dc} (W)	P_{RF} (W)	P_{diss} (W)	θ_R (°C/W)	D (mils)
17.7	464	2130	0.976	1.73	36.8	17.3	63.7	11	52.7	4.27	4.39
19.9	503	2030	1.15	2.29	37	16.5	84.7	14	70.7	3.18	4.76
24.8	530	1800	1.5	3.72	37.2	13.9	138	19.2	119	1.89	5.44
29.4	467	1580	1.72	5.06	37	10.4	187	19.4	168	1.34	5.83
34.5	316	1350	1.64	5.66	36.7	6	208	12.5	196	1.15	5.69
39.6	111	1170	0.803	3.18	36.6	1.86	116	2.16	114	1.97	3.98

TABLE 32

CW RESULTS FOR THE PROFILE IN FIGURE 29a AT 60 GHz TAKING INTO ACCOUNT THE THERMAL-RESISTANCE EXPRESSIONS

D(CM) (mils)	θ(CM) (°C/W)	P_{RF}(CM) (W)	D(DM) (mils)	θ(DM) (°C/W)	P_{RF}(DM) (W)	D(CR) (mils)	θ(CR) (°C/W)	P_{RF}(CR) (W)	D(DR) (mils)	θ(DR) (°C/W)	P_{RF}(DR) (W)	J_{dc} (kA/cm^2)
2.37	31	1.27	2.37	12.9	1.27	2.37	18.8	1.27	2.37	8.81	1.27	7.82
2.43	30.1	1.51	2.55	11.7	1.66	2.55	17.2	1.66	2.55	7.94	1.66	8.46
2.25	32.8	1.44	2.71	10.8	2.09	2.71	16	2.09	2.71	7.28	2.09	9.06
1.82	41.8	1.19	3.14	9.01	3.53	3.41	13.4	3.53	3.14	5.94	3.53	10.9
1.74	44	1.14	3.22	8.73	3.89	3.16	13.3	3.76	3.22	5.74	3.89	11.3
1.71	45	1.12	3.28	8.54	4.14	3.10	13.6	3.7	3.28	5.6	4.14	11.5
1.66	46.4	1.08	3.29	8.5	4.22	3.02	14	3.56	3.29	5.57	4.22	11.7
1.47	53.6	0.934	3.54	7.77	5.39	2.68	16.2	3.09	3.54	5.05	5.39	12.9
1.31	61.8	0.816	3.8	7.13	6.88	2.38	18.7	2.7	3.8	4.59	6.88	14.1
1.2	68.5	0.726	3.6	7.61	6.54	2.18	20.7	2.4	3.96	4.35	7.89	15
1.12	74.6	0.657	3.36	8.29	5.92	2.04	22.6	2.17	4.09	4.17	8.77	15.8
1.02	83.3	0.577	3.07	9.26	5.2	1.86	25.2	1.91	4.24	3.98	9.89	16.8

Cont.

Table 32 Cont.

D(CM) (mils)	θ(CM) (°C/W)	P_{RF}(CM) (W)	D(DM) (mils)	θ(DM) (°C/W)	P_{RF}(DM) (W)	D(CR) (mils)	θ(CR) (°C/W)	P_{RF}(CR) (W)	D(DR) (mils)	θ(DR) (°C/W)	P_{RF}(DR) (W)	J_{dc} (kA/cm^2)
0.947	91.9	0.512	2.84	10.2	4.6	1.72	27.8	1.69	4.39	3.8	11	17.7
0.788	116	0.382	2.36	12.9	3.44	1.43	35.2	1.26	4.3	3.91	11.4	19.9
0.534	196	0.185	1.6	21.8	1.67	0.971	59.3	0.613	2.91	6.58	5.52	24.8
0.373	327	0.0798	1.12	36.3	0.719	0.678	98.9	0.264	2.04	11	2.38	29.4
0.245	622	0.023	0.734	69.1	0.208	0.445	188	0.0763	1.34	20.9	0.687	34.5
0.15	1380	0.0031	0.45	154	0.0277	0.273	419	0.0102	0.819	46.6	0.0916	39.6

its higher thermal conductivity and because the device susceptance is much smaller for the Si diode.

In summary, the results at 60 GHz were that the highest efficiency, 19.3 percent, was obtained for the InP hybrid structure. The highest electronic RF power (matched to 1-Ω resistance) was obtained for the uniform GaAs double-drift diode. The maximum efficiency for the Si hybrid was 18.3 percent, only slightly less than for the InP hybrid; however, the electronic RF power at the maximum efficiency point was higher for the Si hybrid. In all cases, the expected CW RF power was highest for the Si hybrid diode.

SECTION 8.

RESULTS AT 94 GHz

Figure 31a shows the doping profile for a GaAs Read single-drift structure simulated at 94 GHz, and Figure 31b gives the dc solution at T = 500°K and J_{dc} = 25 kA/cm^2. Large-signal results at f = 94 GHz and J_{dc} = 25 kA/cm^2 are plotted in Figure 32a and b, and Figure 32c shows a plot of large-signal results vs. J_{dc} at V_{RF} = 6.5 V. Large-signal results vs. J_{dc} are listed in Table 33. The optimum efficiency for this structure was η = 4.04 percent at J_{dc} = 29.6 kA/cm^2, and maximum electronic RF power density was P_{RF} = 31.9 kW/cm^2 at J_{dc} = 71.2 kA/cm^2. When ℓ_2 = 0 and ℓ_1 = 0.5 x 10^{-4} cm, the thermal-resistance expressions are

$$\theta(CM) = \frac{64.27}{d_m} + \frac{37}{d_m^2} , \qquad (64)$$

$$\theta(DM) = \frac{21.42}{d_m} + \frac{37}{d_m^2} , \qquad (65)$$

$$\theta(CR) = \frac{35.35}{d_m} + \frac{37}{d_m^2} \qquad (66)$$

and

$$\theta(DR) = \frac{11.78}{d_m} + \frac{37}{d_m^2} . \qquad (67)$$

Solving Equations 13 through 15 and 64 through 67 gives the CW powers listed in Table 34.

Figure 33a gives the doping profile for a Si hybrid diode simulated at 94 GHz, and Figure 33b gives the dc solution at T = 500°K and J_{dc} = 25 kA/cm^2. Large-signal results vs. V_{RF} at

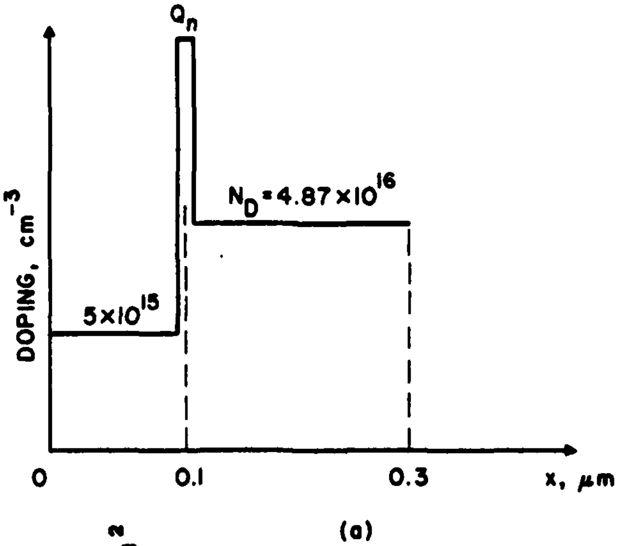

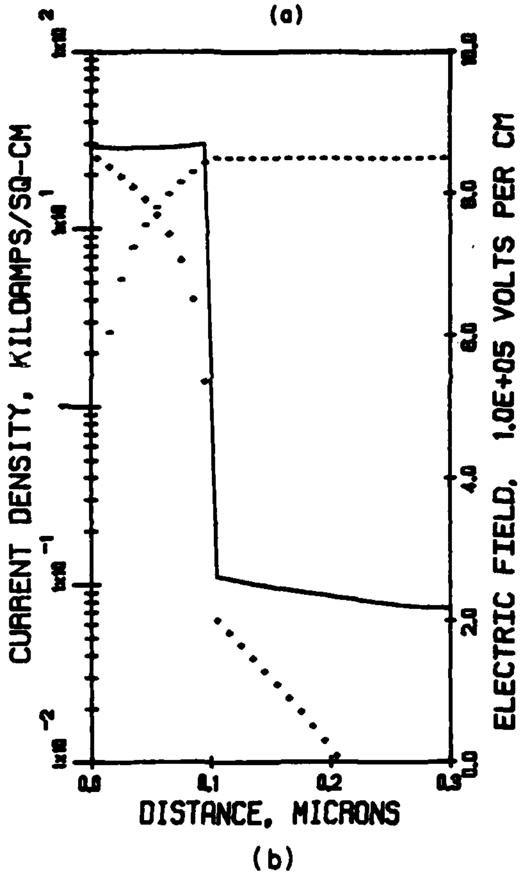

Figure 31. (a) GaAs Single-Drift Diode for 94-GHz Operation and (b) Dc Solution at T = 500°K and J_{dc} = 25 kA/cm². (X_A = 0.1 μm, J_{dc} = 25 kA/cm², E_{max} = 8.68 x 10^5 V/cm, E_{to} = 2.62 x 10^5 V/cm, E(RHS) = 2.18 x 10^5 V/cm and Q_n = 4.21 x 10^{12} cm^{-2})

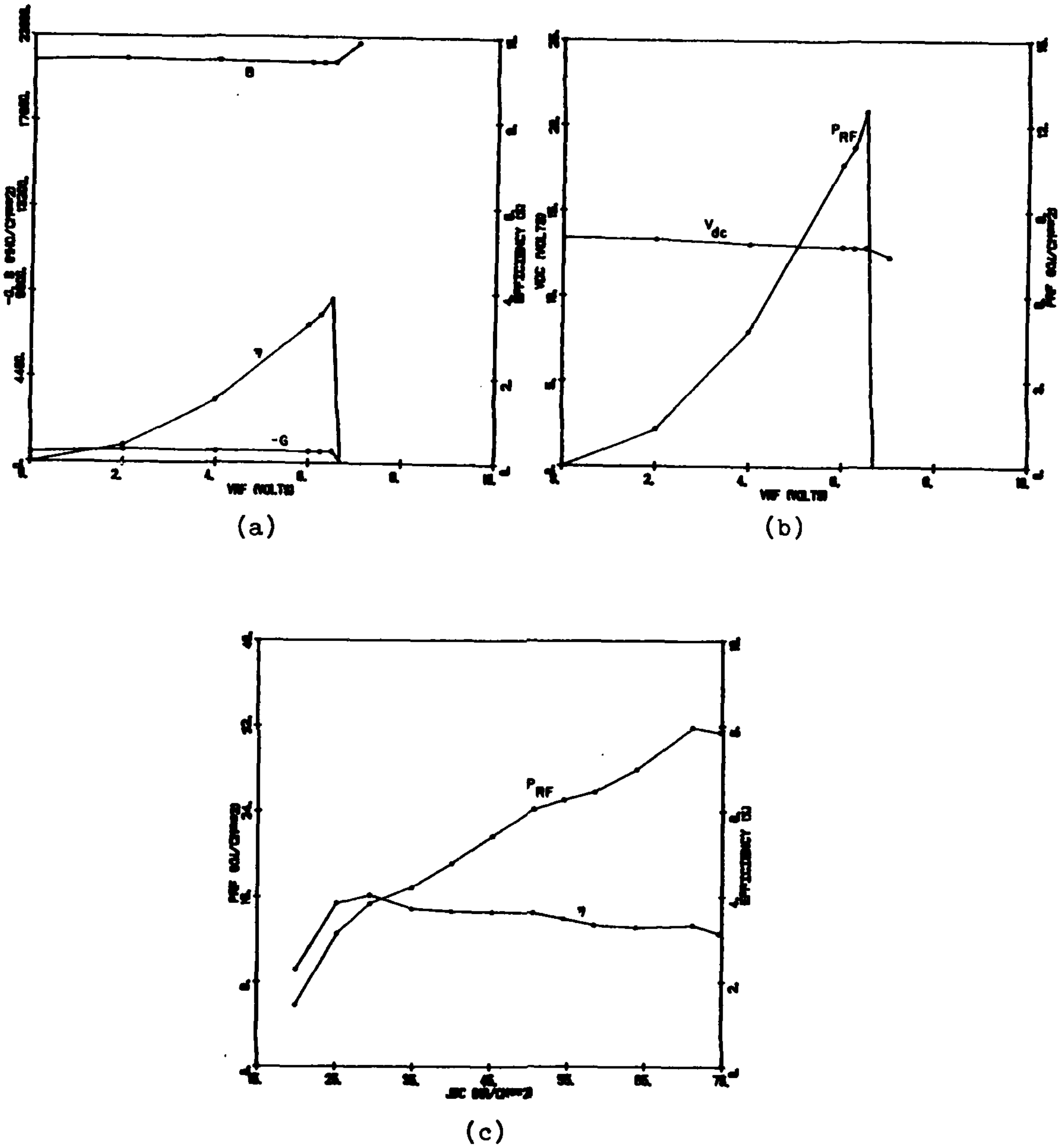

Figure 32. Large-Signal Results for the Profile of Figure 31a at $f = 94$ GHz, $T = 500°K$ and (a and b) $J_{dc} = 25\ kA/cm^2$, (c) $V_{RF} = 6.5$ V.

TABLE 33

LARGE-SIGNAL RESULTS FOR THE GaAs SINGLE-DRIFT READ PROFILE IN FIGURE 31a AND POWER LEVELS

OBTAINED BY MATCHING TO 1-Ω RESISTANCE (f = 94 GHz, V_{RF} = 6.5 V)

J_{dc} (kA/cm^2)	$-G_D$ (mho/cm^2)	B_D (mho/cm^2)	A x 10^{-4} (cm^2)	I_{dc} (A)	V_{dc} (V)	η (Percent)	P_{dc} (W)	P_{RF} (W)	P_{diss} (W)	θ_R (°C/W)	D (mils)
19.9	276	2.11×10^4	6.2×10^{-3}	0.0123	12.8	2.29	0.157	3.6×10^{-3}	0.153	1470	0.35
25.3	592	2.07×10^4	0.0138	0.0349	12.8	3.85	0.447	0.0172	0.43	523	0.522
29.6	726	2.04×10^4	0.0174	0.0515	12.8	4.04	0.659	0.0266	0.632	356	0.586
34.9	799	2.02×10^4	0.0196	0.0684	13	3.72	0.889	0.0331	0.856	263	0.622
40	905	1.99×10^4	0.0228	0.0912	13	3.66	1.18	0.0432	1.14	197	0.671
45.3	1030	1.96×10^4	0.0267	0.121	13.1	3.64	1.58	0.0575	1.52	148	0.726
50.6	1140	1.93×10^4	0.0305	0.154	13.2	3.62	2.03	0.0735	1.96	115	0.776
54.5	1190	1.9×10^4	0.0328	0.179	13.2	3.48	2.36	0.0821	2.28	98.7	0.804
58.5	1220	1.88×10^4	0.0344	0.201	13.2	3.33	2.65	0.0882	2.56	87.9	0.824
63.9	1320	1.84×10^4	0.0388	0.248	13.3	3.28	3.3	0.108	3.19	70.5	0.875
71.2	1510	1.8×10^4	0.0463	0.33	13.4	3.33	4.42	0.147	4.27	52.7	0.956
74.6	1490	1.77×10^4	0.0472	0.352	13.4	3.14	4.72	0.148	4.57	49.2	0.965

TABLE 34

CW RESULTS FOR THE PROFILE IN FIGURE 31a AT 94 GHz TAKING INTO

ACCOUNT THE THERMAL-RESISTANCE EXPRESSIONS

D(CM) (mils)	θ(CM) (°C/W)	P_{RF}(CM) (W)	D(DM) (mils)	θ(DM) (°C/W)	P_{RF}(DM) (W)	D(CR) (mils)	θ(CR) (°C/W)	P_{RF}(CR) (W)	D(DR) (mils)	θ(DR) (°C/W)	P_{RF}(DR) (W)	J_{dc} (kA/cm^2)
0.35	486	3.6×10^{-3}	0.35	363	3.6×10^{-3}	0.35	403	3.6×10^{-3}	0.35	336	3.6×10^{-3}	19.9
0.522	259	0.0172	0.522	177	0.0172	0.522	204	0.0172	0.522	158	0.0172	25.3
0.586	217	0.0266	0.586	144	0.0266	0.586	168	0.0266	0.586	128	0.0266	29.6
0.622	199	0.0331	0.622	130	0.0331	0.622	152	0.0331	0.622	114	0.0331	34.9
0.671	178	0.0432	0.671	114	0.0432	0.671	135	0.0432	0.671	99.7	0.0432	40
0.632	194	0.0438	0.726	99.7	0.0575	0.726	119	0.0575	0.726	86.4	0.0575	45.3
0.497	279	0.0303	0.776	89	0.0735	0.776	107	0.0735	0.776	76.6	0.0735	50.6
0.419	364	0.0223	0.804	83.9	0.0821	0.762	110	0.0737	0.804	71.9	0.0821	54.5
0.35	486	0.0159	0.824	80.5	0.0882	0.636	147	0.0527	0.824	68.8	0.0882	58.5
0.265	771	9.9×10^{-3}	0.794	85.6	0.0891	0.481	233	0.0327	0.875	61.8	0.108	63.9
0.173	1600	4.83×10^{-2}	0.52	178	0.0435	0.315	485	0.016	0.945	53.9	0.144	71.2
0.138	2420	3.02×10^{-3}	0.413	268	0.0272	0.25	731	9.98×10^{-3}	0.751	81.2	0.0898	74.6

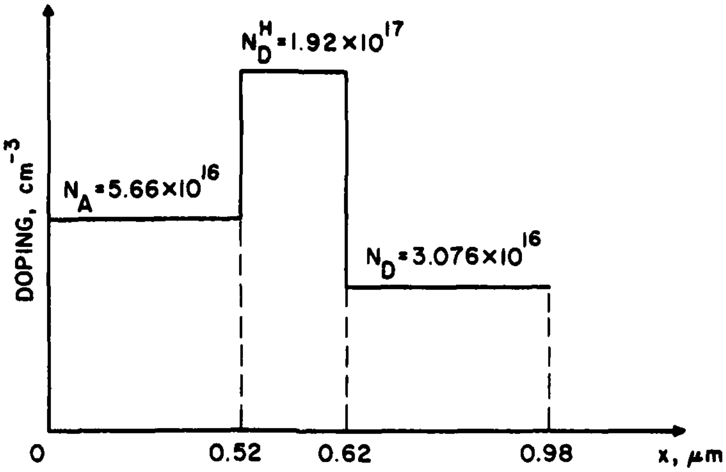

(a)

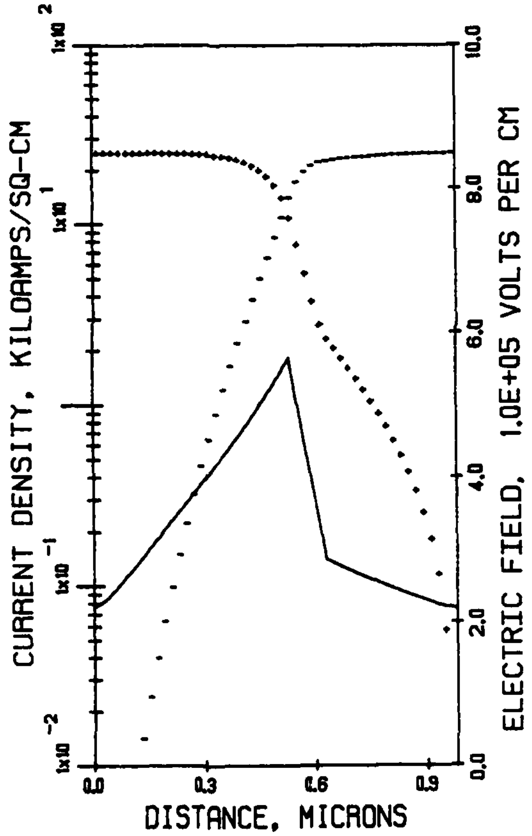

(b)

Figure 33. (a) Si Hybrid Structure for 94-GHz Operation and (b) Dc Solution at T = 500°K and J_{dc} = 25 kA/cm^2. (X_A = 0.38 μm, J_{dc} = 25 kA/cm^2, E(LHS) = 2.24 x 10^5 V/cm, E_{max} = 5.656 x 10^5 V/cm and E(RHS) = 2.208 x 10^5 V/cm)

$f = 94$ GHz and $J_{dc} = 25$ kA/cm² are plotted in Figure 34a and b, and large-signal results vs. J_{dc} at $V_{RF} = 19$ V are plotted in Figure 34c. Large-signal results vs. J_{dc} are listed in Table 35. Using $\ell_2 = 0.52 \times 10^{-4}$ cm from Figure 33a, assuming $\ell_1 = 0.5 \times 10^{-4}$ cm as before, and then reducing the final two terms of Equation 1 by 1/3 to account for higher thermal conductivity in Si obtains the thermal-resistance expressions as follows:

$$\theta(CM) = \frac{64.27}{d_m} + \frac{18.05}{d_m^2} , \tag{68}$$

$$\theta(DM) = \frac{21.42}{d_m} + \frac{18.05}{d_m^2} , \tag{69}$$

$$\theta(CR) = \frac{35.35}{d_m} + \frac{18.05}{d_m^2} \tag{70}$$

and

$$\theta(DR) = \frac{11.78}{d_m} + \frac{18.05}{d_m^2} . \tag{71}$$

Solving Equations 13 through 15 and 68 through 71 yields the expected CW powers listed in Table 36. These RF powers are quite high due to the high thermal conductivity of Si and the smaller susceptance values for Si IMPATTs.

Figure 35a shows a GaAs double Read structure simulated at 94 GHz, and Figure 35b shows the dc solution at $T = 500°K$ and $J_{dc} = 25$ kA/cm². Large-signal results for this structure vs. V_{RF} at $f = 94$ GHz and $J_{dc} = 25$ kA/cm² are plotted in Figure 36a and b, and large-signal results vs. J_{dc} at $V_{RF} = 11$ V are plotted in Figure 36c. Large-signal results vs. J_{dc} are listed in Table 37. From Figure 35a, the p-region length is $\ell_2 = 0.26 \times 10^{-4}$ cm, and when $\ell_1 = 0.5 \times 10^{-4}$ cm, the thermal-resistance expressions become

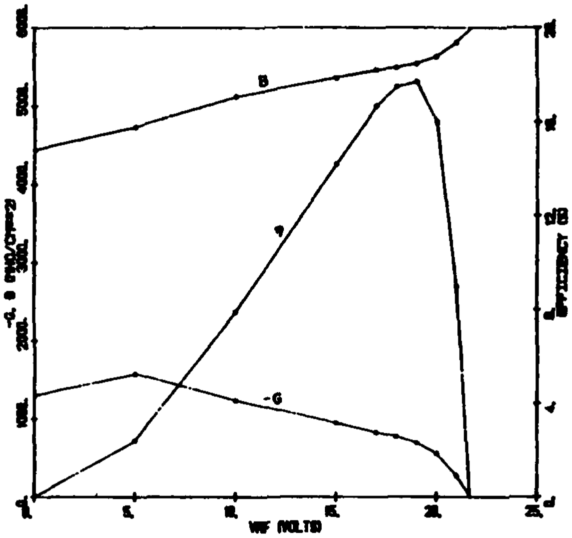

(a)

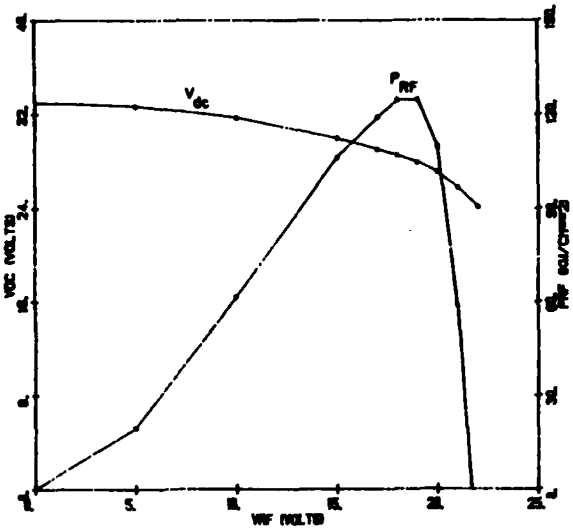

(b)

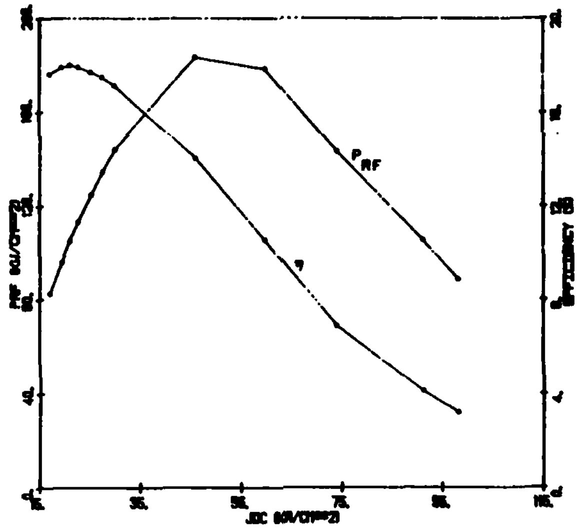

(c)

Figure 34. Large-Signal Results for the Profile of Figure 33a at $T = 500°K$, $f = 94$ GHz and (a and b) $J_{dc} = 25\ kA/cm^2$, (c) $V_{RF} = 19$ V.

TABLE 35

LARGE-SIGNAL RESULTS FOR THE Si HYBRID STRUCTURE IN FIGURE 33a AND POWER LEVELS

OBTAINED BY MATCHING TO 1-Ω RESISTANCE (f = 94 GHz, V_{RF} = 19 V)

J_{dc} (kA/cm^2)	$-G_D$ (mho/cm^2)	B_D (mho/cm^2)	A $\times 10^{-4}$ (cm^2)	I_{dc} (A)	V_{dc} (V)	η (Percent)	P_{dc} (W)	P_{RF} (W)	P_{diss} (W)	θ_R (°C/W)	D (mils)
17	458	5870	0.132	0.224	27.6	17.6	6.18	1.09	5.09	44.2	1.61
19.4	532	5780	0.158	0.306	27.7	17.9	8.48	1.52	6.96	32.3	1.76
21	583	5710	0.177	0.372	27.8	18	10.3	1.85	8.45	26.6	1.87
22.7	627	5640	0.195	0.443	27.9	17.9	12.4	2.22	10.2	22	1.96
25.2	691	5540	0.222	0.559	28	17.7	15.6	2.76	12.8	17.6	2.09
27.4	746	5450	0.246	0.674	28	17.5	18.9	3.31	15.6	14.4	2.2
29.9	799	5350	0.273	0.819	28.1	17.1	23	3.93	19.1	11.8	2.32
45.9	1020	4690	0.443	2.03	28.4	14	57.6	8.06	49.5	4.54	2.96
59.7	989	4130	0.548	3.27	28.3	10.5	92.5	9.71	82.8	2.72	3.29
74	793	3610	0.58	4.29	28.1	6.88	120	8.26	112	2	3.38
91.1	584	3090	0.59	5.37	28.1	4.11	151	6.21	145	1.55	3.41
98.1	491	2910	0.564	5.53	28.2	3.21	156	5.01	151	1.49	3.34

TABLE 36

CW RESULTS FOR THE PROFILE IN FIGURE 33a AT 94 GHz TAKING INTO

ACCOUNT THE THERMAL-RESISTANCE EXPRESSIONS

D(CM) (mils)	θ(CM) (°C/W)	P_{RF}(CM) (W)	D(DM) (mils)	θ(DM) (°C/W)	P_{RF}(DM) (W)	D(CR) (mils)	θ(CR) (°C/W)	P_{RF}(CR) (W)	D(DR) (mils)	θ(DR) (°C/W)	P_{RF}(DR) (W)	J_{dc} (kA/cm²)
1.51	50.6	0.949	1.61	20.3	1.09	1.61	28.9	1.09	1.61	14.3	1.09	17
1.28	60.9	0.805	1.76	18	1.52	1.76	25.9	1.52	1.76	12.5	1.52	19.4
1.16	68.6	0.719	1.87	16.6	1.85	1.87	24.1	1.85	1.87	11.5	1.85	21
1.05	77.8	0.631	1.96	15.6	2.22	1.9	23.5	2.08	1.96	10.7	2.22	22.7
0.909	92.6	0.523	2.09	14.4	2.76	1.65	28	1.73	2.09	9.77	2.76	25.2
0.811	107	0.447	2.2	13.5	3.31	1.47	32.3	1.48	2.2	9.08	3.31	27.4
0.711	126	0.368	2.13	14	3.31	1.29	38.1	1.22	2.32	8.43	3.93	29.9
0.335	352	0.104	1.01	39.1	0.936	0.61	106	0.344	1.83	11.8	3.1	45.9
0.176	947	0.0278	0.528	105	0.251	0.32	287	0.092	0.96	31.8	0.829	59.7
0.0759	3980	0.0042	0.228	442	0.0376	0.138	1200	0.0138	0.414	134	0.124	74
5.95×10^{-4}	5.11×10^{7}	1.89×10^{-5}	1.78×10^{-3}	5.7×10^{6}	1.7×10^{-6}	1.08×10^{-3}	1.5×10^{7}	6.2×10^{-7}	3.2×10^{-3}	1.7×10^{6}	5.6×10^{-6}	91.1
--	--	--	--	--	--	--	--	--	--	--	--	98.1

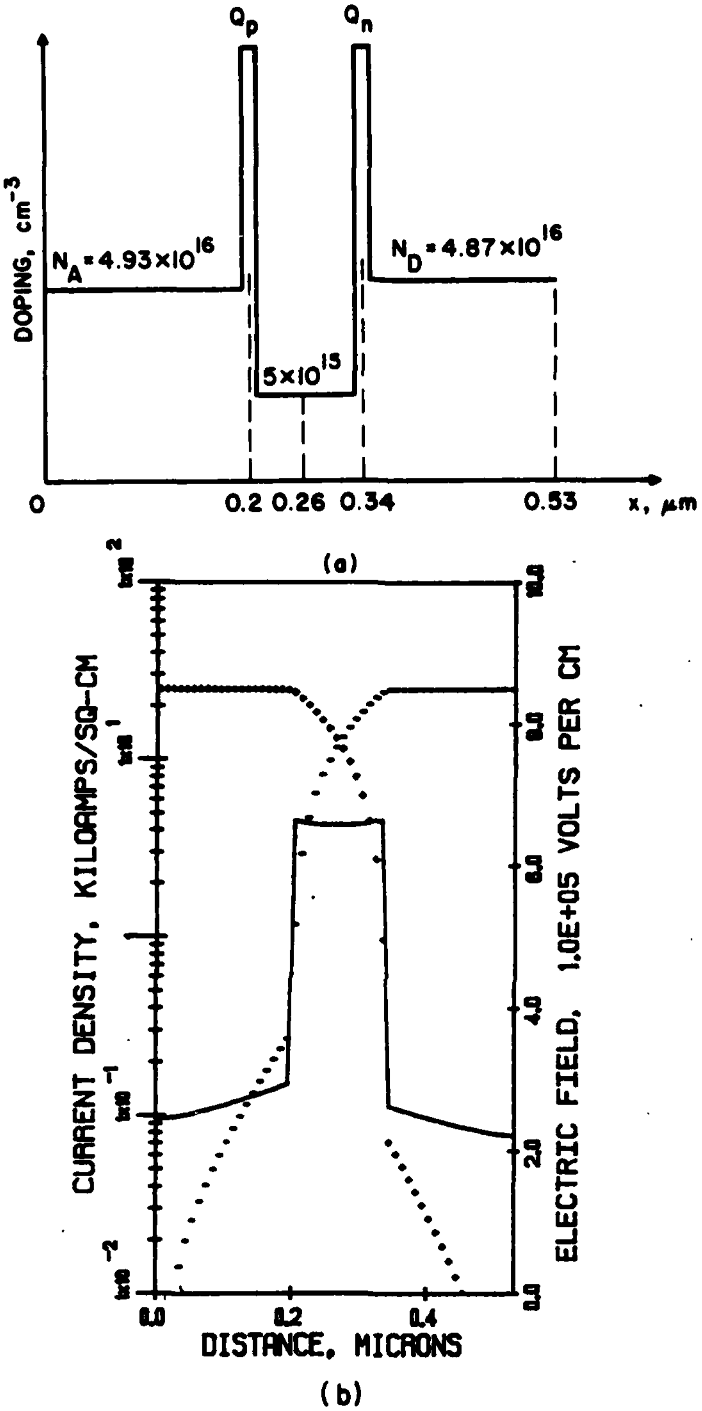

Figure 35. (a) Doping Profile of Double-Read GaAs Diode for 94-GHz Operation and (b) Dc Solution at T = 500°K and J_{dc} = 25 kA/cm^2. (X_A = 0.13 μm, J_{dc} = 25 kA/cm^2, E(LHS) = 2.45 x 10^5 V/cm, E_{to}(LHS) = 2.94 x 10^5 V/cm, E_{max} = 6.65 x 10^5 V/cm, E_{to}(RHS) = 2.64 x 10^5 V/cm, E(RHS) = 2.227 x 10^5 V/cm, Q_n = 2.8 x 10^{12} cm^{-2} and Q_p = 2.58 x 10^{12} cm^{-2})

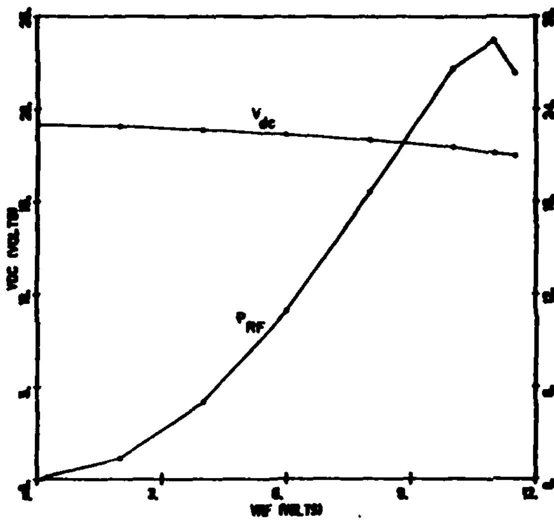

(a)

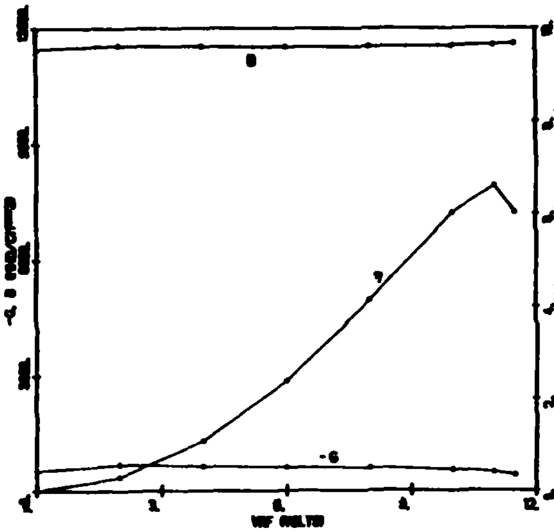

(b)

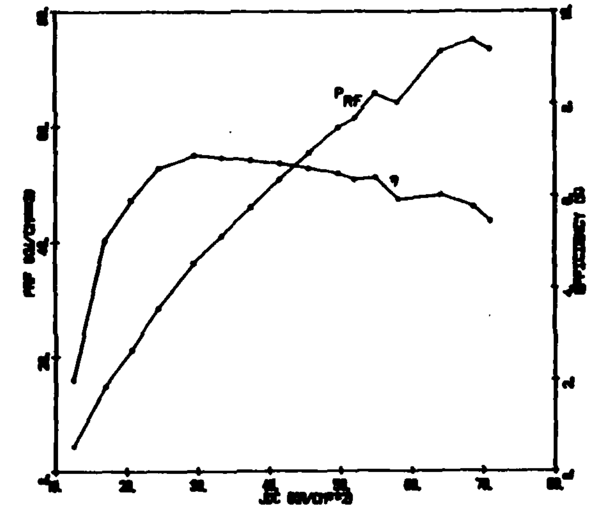

(c)

Figure 36. Large-Signal Results for the Profile of Figure 35a at $f = 94$ GHz, $T = 500°K$ and (a and b) $J_{dc} = 25$ kA/cm^2, (c) $V_{RF} = 11$ V.

TABLE 37

LARGE-SIGNAL RESULTS FOR THE DOUBLE READ GaAs PROFILE IN FIGURE 35a AND POWER LEVELS

OBTAINED BY MATCHING TO 1-Ω RESISTANCE (f = 94 GHz, V_{RF} = 11 V)

J_{dc} (kA/cm^2)	$-G_D$ (mho/cm^2)	B_D (mho/cm^2)	A x10^{-4} (cm^2)	I_{dc} (A)	V_{dc} (V)	η (Percent)	P_{dc} (W)	P_{RF} (W)	P_{diss} (W)	θ_R (°C/W)	D (mils)
12.5	70.5	12,100	4.82×10^{-3}	6.02×10^{-3}	17.1	1.99	0.103	0.002	0.101	2230	0.308
17	245	11,900	0.0173	0.0294	17.4	5.04	0.512	0.0258	0.486	463	0.584
20.6	352	11,700	0.0257	0.0529	17.5	5.91	0.926	0.0547	0.871	258	0.712
24.4	470	11,600	0.0349	0.0852	17.6	6.6	1.5	0.099	1.4	161	0.83
29.4	601	11,400	0.0461	0.136	17.9	6.88	2.43	0.167	2.26	99.6	0.954
33.3	679	11,200	0.0539	0.179	18.1	6.83	3.24	0.221	3.02	74.5	1.03
37.4	762	11,100	0.0616	0.23	18.2	6.77	4.19	0.284	3.91	57.5	1.1
41.4	840	10,900	0.0703	0.291	18.3	6.7	5.32	0.356	4.96	45.4	1.18
45.5	916	10,700	0.0794	0.361	18.5	6.6	6.68	0.441	6.24	36	1.25
49.6	988	10,600	0.0872	0.432	18.6	6.48	8.04	0.521	7.52	29.9	1.31
51.9	1020	10,500	0.0916	0.475	18.6	6.36	8.84	0.562	8.28	27.2	1.34
54.9	1090	10,400	0.0997	0.547	18.7	6.4	10.2	0.653	9.55	23.6	1.4

Cont.

Table 37 Cont.

J_{dc} (kA/cm^2)	$-G_D$ (mho/cm^2)	B_D (mho/cm^2)	A x 10^{-4} (cm^2)	I_{dc} (A)	V_{dc} (V)	η (Percent)	P_{dc} (W)	P_{RF} (W)	P_{diss} (W)	θ_R (°C/W)	D (mils)
58	1060	10,200	0.101	0.586	18.7	5.93	11	0.652	10.3	21.8	1.41
64	1210	9960	0.12	0.768	18.9	6.03	14.5	0.874	13.6	16.5	1.54
68.6	1240	9760	0.128	0.878	19	5.76	16.7	0.962	15.7	14.3	1.59
71	1210	9650	0.128	0.909	18.9	5.46	17.2	0.939	16.3	13.8	1.59

$$\theta(CM) = \frac{64.27}{d_m} + \frac{45.56}{d_m^2} , \quad (72)$$

$$\theta(DM) = \frac{21.42}{d_m} + \frac{45.56}{d_m^2} , \quad (73)$$

$$\theta(CR) = \frac{35.35}{d_m} + \frac{45.56}{d_m^2} \quad (74)$$

and

$$\theta(DR) = \frac{11.78}{d_m} + \frac{45.56}{d_m^2} . \quad (75)$$

Solving for Equations 13 through 15 and 72 through 75 yields the expected CW powers listed in Table 38. Comparison with Table 36 shows that the Si hybrid can generate significantly more CW power than the GaAs double Read structure at 94 GHz.

Figure 37a shows the doping profile for a GaAs hybrid structure simulated at 94 GHz, and Figure 37b gives the dc solution at T = 500°K and J_{dc} = 30 kA/cm^2. Large-signal results vs. V_{RF} at f = 94 GHz and J_{dc} = 30 kA/cm^2 are plotted in Figure 38a and b, and large-signal results vs. J_{dc} at V_{RF} = 12.24 V are plotted in Figure 38c. The best efficiency obtained was η = 7.54 percent at J_{dc} = 30 kA/cm^2 and V_{RF} = 12.25 V, and the largest electronic RF power density was P_{RF} = 121 kW/cm^2 at J_{dc} = 117 kA/cm^2 and V_{RF} = 12.25 V. Large-signal results vs. J_{dc} are listed in Table 39. From Figure 37a, the active region length is $\ell_2 = 0.25 \times 10^{-4}$ cm, and when $\ell_1 = 0.5 \times 10^{-4}$ cm as before, the following thermal-resistance expressions are obtained:

$$\theta(CM) = \frac{64.27}{d_m} + \frac{45.23}{d_m^2} , \quad (76)$$

TABLE 38

CW RESULTS FOR THE PROFILE IN FIGURE 35a AT 94 GHz TAKING INTO

ACCOUNT THE THERMAL-RESISTANCE EXPRESSIONS

D(CM) (mils)	θ(CM) (°C/W)	P_{RF}(CM) (W)	D(DM) (mils)	θ(DM) (°C/W)	P_{RF}(DM) (W)	D(CR) (mils)	θ(CR) (°C/W)	P_{RF}(CR) (W)	D(DR) (mils)	θ(DR) (°C/W)	P_{RF}(DR) (W)	J_{dc} (kA/cm²)
0.308	689	0.144	0.308	550	0.002	0.308	595	0.002	0.308	518	0.002	12.5
0.584	244	0.232	0.584	170	0.0258	0.584	194	0.0258	0.584	154	0.0258	17
0.712	180	0.19	0.712	120	0.0547	0.712	140	0.0547	0.712	106	0.0547	20.6
0.83	144	0.148	0.83	92	0.099	0.83	109	0.099	0.83	80.3	0.099	24.4
0.701	184	0.0901	0.954	72.5	0.167	0.954	87.1	0.167	0.954	62.4	0.167	29.4
0.521	291	0.0567	1.03	63.7	0.221	0.948	88	0.187	1.03	54.4	0.221	33.3
0.38	485	0.0337	1.1	57.1	0.284	0.69	147	0.111	1.1	48.4	0.284	37.4
0.268	871	0.0185	0.806	96.8	0.167	0.488	264	0.0613	1.18	42.7	0.356	41.4
0.17	1960	8.13×10^{-3}	0.51	217	0.0731	0.309	592	0.0269	0.927	65.8	0.242	45.5
0.092	6090	2.56×10^{-3}	0.276	677	0.023	0.167	1840	8.46×10^{-3}	0.501	205	0.0761	49.6
0.0554	1.6×10^{4}	9.56×10^{-4}	0.166	1780	8.6×10^{-3}	0.101	4840	3.16×10^{-3}	0.302	537	0.0284	51.9

Cont.

Table 38 Cont.

D(CM) (mils)	θ(CM) (°C/W)	P_{RF}(CM) (W)	D(DM) (mils)	θ(DM) (°C/W)	P_{RF}(DM) (W)	D(CR) (mils)	θ(CR) (°C/W)	P_{RF}(CR) (W)	D(DR) (mils)	θ(DR) (°C/W)	P_{RF}(DR) (W)	J_{dc} (kA/cm^2)
0.0101	4.5×10^5	3.4×10^{-5}	0.0303	5.02×10^4	3.06×10^{-4}	0.0184	1.37×10^5	1.12×10^{-4}	0.0552	1.52×10^4	1.01×10^{-3}	54.9
--	--	--	--	--	--	--	--	--	--	--	--	58
--	--	--	--	--	--	--	--	--	--	--	--	64
--	--	--	--	--	--	--	--	--	--	--	--	68.6
--	--	--	--	--	--	--	--	--	--	--	--	71

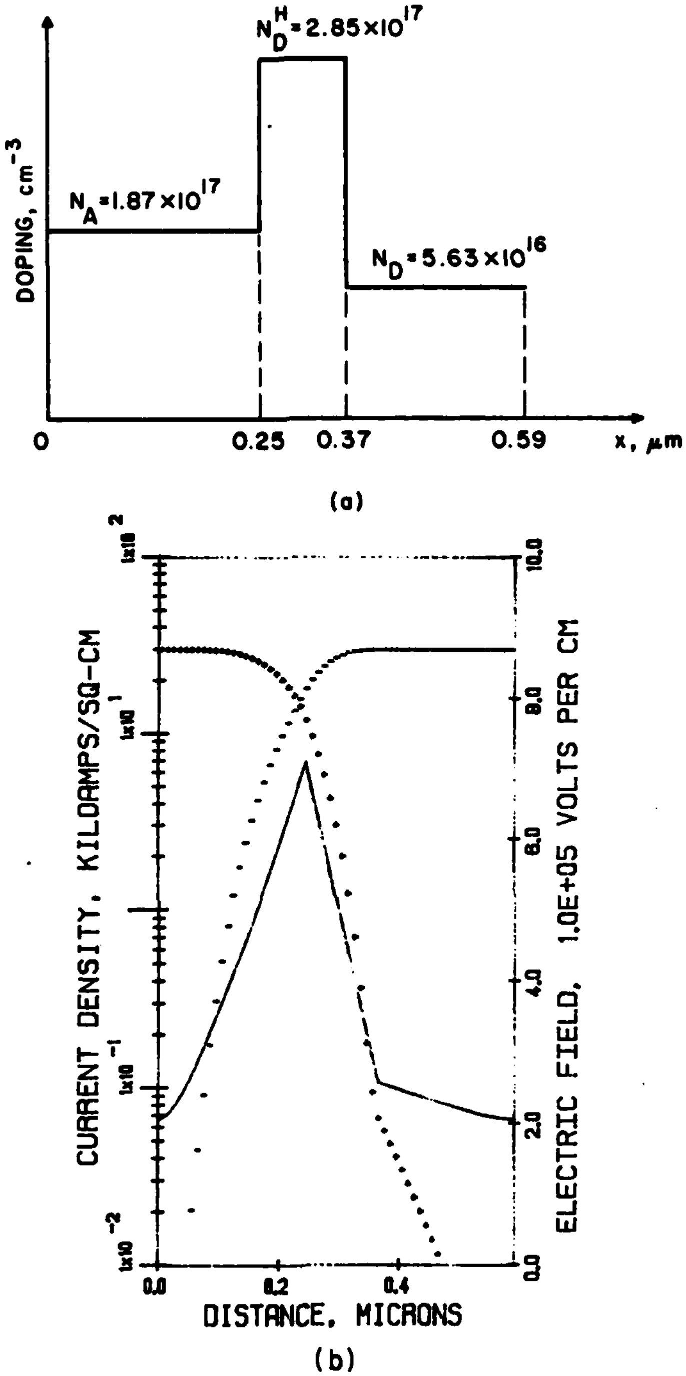

Figure 37. (a) Doping Profile for GaAs Hybrid Structure for 94-GHz Operation and (b) Dc Solution at T = 500°K and J_{dc} = 30 kA/cm^2. (X_A = 0.19 μm, J_{dc} = 30 kA/cm^2, E(LHS) = 2.068 x 10^5 V/cm, E_{max} = 7.094 x 10^5 V/cm, E_{to} = 2.591 x 10^5 V/cm and E(RHS) = 2.063 x 10^5 V/cm)

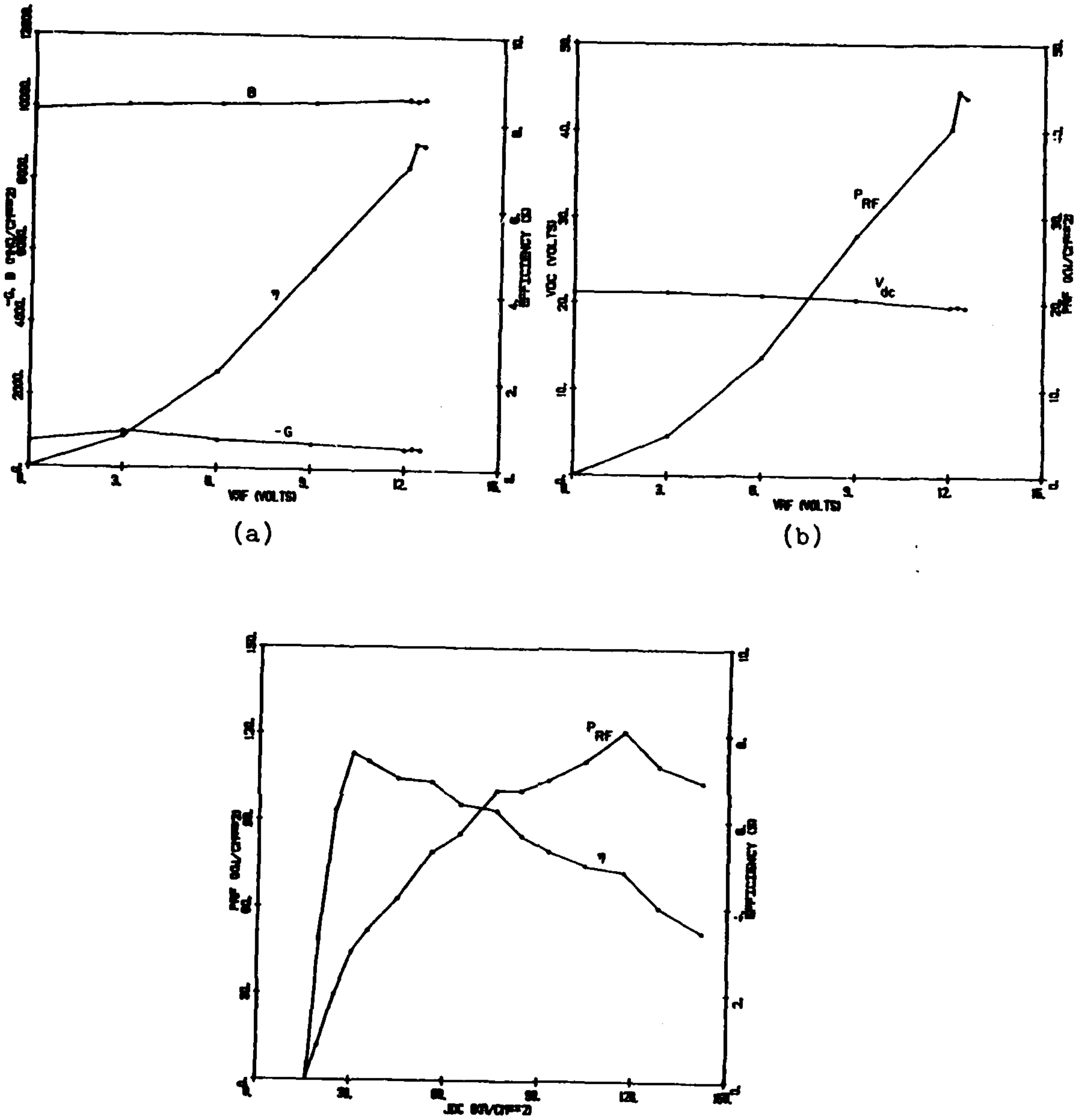

(a) (b)

(c)

Figure 38. Large-Signal Results for the Profile of Figure 37a at $T = 500°K$, $f = 94$ GHz and (a and b) $J_{dc} = 30$ kA/cm^2, (c) $V_{RF} = 12.25$ V.

TABLE 39

LARGE-SIGNAL RESULTS FOR THE GaAs HYBRID PROFILE IN FIGURE 37a AND POWER LEVELS

OBTAINED BY MATCHING TO 1-Ω RESISTANCE (f = 94 GHz, V_{RF} = 12.25 V)

J_{dc} (kA/cm²)	$-G_D$ (mho/cm²)	B_D (mho/cm²)	A x10⁻⁴(cm²)	I_{dc} (A)	V_{dc} (V)	η (Percent)	P_{dc} (W)	P_{RF} (W)	P_{diss} (W)	θ_R (°C/W)	D (mils)
19.5	161	10,800	0.0138	0.0269	19.1	3.25	0.514	0.0167	0.497	453	0.522
24.6	395	10,500	0.0358	0.0881	19.3	6.23	1.7	0.106	1.59	142	0.84
30	593	10,200	0.0568	0.17	19.6	7.54	3.33	0.251	3.08	73	1.06
35.2	688	10,100	0.0671	0.236	20	7.35	4.72	0.347	4.37	51.5	1.15
44.5	839	9740	0.0878	0.391	20.3	6.97	7.94	0.553	7.39	30.4	1.32
55.3	1050	9330	0.119	0.658	20.7	6.89	13.6	0.937	12.7	17.7	1.53
64.2	1140	9010	0.138	0.886	20.9	6.38	18.5	1.18	17.3	13	1.65
76	1340	8540	0.179	1.36	21.2	6.23	28.8	1.79	27	8.[illegible]	1.88
83.8	1340	8250	0.192	1.61	21.2	5.66	34.1	1.93	32.2	6.99	1.95
92.5	1390	7900	0.216	2	21.2	5.3	42.4	2.25	40.2	5.6	2.06
104	1480	7450	0.256	2.66	21.4	4.97	56.9	2.83	54.1	4.16	2.25
117	1620	6920	0.321	3.76	21.5	4.83	80.8	3.9	76.9	2.92	2.52
128	1460	6520	0.327	4.18	21.3	4.01	89	3.57	85.4	2.63	2.54
142	1380	6030	0.361	5.13	21.2	3.45	109	3.76	105	2.14	2.67

$$\theta(DM) = \frac{21.42}{d_m} + \frac{45.23}{d_m^2} , \quad (77)$$

$$\theta(CR) = \frac{35.35}{d_m} + \frac{45.23}{d_m^2} , \quad (78)$$

and

$$\theta(DR) = \frac{11.78}{d_m} + \frac{45.23}{d_m^2} . \quad (79)$$

Solving Equations 13 through 15 and 76 through 79 yields the CW powers given in Table 40.

Figure 39a shows the doping profile for the InP hybrid structure simulated at 94 GHz, and Figure 39b gives the dc solution at $T = 500°K$ and $J_{dc} = 25$ kA/cm². Large-signal results vs. V_{RF} at $f = 94$ GHz and $J_{dc} = 25$ kA/cm² are plotted in Figure 40a and b, and large-signal results vs. J_{dc} at $V_{RF} = 17$ V are plotted in Figure 40c. Large-signal results vs. J_{dc} are listed in Table 41. The best efficiency was $\eta = 13.4$ percent at $J_{dc} = 24.6$ kA/cm², and the maximum RF power density was $P_{RF} = 162$ kW/cm² at $J_{dc} = 92.6$ kA/cm². Using $\ell_2 = 0.3 \times 10^{-4}$ cm from Figure 39a and $\ell_1 = 0.5 \times 10^{-4}$ cm as before, and reducing the final two terms in Equation 1 by 0.8 to account for the higher thermal conductivity of InP yields the following thermal-resistance expressions:

$$\theta(CM) = \frac{64.27}{d_m} + \frac{37.5}{d_m^2} , \quad (80)$$

$$\theta(DM) = \frac{21.42}{d_m} + \frac{37.5}{d_m^2} , \quad (81)$$

$$\theta(CR) = \frac{35.35}{d_m} + \frac{37.5}{d_m^2} \quad (82)$$

TABLE 40

CW RESULTS FOR THE PROFILE IN FIGURE 37a AT 94 GHz TAKING INTO

ACCOUNT THE THERMAL-RESISTANCE EXPRESSIONS

D(CM) (mils)	θ(CM) (°C/W)	P_{RF}(CM) (W)	D(DM) (mils)	θ(DM) (°C/W)	P_{RF}(DM) (W)	D(GR) (mils)	θ(CR) (°C/W)	P_{RF}(CR) (W)	D(DR) (mils)	θ(DR) (°C/W)	P_{RF}(DR) (W)	J_{dc} (kA/cm^2)
0.522	289	0.0167	0.522	207	0.0167	0.522	234	0.0167	0.522	188	0.0167	19.5
0.84	141	0.106	0.84	89.6	0.106	0.84	106	0.106	0.84	78.1	0.106	24.6
0.567	254	0.0722	1.06	60.5	0.251	1.03	76.8	0.239	1.06	51.4	0.251	30
0.355	539	0.0331	1.07	59.8	0.298	0.646	163	0.110	1.15	44.4	0.347	35.2
0.118	3770	4.47×10^{-3}	0.355	419	0.0402	0.215	1140	0.0148	0.646	127	0.133	44.5
--	--	--	--	--	--	--	--	--	--	--	--	55.3

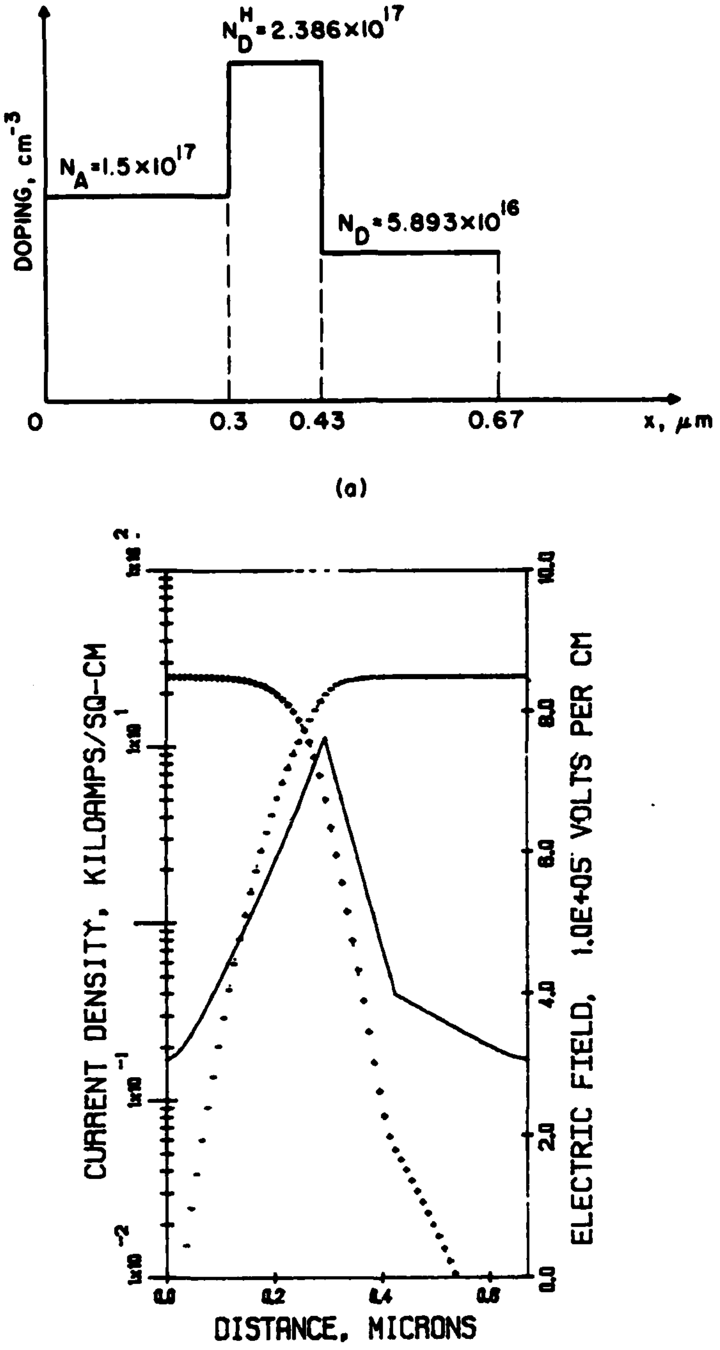

(b)

Figure 39. (a) InP Hybrid Doping Profile for 94-GHz Operation and (b) Dc Solution at T = 500°K and J_{dc} = 25 kA/cm². (X_A = 0.19 μm, J_{dc} = 25 kA/cm², E(LHS) = 3.09 x 10^5 V/cm, E_{max} = 7.64 x 10^5 V/cm, E_{to} = 4.0 x 10^5 V/cm and E(RHS) = 3.081 x 10^5 V/cm)

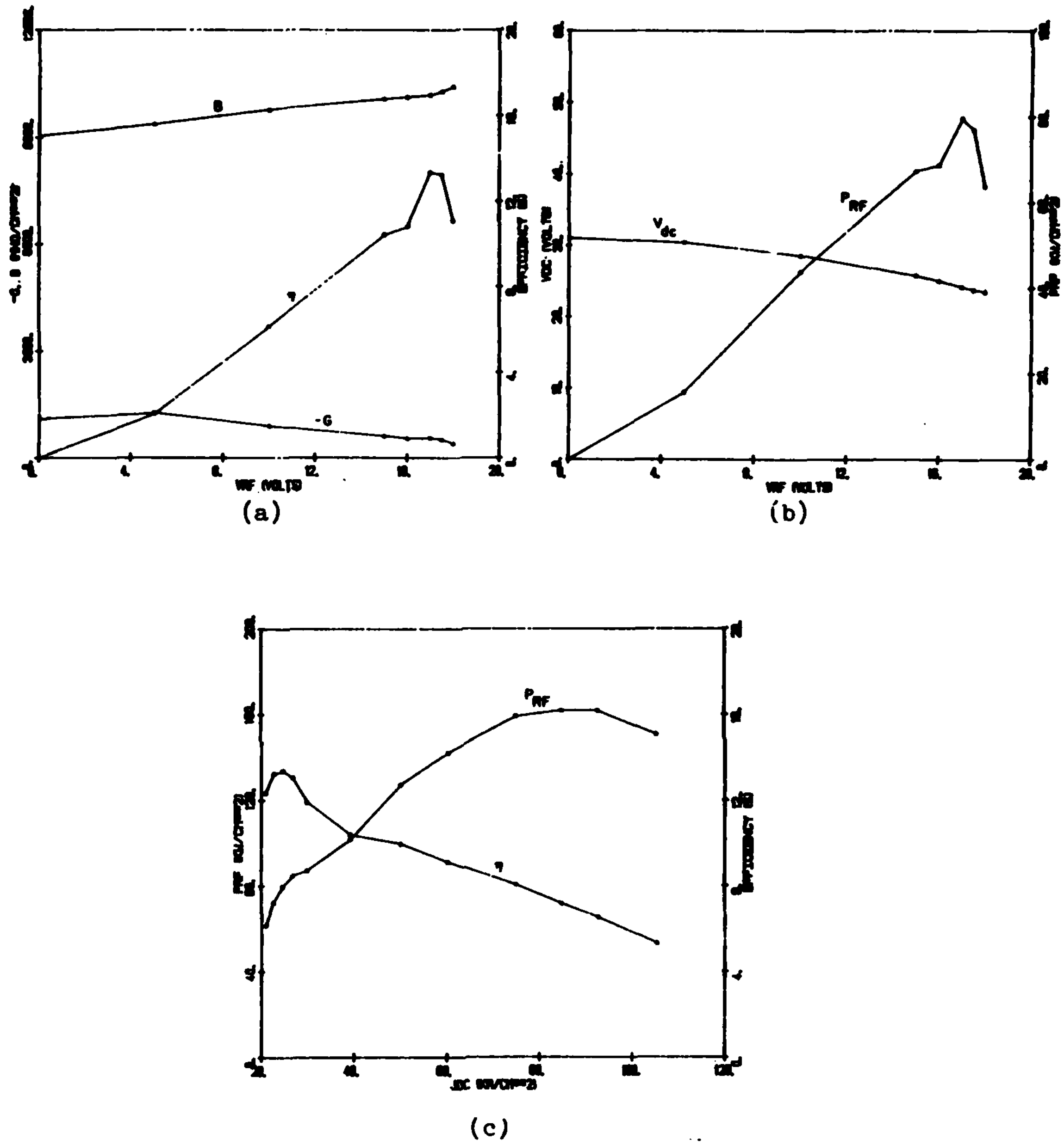

Figure 40. Large-Signal Results for the Profile of Figure 39a at $f = 94$ GHz, $T = 500°K$ and (a and b) $J_{dc} = 25$ kA/cm^2, (c) $V_{RF} = 17$ V.

TABLE 41

LARGE-SIGNAL RESULTS FOR THE InP HYBRID PROFILE IN FIGURE 39a AND POWER LEVELS

OBTAINED BY MATCHING TO 1-Ω RESISTANCE (f = 94 GHz, V_{RF} = 17 V)

J_{dc} (kA/cm²)	$-G_D$ (mho/cm²)	B_D (mho/cm²)	A x 10^{-4} (cm²)	I_{dc} (A)	V_{dc} (V)	η (Percent)	P_{dc} (W)	P_{RF} (W)	P_{diss} (W)	θ_R (°C/W)	D (mils)
20.9	426	1.04×10^4	0.0393	0.0821	23.9	12.3	1.96	0.241	1.72	131	0.881
22.7	500	1.03×10^4	0.047	0.107	24	13.2	2.57	0.339	2.23	101	0.963
24.6	551	1.02×10^4	0.0528	0.13	24.2	13.4	3.15	0.422	2.73	82.4	1.02
26.7	585	1.01×10^4	0.0572	0.153	24.2	13	3.7	0.481	3.22	69.9	1.06
29.8	603	9990	0.0602	0.179	24.5	11.9	4.38	0.521	3.86	58.3	1.09
39.2	704	9700	0.0744	0.292	25	10.4	7.3	0.759	6.54	34.4	1.21
50	880	9290	0.101	0.505	25.5	9.97	12.9	1.29	11.6	19.4	1.41
60.2	982	8910	0.122	0.734	25.9	9.11	19	1.73	17.3	13	1.55
75	1100	8340	0.155	1.16	26.4	8.04	30.6	2.46	28.1	8.01	1.75
84.8	1120	7970	0.173	1.47	26.6	7.16	39.1	2.8	36.3	6.2	1.85
92.6	1120	7640	0.188	1.74	26.8	6.53	46.6	3.04	43.6	5.16	1.93
105	1040	7210	0.196	2.06	27	5.31	55.6	2.95	52.6	4.28	1.97

and

$$\theta(DR) = \frac{11.78}{d_m} + \frac{37.5}{d_m^2} . \qquad (83)$$

Solving Equations 13 through 15 and 80 through 83 yields the CW power levels given in Table 42.

Figure 41a gives the doping profile for a uniform GaAs double-drift IMPATT simulated at 94 GHz, and Figure 41b shows the dc solution at $T = 500°K$ and $J_{dc} = 60$ kA/cm². Selected large-signal results for different values of J_{dc} and V_{RF} at f = 94 GHz are given in Table 43. The best efficiency obtained was $\eta = 7.92$ percent at $J_{dc} = 69.7$ kA/cm² and $V_{RF} = 15$ V, and maximum RF power density was $P_{RF} = 196$ kW/cm² at $J_{dc} = 178$ kA/cm² and $V_{RF} = 15$ V. From Figure 41a, $\ell_2 = 0.32 \times 10^{-4}$ cm, and when $\ell_1 = 0.5 \times 10^{-4}$ cm as before, the thermal-resistance expressions become

$$\theta(CM) = \frac{64.27}{d_m} + \frac{47.53}{d_m^2} , \qquad (84)$$

$$\theta(DM) = \frac{21.42}{d_m} + \frac{47.53}{d_m^2} , \qquad (85)$$

$$\theta(CR) = \frac{35.35}{d_m} + \frac{47.53}{d_m^2} \qquad (86)$$

and

$$\theta(DR) = \frac{11.78}{d_m} + \frac{47.53}{d_m^2} . \qquad (87)$$

Solving Equations 13 through 15 and 84 through 87 yields the expected CW powers given in Table 44.

Figure 42a gives the doping profile for a uniformly doped Si double-drift IMPATT simulated at 94 GHz, and Figure 42b gives the dc solution at $T = 500°K$, and $J_{dc} = 25$ kA/cm². Large-signal

TABLE 42

CW RESULTS FOR THE PROFILE IN FIGURE 39a AT 94 GHz TAKING INTO

ACCOUNT THE THERMAL-RESISTANCE EXPRESSIONS

D(CM) (mils)	θ(CM) (°C/W)	P_{RF}(CM) (W)	D(DM) (mils)	θ(DM) (°C/W)	P_{RF}(DM) (W)	D(CR) (mils)	θ(CR) (°C/W)	P_{RF}(CR) (W)	D(DR) (mils)	θ(DR) (°C/W)	P_{RF}(DR) (W)	J_{dc} (kA/cm^2)
0.881	121	0.241	0.881	72.6	0.241	0.881	88.4	0.241	0.881	61.7	0.241	20.9
0.878	122	0.28	0.963	62.7	0.339	0.963	77.1	0.339	0.963	52.7	0.339	22.7
0.757	150	0.231	1.02	57	0.422	1.02	70.7	0.422	1.02	47.6	0.422	24.6
0.646	190	0.177	1.06	53.6	0.481	1.06	66.7	0.481	1.06	44.5	0.481	26.7
0.491	287	0.106	1.09	51.2	0.521	0.892	86.7	0.35	1.09	42.4	0.521	29.8
0.203	1220	0.0214	0.61	136	0.192	0.37	370	0.0706	1.11	41.1	0.635	39.2
0.0184	1.14×10^{5}	2.18×10^{-4}	0.0552	1.27×10^{4}	1.96×10^{-3}	0.0335	3.45×10^{4}	0.72×10^{-3}	0.1	3840	6.5×10^{-3}	50
--	--	--	--	--	--	--	--	--	--	--	--	60.2

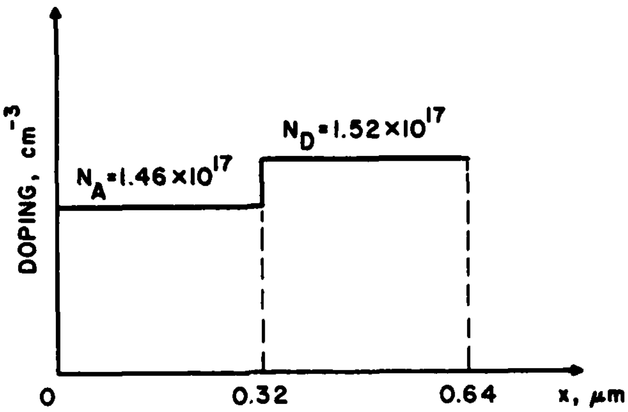

(a)

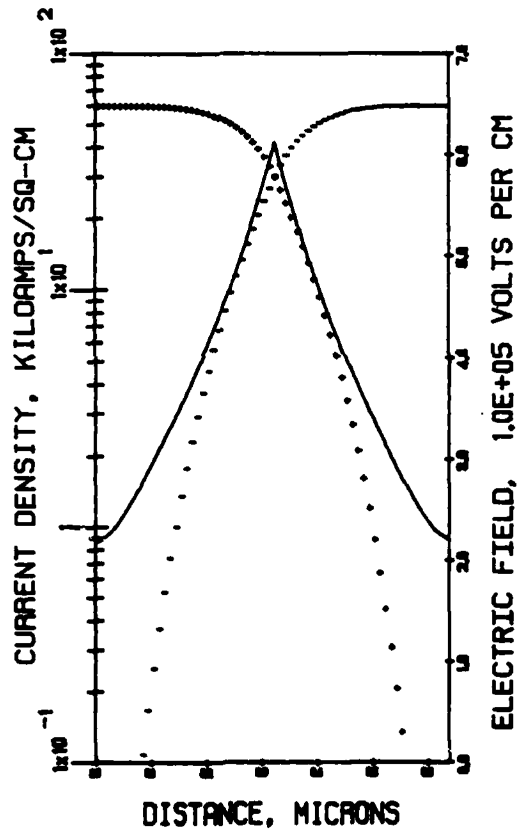

(b)

Figure 41. (a) Doping Profile for Uniformly Doped GaAs Double-Drift IMPATT at 94 GHz and (b) Dc Solution at T = 500°K and J_{dc} = 60 kA/cm². (X_A = 0.28 μm, E(LHS) = 2.192 x 10^5 V/cm, E_{max} = 6.122 x 10^5 V/cm and E(RHS) = 2.228 x 10^5 V/cm)

TABLE 43

LARGE-SIGNAL RESULTS FOR THE DOUBLE-DRIFT GaAs PROFILE IN FIGURE 41a AND POWER LEVELS

OBTAINED BY MATCHING TO 1-Ω RESISTANCE (f = 94.GHz)

J_{dc} (kA/cm^2)	$-G_D$ (mho/cm^2)	B_D (mho/cm^2)	A $\times 10^{-4}$ (cm^2)	I_{dc} (A)	V_{dc} (V)	η (Percent)	P_{dc} (W)	P_{RF} (W)	P_{diss} (W)	θ_R (°C/W)	D (mils)	V_{RF} (V)
27.3	17.7	1.02×10^4	0.0017	0.00464	19.9	0.366	0.0923	3.38×10^{-4}	0.092	2440	0.183	15
29.4	126	1.01×10^4	0.0123	0.0362	20.1	2.4	0.728	0.0175	0.71	317	0.493	15
34.4	247	9830	0.0255	0.0877	20.2	4	1.77	0.0708	1.7	132	0.709	15
39.7	399	9560	0.0436	0.173	20.4	5.53	3.53	0.195	3.34	67.4	0.928	15
45.1	538	9290	0.0621	0.28	20.6	6.5	5.77	0.375	5.4	41.7	1.11	15
49.5	623	9100	0.0749	0.371	20.7	6.83	7.68	0.524	7.16	31.4	1.22	15
54.1	756	8880	0.0952	0.515	21	7.5	10.8	0.81	9.99	22.5	1.37	15
59.4	843	8680	0.111	0.659	21.1	7.57	13.9	1.05	12.8	17.6	1.48	15
29.5	234	9920	0.0238	0.0702	20.4	3.81	1.43	0.0545	1.38	163	0.685	14
29.7	352	9740	0.037	0.11	20.7	4.84	2.28	0.11	2.17	104	0.854	13
29.6	444	9620	0.0479	0.142	21	5.13	2.98	0.153	2.83	79.5	0.972	12

Cont.

Table 43 Cont.

J_{dc} (kA/cm^2)	$-G_D$ (mho/cm^2)	B_D (mho/cm^2)	A x 10^{-4} (cm^2)	I_{dc} (A)	V_{dc} (V)	η (Percent)	P_{dc} (W)	P_{RF} (W)	P_{diss} (W)	θ_R (°C/W)	D (mils)	V_{RF} (V)
29.7	521	9500	0.0576	0.171	21.2	5	3.62	0.181	3.44	65.4	1.07	11
69.7	1060	8300	0.151	1.05	21.5	7.92	22.6	1.79	20.8	10.8	1.73	15
178	1740	5070	0.606	10.8	22.4	4.88	242	11.8	230	0.978	3.46	15

TABLE 44

CW RESULTS FOR THE PROFILE IN FIGURE 41a AT 94 GHz TAKING INTO ACCOUNT THE THERMAL-RESISTANCE EXPRESSIONS

D(CM) (mils)	θ(CM) (°C/W)	P_{RF}(CM) (W)	D(DM) (mils)	θ(DM) (°C/W)	P_{RF}(DM) (W)	D(CR) (mils)	θ(CR) (°C/W)	P_{RF}(CR) (W)	D(DR) (mils)	θ(DR) (°C/W)	P_{RF}(DR) (W)	J_{dc} (V_{RF}) (kA/cm²)
0.183	1770	3.38×10^{-4}	0.183	1540	3.38×10^{-4}	0.183	1610	3.38×10^{-4}	0.183	1480	3.38×10^{-4}	27.3 (15)
0.458	366	0.0151	0.493	239	0.0175	0.493	267	0.0175	0.493	219	0.0175	29.4 (15)
0.296	759	0.0123	0.709	125	0.0708	0.538	230	0.0408	0.709	111	0.0708	34.4 (15)
0.163	2170	6.06×10^{-3}	0.49	241	0.0546	0.297	657	0.02	0.891	73	0.18	39.7 (15)
0.0558	1.64×10^{4}	9.51×10^{-4}	0.167	1830	8.56×10^{-3}	0.101	4970	3.14×10^{-3}	0.304	552	0.0283	45.1 (15)
--	--	--	--	--	--	--	--	--	--	--	--	49.5 (15)
--	--	--	--	--	--	--	--	--	--	--	--	54.1 (15)
--	--	--	--	--	--	--	--	--	--	--	--	59.4 (15)
0.454	372	0.0239	0.685	132	0.0545	0.685	153	0.0545	0.685	118	0.0545	29.5 (14)
0.441	390	0.0294	0.854	90.2	0.11	0.802	118	0.0971	0.854	79	0.11	29.7 (13)
0.432	403	0.0302	0.972	72.3	0.153	0.785	122	0.0997	0.972	62.4	0.153	29.6 (12)
0.415	430	0.0275	1.07	61.5	0.181	0.755	130	0.091	1.07	52.5	0.181	29.7 (11)

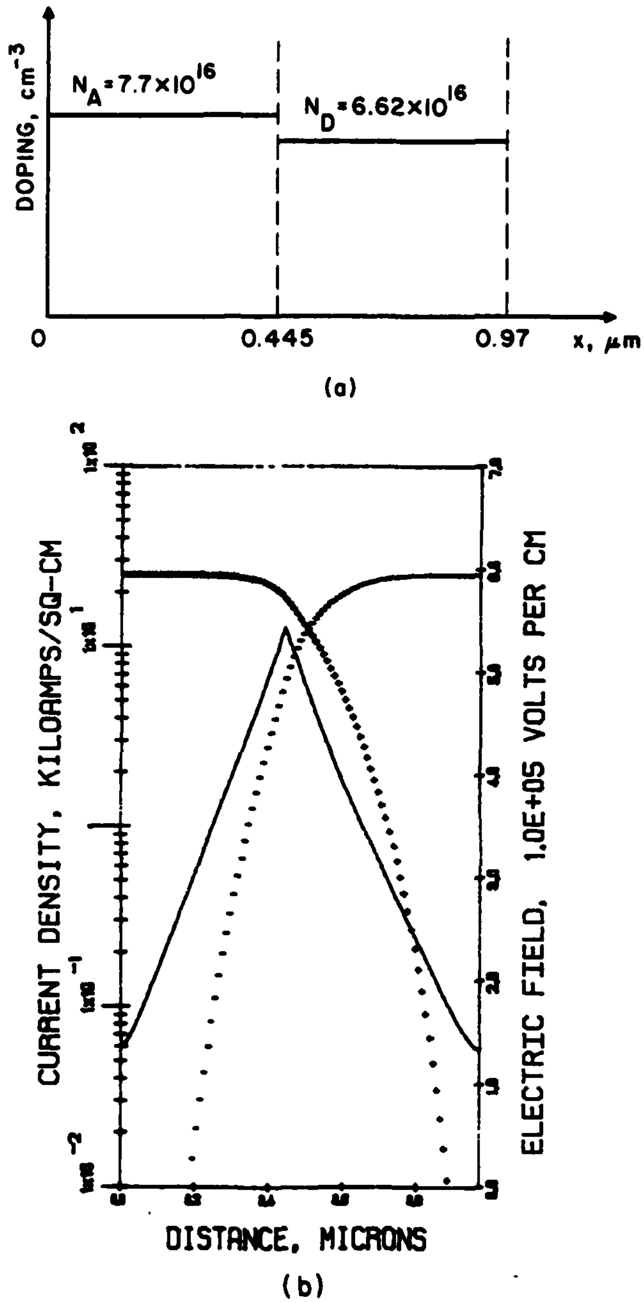

Figure 42. (a) Doping Profile for Uniformly Doped Si Double-Drift IMPATT at 94 GHz and (b) Dc Solution at T = 500°K and J_{dc} = 25 kA/cm^2. (X_A = 0.37 μm, E(LHS) = 1.368 x 10^5 V/cm, E_{max} = 5.436 x 10^5 V/cm and E(RHS) = 1.342 x 10^5 V/cm)

results vs. V_{RF} at f = 94 GHz and J_{dc} = 25 kA/cm^2 are plotted in Figure 43a and b, and large-signal results vs. J_{dc} at V_{RF} = 18 V are plotted in Figure 43c. Large-signal results vs. J_{dc} are listed in Table 45. Using ℓ_2 = 0.445 μm from Figure 42a, assuming ℓ_1 = 0.5 μm as before, and then reducing the final two terms of Equation 1 by 1/3 to account for higher thermal conductivity in Si yields the following thermal-resistance expressions:

$$\theta(CM) = \frac{64.27}{d_m} + \frac{17.21}{d_m^2} , \quad (88)$$

$$\theta(DM) = \frac{21.42}{d_m} + \frac{17.21}{d_m^2} , \quad (89)$$

$$\theta(CR) = \frac{35.35}{d_m} + \frac{17.21}{d_m^2} \quad (90)$$

and

$$\theta(DR) = \frac{11.78}{d_m} + \frac{17.21}{d_m^2} . \quad (91)$$

Solving Equations 13 through 15 and 88 through 91 yields the expected CW powers listed in Table 46.

When the results obtained at 94 GHz are summarized, it is found that the Si hybrid and uniformly doped double-drift devices are capable of generating more CW power than any other structure for all combinations of diode geometry and heat-sink material. The Si hybrid has the highest RF conversion efficiency. The uniform GaAs double-drift device yielded the highest maximum electronic RF power (matching into 1-Ω resistance and ignoring thermal effects). The uniform Si double-drift device was capable of generating almost half the peak RF electronic power generated by the uniform GaAs double-drift structure.

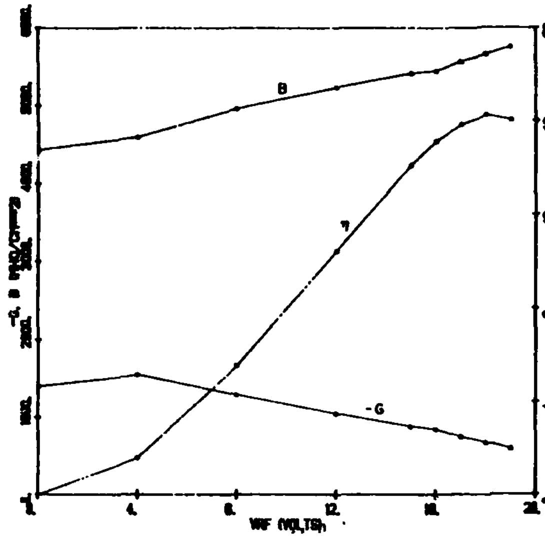

(a)

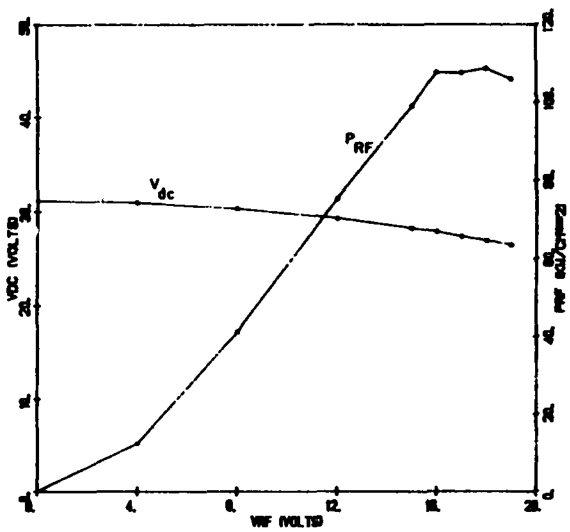

(b)

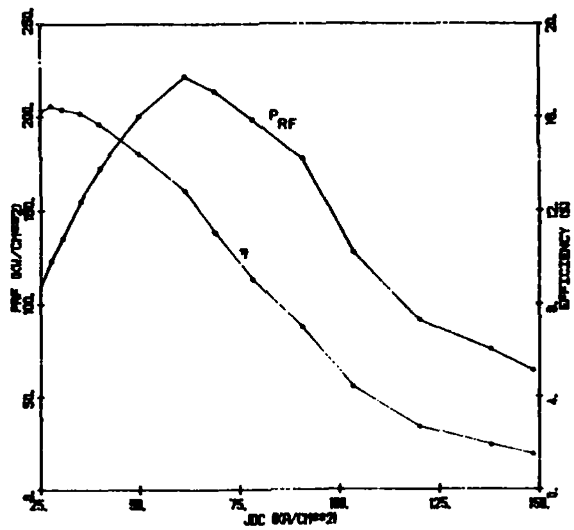

(c)

Figure 43. Large-Signal Results for the Profile of Figure 42a at $f = 94$ GHz, $T = 500^{\circ}K$ and (a and b) $J_{dc} = 25$ kA/cm^2, (c) $V_{RF} = 18$ V.

TABLE 45

LARGE-SIGNAL RESULTS FOR THE UNIFORM Si DOUBLE-DRIFT PROFILE IN FIGURE 42a AND POWER LEVELS

OBTAINED BY MATCHING TO 1-Ω RESISTANCE (f = 94 GHz)

J_{dc} (kA/cm^2)	$-G_D$ (mho/cm^2)	B_D (mho/cm^2)	A (cm^2)	I_{dc} (A)	V_{dc} (V)	η (Percent)	P_{dc} (W)	P_{RF} (W)	P_{diss} (W)	θ_R (°C/W)	D (mils)
7.9	50.3	6607	1.15×10^{-6}	9.08×10^{-3}	25.9	3.98	0.235	9.35×10^{-3}	0.226	996	0.476
11.8	207	6387	5.07×10^{-6}	0.0598	26.2	10.87	1.57	0.171	1.4	161	1.0
15.8	360	6159	9.46×10^{-6}	0.149	26.4	13.96	3.93	0.549	3.38	66.6	1.37
19.2	482	5962	1.35×10^{-5}	0.259	26.6	15.26	6.89	1.05	5.84	38.5	1.63
22.1	586	5800	1.72×10^{-5}	0.38	26.8	16.03	10.2	1.64	8.56	26.3	1.84
24.9	671	5649	2.07×10^{-5}	0.515	26.9	16.2	13.8	2.24	11.6	19.4	2.02
27.7	762	5499	2.47×10^{-5}	0.684	27.1	16.4	18.5	3.03	15.5	14.5	2.21
30.5	834	5355	2.84×10^{-5}	0.866	27.2	16.3	23.6	3.85	19.8	11.4	2.37
35	957	5124	3.52×10^{-5}	1.23	27.4	16.2	33.7	5.46	28.2	7.98	2.64
39.8	1065	4887	4.26×10^{-5}	1.7	27.6	15.7	46.9	7.36	39.5	5.7	2.9
49.8	1236	4407	5.9×10^{-5}	2.94	27.9	14.4	82	11.8	70.2	3.2	3.41
61.1	1368	3856	8.17×10^{-5}	4.99	28.2	12.8	141	18	123	1.83	4.01

Cont.

Table 45 Cont.

J_{dc} (kA/cm^2)	$-G_D$ (mho/cm^2)	B_D (mho/cm^2)	A (cm^2)	I_{dc} (A)	V_{dc} (V)	η (Percent)	P_{dc} (W)	P_{RF} (W)	P_{diss} (W)	θ_R (°C/W)	D (mils)
68.6	1318	3512	9.37×10^{-5}	6.43	28.1	11.1	181	20.1	161	1.4	4.3
78.2	1225	3092	1.11×10^{-4}	8.68	28.0	9.06	243	22	221	1.02	4.68
90.5	1096	2610	1.37×10^{-4}	12.4	28.9	7.0	347	24.3	323	0.696	5.2
103	787	2232	1.4×10^{-4}	14.4	27.9	4.42	402	17.8	384	0.586	5.26
120	562	1807	1.57×10^{-4}	18.8	28.1	2.7	528	14.2	514	0.438	5.57
138	466	1396	2.15×10^{-4}	29.7	28.5	1.92	846	16.2	830	0.271	6.51
148	396	1228	2.38×10^{-4}	35.2	28.7	1.5	1010	15.2	995	0.226	6.85

TABLE 46

CW RESULTS FOR THE PROFILE IN FIGURE 42a AT 94 GHz TAKING INTO

ACCOUNT THE THERMAL-RESISTANCE EXPRESSIONS

D(CM) (mils)	θ(CM) (°C/W)	P_{RF}(CM) (W)	D(DM) (mils)	θ(DM) (°C/W)	P_{RF}(DM) (W)	D(CR) (mils)	θ(CR) (°C/W)	P_{RF}(CR) (W)	D(DR) (mils)	θ(DR) (°C/W)	P_{RF}(DR) (W)	J_{dc} (kA/cm^2)
0.476	996	9.35×10^{-3}	0.476	996	9.35×10^{-3}	0.476	996	9.35×10^{-3}	0.476	996	9.35×10^{-3}	7.9
1.0	161	0.171	1.0	161	0.171	1.0	161	0.171	1.0	161	0.171	11.8
1.37	66.6	0.549	1.37	66.6	0.549	1.37	66.6	0.549	1.37	66.6	0.549	15.8
1.32	58.4	0.694	1.63	38.5	1.05	1.63	38.5	1.05	1.63	38.5	1.05	19.2
1.12	71.0	0.605	1.84	26.3	1.64	1.84	26.3	1.64	1.84	26.3	1.64	22.1
0.964	85.2	0.511	2.02	19.4	2.24	1.75	25.8	1.69	2.02	19.4	2.24	24.9
0.835	102	0.436	2.21	14.5	3.03	1.52	30.7	1.44	2.21	14.5	3.03	27.7
0.729	120	0.364	2.19	13.4	3.28	1.32	36.5	1.2	2.37	11.4	3.85	30.5
0.592	158	0.275	1.77	17.5	2.47	1.08	47.7	0.909	2.64	7.98	5.46	35
0.478	210	0.2	1.43	23.3	1.8	0.869	63.5	0.66	2.6	7.06	5.94	39.8
0.313	381	0.0994	0.939	42.3	0.895	0.569	115	0.329	1.71	12.8	2.96	49.8
0.192	804	0.0412	0.575	89.3	0.371	0.348	243	0.136	1.04	27	1.23	61.1

Cont.

Table 46

D(CM) (mils)	θ(CM) (°C/W)	P_{RF}(CM) (W)	D(DM) (mils)	θ(DM) (°C/W)	P_{RF}(DM) (W)	D(CR) (mils)	θ(CR) (°C/W)	P_{RF}(CR) (W)	D(DR) (mils)	θ(DR) (°C/W)	P_{RF}(DR) (W)	J_{dc} (kA/cm^2)
0.135	1420	0.0197	0.405	158	0.178	0.246	429	0.0652	0.736	47.7	0.587	68.6
0.0788	3585	6.25×10^{-3}	0.236	398	0.0562	0.143	1084	0.0207	0.43	120	0.186	78.2
0.0249	3.03×10^{4}	5.58×10^{-4}	0.0747	3.35×10^{3}	5.02×10^{-3}	0.0453	9171	1.84×10^{-3}	0.136	1019	0.0166	90.5
--	--	--	--	--	--	--	--	--	--	--	--	103
--	--	--	--	--	--	--	--	--	--	--	--	120
--	--	--	--	--	--	--	--	--	--	--	--	138

SECTION 9.

SUMMARY OF RESULTS

Table 47 presents a summary of the expected maximum CW powers obtained for all combinations of frequency, diode structure, mesa geometry and heat-sink material studied. It is seen that Si devices yield the maximum power in all cases.

It should be kept in mind that the thermal-resistance expressions used were quite optimistic since the mounting term, R_{PKG}, in Equation 1 was ignored. Also, the contributions due to intervening metallization layers were not considered. Therefore, it is expected that the CW powers in Table 47 represent "best case" estimates. Figure 44 gives plots of the CW powers vs. frequency for all four combinations of mesa geometry and heat-sink material for the Si, GaAs and InP hybrid structures.

Table 48 lists the peak electronic RF power obtained by matching each diode to 1-Ω circuit resistance, excluding thermal considerations. Results for the uniformly doped GaAs double-drift diode at 94 GHz in Table 48 are not for the structure examined previously in this report, but rather a structure recently found[18] to have optimum electronic power generating capability at 94 GHz was simulated. This structure has $N_A = 2.2 \times 10^{17}$ cm^{-3}, $N_D = 2.23 \times 10^{17}$ cm^{-3}, and $W_n = W_p = 0.32$ μm. The very large powers in Table 48 for the uniform double-drift structures are brought about by a large increase in device area required to match into 1-Ω circuit resistance as J_{dc} increases. Both $|G|$ and B decrease (beyond a certain point) with increasing J_{dc}, and also the ratio

TABLE 47

SUMMARY OF CW RF POWER FOR ALL FREQUENCIES, DIODE STRUCTURES AND MESA GEOMETRY, HEAT-SINK MATERIAL COMBINATIONS (W)

Diode Type	Frequency (GHz) 30	40	60	94
Single Mesa, Copper Heat Sink				
Si Hybrid	4.47	2.94	1.51	0.949
Si Uniform Double Drift				0.694
GaAs Hybrid	1.56	1.06	0.411	0.106
InP Hybrid	2.53	1.86	0.548	0.28
GaAs Double Read	2.94	1.84	0.507	0.232
GaAs Uniform Double Drift			0.19	0.0302
GaAs Single Drift			0.375	0.0438
Single Mesa, Diamond Heat Sink				
Si Hybrid	15.3	11.8	6.88	3.31
Si Uniform Double Drift				3.28
GaAs Hybrid	9.43	4.78	1.74	0.298
InP Hybrid	8.75	5.9	2.84	0.521
GaAs Double Read	10.3	4.96	1.41	0.284
GaAs Uniform Double Drift			1.18	0.181
GaAs Single Drift			0.514	0.0891
Ring Geometry, Copper Heat Sink				
Si Hybrid	9.23	6.09	3.76	2.08
Si Uniform Double Drift				1.69
GaAs Hybrid	4.5	3.02	1.08	0.239
InP Hybrid	5.94	4.01	1.73	0.481
GaAs Double Read	7.28	2.96	1.01	0.187
GaAs Uniform Double Drift			0.628	0.0997
GaAs Single Drift			0.514	0.0737

Cont.

Table 47 Cont.

Diode Type	Frequency (GHz) 30	40	60	94
Ring Geometry, Diamond Heat Sink				
Si Hybrid	29.2	18.8	11.4	3.93
Si Uniform Double Drift				5.94
GaAs Hybrid	15.8	7.47	2.32	0.347
InP Hybrid	13.9	7.64	3.06	0.635
GaAs Double Read	16.6	6.09	1.9	0.356
GaAs Uniform Double Drift			1.8	0.181
GaAs Single Drift			0.514	0.144

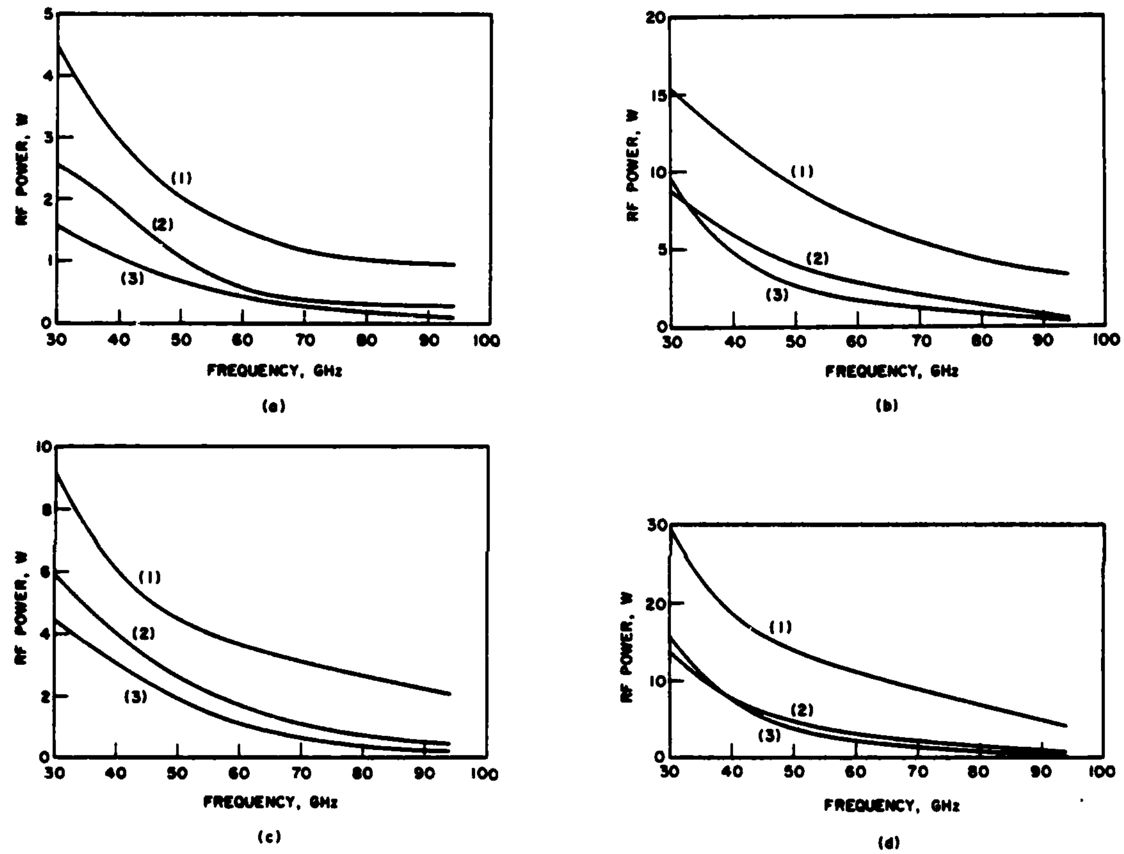

Figure 44. Summary of Maximum CW RF Powers Obtained for (1) Si Hybrid Structure, (2) InP Hybrid Structure, and (3) GaAs Hybrid Structure vs. Frequency. (a) Single Mesa, Copper Heat Sink, (b) Single Mesa, Diamond Heat Sink, (c) Ring Geometry, Copper Heat Sink, and (d) Ring Geometry, Diamond Heat Sink.

TABLE 48

SUMMARY OF PEAK ELECTRONIC RF POWERS OBTAINED BY MATCHING TO 1-Ω RESISTANCE (W)

Diode Type	Frequency (GHz) 30	40	60	94
Si Hybrid	36.7	29.2	19.4	9.71
GaAs Hybrid	39	20.3	10.6	3.9
InP Hybrid	30.9	19.5	10.6	3.04
GaAs Double Read	18.7	7.66	2.52	0.962
GaAs Uniform Double Drift			122	60.4*
GaAs Single Drift			0.514	0.148
Si Uniform Double Drift				24.3

*Calculated for Structure D7 in Reference 18.

$B/|G|$ decreases, both effects increasing $A = -G/(G^2 + B^2)$. The powers in Table 48 occur for J_{dc} well above the J_{dc} for maximum RF power density. It is doubtful that these peak powers could be observed experimentally since the required pulse width would be extremely short.

LIST OF REFERENCES

1. Mains, R. K. and Haddad, G. I., "Properties of High-Efficiency X-Band GaAs IMPATT Diodes," Tech. Report No. AFWAL-TR-81-1066, Electron Physics Laboratory, The University of Michigan, Ann Arbor, June 1981.

2. Froelich, R. K., "Computer Modeling of Millimeter-Wave IMPATT Diodes," Ph.D. Dissertation, The University of Michigan, Ann Arbor, 1982.

3. Bauhahn, P. E., "Properties of Semiconductor Materials and Microwave Transit-Time Devices," Ph.D. Dissertation, The University of Michigan, Ann Arbor, 1977.

4. Steele, S. R., Johnson, K. K., Lauterwasser, B. D., Baras, A. D. and Holway, L., Jr., "P-Type Gallium Arsenide Epitaxial Growth," Tech. Report No. AFAL-TR-79-1144, Raytheon Company, Waltham, MA, October 1979.

5. Blakey, P. A., private communication.

6. Cornell Hot Electron Workshop, July 1978; presented by Kao and Crowell from the University of Southern California, Los Angelos. Blakey, P. A., private communication.

7. Kao, C. W. and Crowell, C. R., "Impact Ionization by Electrons and Holes in InP," Solid-State Electronics, vol. 23, No. 8, pp. 881-891, August 1980.

8. Fawcett, W. and Hill, G., "Temperature Dependence of the Velocity/Field Characteristic of Electrons in InP," Electronic Letters, vol. 11, No. 4, pp. 80-81, 20 February 1975.

9. Belova, N. A., Galchenkov, L. A., Skvortsova, N. E. and Sokolov, Yu. F., "Investigation of the Carrier Mobility in Epitaxial InP Films Grown on Heavily Doped Substrates," Sov. Phys. Semicon., vol. 13, No. 9, pp. 1045-1047, September. 1979.

10. Majerfeld, A., Potter, K. E. and Rolson, P. N., "Temperature Dependence of the Subthreshold Velocity/Field Characteristic for Epitaxial InP," Electronic Letters, vol. 11, No. 4, pp. 81-82, 20 February 1975.

11. Bauhahn, P. E., Haddad, G. I. and Masnari, N. A., "Comparison of the Hot Electron-Diffusion Rates for GaAs and InP," Electronic Letters, vol. 9, No. 19, pp. 460-461, 20 September 1973.

12. Microwave Associates, Burlington, MA, private communication.

13. Kennedy, D. P., "Spreading Resistance in Cylindrical Semiconductor Devices," J. Appl. Phys., vol. 31, No. 8, pp. 1490-1497, August 1960.

14. Olson, H. M., "Temperature Transients in IMPATT Diodes," IEEE Trans. on Electron Devices, vol. ED-23, No. 5, pp. 484-503, May 1976.

15. Maycock, P. D., "Thermal Conductivity of Silicon, Germanium, III-V Compounds and III-V Alloys," Solid-State Electronics, vol. 10, No. 3, pp. 161-168, March 1967.

16. Gilden, M. and Hines, M. E., "Electronic Tuning Effects in the Read Microwave Avalanche Diode," IEEE Trans. on Electron Devices, vol. ED-13, No. 1, pp. 169-175, January 1966.

17. Massé, D., Barlas, A. D., Holway, L., Adlerstein, M., Johnson, K. K. and Mozzi, R., "EHF GaAs Double-Drift IMPATT Diodes," Tech. Report AFAL-TR-79-1204, Raytheon Research Division, Waltham, MA, December 1979.

18. Cherensky, S., "Assessment and Optimization of Uniformly Doped Double-Drift GaAs Millimeter Wave IMPATT Diodes," Electron Physics Laboratory, The University of Michigan, Ann Arbor, January 1982.

END

FILMED

2-83

DTIC